CMS-SMP-23-002

# High-precision measurement of the W boson mass with the CMS experiment at the LHC

The CMS Collaboration*

## Abstract

In the standard model of particle physics, the masses of the carriers of the weak interaction, the W and Z bosons, are uniquely related. Physics beyond the standard model could change this relationship through the effects of quantum loops of virtual particles, thus making it of great importance to measure these masses with the highest possible precision. Although the mass of the Z boson is known to the remarkable precision of 22 parts per million (2.0 MeV), the W boson mass is known much less precisely, given the difficulty of the measurement. A global fit to electroweak data, used to predict the W boson mass in the standard model, yields an uncertainty of 6 MeV. Reaching a comparable experimental precision would be a sensitive and fundamental test of the standard model. Furthermore, a precision measurement of the W boson mass performed by the CDF Collaboration at the Fermilab Tevatron has challenged the standard model by significantly disagreeing with the prediction of the global electroweak fit and the average of other $m_W$ measurements. We report the first W boson mass measurement by the CMS Collaboration at the CERN LHC, based on a data sample collected in 2016 at the proton-proton collision energy of 13 TeV. The W boson mass is measured using a large sample of W $\rightarrow \mu\nu$ events via a highly granular binned maximum likelihood fit to the kinematic properties of the muons produced in the $W^+$ and $W^-$ boson decays. The significant in situ constraints of theoretical inputs and their corresponding uncertainties, together with an accurate determination of the experimental effects, lead to a precise W boson mass measurement, $m_W = 80\,360.2 \pm 9.9$ MeV, in agreement with the standard model prediction.

*Submitted to Nature*

*See Appendix B for the list of collaboration members

# 1  Importance of measuring the W boson mass

Precision measurements of fundamental parameters have played a major role in the development of the standard model (SM) of particle physics, which provides a remarkably accurate description of the known elementary particles and their interactions. Over the span of several decades, they provided increasingly precise estimates for the masses of the W and Z bosons, top quark, and Higgs boson, which helped guide the experimental programs aimed at their discoveries [1, 2]. With the observation of the Higgs boson at the CERN LHC and the determination of its mass, all the parameters in the electroweak (EW) sector of the SM are now constrained by experimental measurements. Nevertheless, the standard model is widely believed to be incomplete, given that it does not explain certain fundamental observations, such as the asymmetry of matter and antimatter in the universe and the existence of dark matter. In the SM, the masses of the $W^{\pm}$ and Z bosons, $m_W$ and $m_Z$, are uniquely related to the coupling strengths of the weak and electromagnetic interactions. If the measured masses and couplings deviate from the predicted relation, it would be a clear sign of physics beyond the SM (BSM), most likely in the form of new particles at mass scales above those that existing accelerators and experiments can probe directly. Such BSM physics could manifest itself through modifications of $m_Z$ or $m_W$ via quantum loop interactions with the W and Z bosons [3, 4].

The Z boson mass has been measured with the exceptional precision of 22 parts per million ($m_Z = 91\,188.0 \pm 2.0\,\text{MeV}$) [5] by the experiments operating at the CERN LEP collider, through measurements of resonant Z boson production in precise beam energy scans [6]. The $m_W$ measurement at LEP was based on the direct reconstruction of pair-produced W bosons, which has a production rate in electron-positron collisions several orders of magnitude lower than that of Z boson production. Consequently, the uncertainty in the $m_W$ measurement was an order of magnitude larger than that of $m_Z$. Subsequent measurements performed at the Fermilab Tevatron [7] and the LHC [8–10] contributed to the current experimental average of $m_W = 80\,369.2 \pm 13.3\,\text{MeV}$ [5]. The value of $m_W$ derived from the predicted relationships of EW parameters in the SM and independently measured observables, known as a global EW fit, $m_W = 80\,353 \pm 6\,\text{MeV}$ [5], is significantly more precise. As such, improving the direct measurement of $m_W$ provides an important test of the SM and enhances the sensitivity to BSM physics. Furthermore, the experimental combination does not include the most precise single measurement, performed by the CDF Collaboration, $m_W = 80\,433.5 \pm 9.4\,\text{MeV}$ [11]. The strong disagreement between this value and both the SM expectation and the other measurements [12] represents a major puzzle in the field of particle physics. An independent high-precision $m_W$ measurement is, therefore, of the utmost importance. In this paper we report the results of the first W boson mass determination by the CMS Collaboration, based on a sample of proton-proton (pp) collisions at a center-of-mass energy of 13 TeV. Our measurement is based on the analysis of more than 100 million reconstructed W boson decays, an event sample that is an order of magnitude larger than those used for the previous $m_W$ measurements. Together with an accurate determination of the experimental effects, this large dataset allows us to significantly reduce the theoretical and experimental uncertainties in our measurement. This result constitutes a substantial step towards resolving the W boson mass puzzle.

# 2  Analysis strategy

At hadron colliders, jets from the hadronization of the quark-antiquark pair produced in the decay of the W boson cannot be selected and calibrated with sufficient accuracy for a precise $m_W$ measurement. Therefore, measurements of $m_W$ rely on the W boson decay to a charged lepton $\ell$ and a neutrino $\nu$, $W \to \ell\nu$, in which the W boson cannot be fully reconstructed be-

cause neutrinos are not directly measurable in collider detectors. The kinematic distributions of the lepton and neutrino from the W boson decay are sensitive to $m_W$ because, in the rest frame of the decaying W boson, the mass of the W boson is equally shared between the momenta of the neutrino and of the lepton. In the laboratory frame, the transverse components of the lepton and neutrino momenta ($p_T^\ell$ and $p_T^\nu$) exhibit characteristic Jacobian peaks at around $m_W/2$, though their exact distributions depend on the transverse momentum of the W boson itself, $p_T^W$. Therefore, the $m_W$ value can be indirectly measured through $p_T^\ell$ or by the transverse component of the negative vector momentum sum of all measured particles in the event, $\vec{p}_T^{\text{miss}}$, which is an estimator of $p_T^\nu$. The resolution of the $p_T^{\text{miss}}$ measurement degrades in the presence of a large number of pp collisions in the same or adjacent bunch crossings (pileup), reducing its sensitivity to $m_W$. The transverse mass, $m_T^W = \sqrt{2\, p_T^\ell\, p_T^{\text{miss}}\, (1 - \cos\Delta\phi_{\ell\vec{p}_T^{\text{miss}}})}$, where $\Delta\phi_{\ell\vec{p}_T^{\text{miss}}}$ is the azimuthal angle difference between the lepton and $\vec{p}_T^{\text{miss}}$ trajectories in the plane transverse to the beam line, is a powerful observable in the $m_W$ measurements performed at the Tevatron [7, 11]. However, due to the poorer $p_T^{\text{miss}}$ resolution, it has limited sensitivity to $m_W$ in LHC measurements [8–10]. The dataset used for our measurement has more than twice the pileup of that used for any previous $m_W$ measurement. These considerations inform the strategy of our $m_W$ determination, which is based on the kinematic distributions of the charged lepton in W $\to \ell\nu$ events.

Among the three leptonic decays (electron, muon, or $\tau$ lepton), we exploit the muon channel, since it offers the best experimental precision with the multipurpose, nearly hermetic CMS detector [13]. The CMS apparatus [13] is designed to trigger on [14–16] and identify electrons, muons, photons, and (charged and neutral) hadrons [17–19]. A global event reconstruction algorithm [20] aims to reconstruct all individual particles in an event, combining information provided by the all-silicon inner tracker and by the crystal electromagnetic and brass-scintillator hadron calorimeters, operating inside a 3.8 T superconducting solenoid, with data from the gas-ionization muon detectors embedded in the flux-return yoke outside the solenoid. Charged-particle trajectories (tracks) are built from energy deposits in each layer of the silicon detector, referred to as "hits." Muon tracks typically have at least 12 hits, each of which is measured with an accuracy of $\approx$15 $\mu$m in the bending plane. The momentum of muons is derived from the curvature of the corresponding track.

To perform a high-precision $m_W$ measurement, we rely on a deep understanding of both the experimental and theoretical sources of systematic uncertainty. The muon momentum scale (the largest source of uncertainty in the measurement) is calibrated to a few parts per hundred-thousand by using a sample of dimuon decays of the J/$\psi$ resonance. Muons from $\Upsilon$(1S) meson and Z boson decays are used for independent validations. Although the $p_T^\mu$ distribution is sensitive to $m_W$, it also depends on the theoretical modeling of the $p_T^W$ distribution and on the parton distribution functions (PDFs), which describe the momentum distributions of the quarks and gluons inside the protons. The PDFs strongly affect the W boson polarization and, hence, the kinematic distributions of the decay leptons [21]. To minimize the dependence of our $m_W$ measurement on the uncertainties in modeling the W boson production, we aggregate selected data and simulated W $\to \mu\nu$ events into a highly-granular three-dimensional distribution depending on $p_T^\mu$, $\eta^\mu$, and $q^\mu$, where $\eta^\mu = -\ln\tan(\theta/2)$ is the muon's pseudorapidity, $\theta$ is the polar angle of the muon with respect to the beam line, and $q^\mu$ is the muon electric charge. The three-dimensional distribution is divided into 48 $\eta^\mu$ bins from $-2.4$ to 2.4 and 30 $p_T^\mu$ bins from 26 to 56 GeV, besides two bins in $q^\mu$ ($+1$ or $-1$). The $m_W$ value is extracted from a binned maximum likelihood fit to this distribution, using template shapes for the signal and background processes.

Our analysis uses state-of-the-art calculations to describe the W and Z boson production. The predictions combine an all-order resummation of logarithmically enhanced soft and collinear gluon emissions at next-to-next-to-next-to-leading logarithmic ($N^3LL$) accuracy with next-to-next-to-leading order (NNLO) accuracy in perturbative quantum chromodynamics (QCD) [22]. They also incorporate a phenomenological model for the nonperturbative motion of the partons inside the proton [23]. We incorporate a novel proposal for "theory nuisance parameters" (TNPs) [24], which exploits the known structure of the resummation calculation to parameterize the impact of unknown perturbative corrections. These models, combined with uncertainty profiling [5] in the binned maximum likelihood fit to the $(p_T^\mu, \eta^\mu, q^\mu)$ distribution, allow the $p_T^W$ spectrum to be determined in situ by our $W \to \mu\nu$ data and reduce its uncertainty to subleading importance in the measurement. In contrast to previous $m_W$ measurements at hadron colliders [7, 9–11], we do not rely on measurements of Z boson production to modify the predicted $p_T^W$ distribution. As shown in Ref. [25], our procedure also significantly constrains the PDFs, the second largest source of uncertainty in our $m_W$ measurement.

We have also developed an alternative $m_W$ analysis approach that reduces the sensitivity to theoretical inputs by extracting $m_W$ simultaneously with the angular distributions of the muon from the W boson decay. This procedure is based on the general parameterization of the production cross section of a spin-1 vector boson and its decay to leptons in terms of nine helicity states [26]. For each bin in the two-dimensional $p_T^W$ and W boson rapidity ($y^W$) space, and separately for the $W^+$ and $W^-$ bosons, each helicity component leads to a different $(p_T^\mu, \eta^\mu)$ distribution. We perform a differential analysis, encoding the variations of the helicity components as alternative templates fitted to the $(p_T^\mu, \eta^\mu, q^\mu)$ distributions. While this method, referred to as "helicity fit", reduces the measurement sensitivity to $m_W$, it provides a valuable cross-check of the nominal result by relaxing some assumptions about the W boson production and, hence, reducing the dependence of the analysis on theoretical predictions and their uncertainties.

To validate the experimental and theoretical inputs of the measurement, we perform two Z boson mass measurements. First we extract $m_Z$ through a maximum likelihood fit to the $Z \to \mu\mu$ dimuon mass distribution. Then we perform a "W-like measurement" of $m_Z$ using only one of the two decay muons, to mimic the conditions of the $m_W$ measurement. We model Z and W boson production with predictions at the same perturbative accuracy and parameterize their independent uncertainties with a common strategy. Given the similarity between the Z and W production mechanisms, the predictions and their uncertainties can be validated by the W-like $m_Z$ analysis, where the predicted $p_T^Z$ distribution can be directly compared with the measured $p_T^{\mu\mu}$ spectrum. These two measurements, validated by comparing them with the precise $m_Z$ value obtained at LEP, are a crucial step of our analysis procedure, ensuring the robustness of the $m_W$ measurement.

The vector-boson (V = W or Z) mass and width are defined in the running-width scheme [27]. The analysis is conducted following the "data blinding" concept [28]: it is optimized on simulated event samples and a random offset, between $-500$ and $500\,\text{MeV}$, is applied to the $m_W$ and $m_Z$ values until all the procedures are established. In the following sections we briefly discuss the most important aspects of the $m_W$ measurement, with further details given in the Methods section (Section A).

## 3 Event samples and selection criteria

The measurements are made using a sample of pp collisions at a center-of-mass energy of $13\,\text{TeV}$, collected in 2016 and corresponding to an integrated luminosity of $16.8\,\text{fb}^{-1}$ ($\pm1.2\%$) [29].

This dataset, roughly half of the full 2016 event sample, is selected to ensure an optimal performance of the CMS detector, especially for the reconstruction of charged particle tracks [30]. The data were processed with the most recent version of the reconstruction software, including improvements to particle identification and reconstruction developed for this analysis, and with the latest detector calibration and description of the operating conditions.

The events are preselected by an online trigger algorithm that requires the presence of at least one muon with $p_T^\mu > 24\,\text{GeV}$, isolated from other energy deposits in the detector and satisfying quality criteria for tracks reconstructed in the silicon tracker and muon detectors [13, 14, 16]. This filter selects the events used in both the $m_Z$ and $m_W$ analyses, to guarantee maximal consistency between them in terms of event selection and efficiency corrections. Selected $W \to \mu\nu$ events are required to have a muon in the $|\eta^\mu| < 2.4$ and $26 < p_T^\mu < 56\,\text{GeV}$ acceptance window. The selected muon must be compatible with the object that triggered the event, be isolated from other particles, and satisfy selection criteria meant to reduce backgrounds and ensure a high-quality reconstruction. The $p_T^\mu$ thresholds restrict the selected events to the $p_T^\mu$ range where the trigger and reconstruction efficiencies are measured most accurately. Machine-learning techniques are used to improve the resolution of the reconstructed $p_T^\text{miss}$ [31], which narrows $m_T^W$ distribution for true $W \to \mu\nu$ events and, hence, improves the separation between the signal and background events. We enhance the purity of the signal by requiring $m_T^W > 40\,\text{GeV}$ and by rejecting events with electrons (or additional muons) with $p_T > 10\,(15)\,\text{GeV}$ satisfying looser identification criteria [17, 18]. A total of 117 million data events are selected by these criteria. The estimated selection efficiency for simulated $W \to \mu\nu$ events is 85% and the estimated fraction of $W \to \mu\nu$ events in the selected data sample is 89%.

The event selection for the dimuon and W-like $m_Z$ measurements is designed to be maximally consistent with the one used for the $m_W$ measurement. The selected events must have two muons satisfying the same selection criteria, except that the $p_T^\mu$ window is extended to 60 GeV because the Z boson is heavier than the W boson. The two muons must have opposite electric charge and a dimuon invariant mass in the $60 < m_{\mu\mu} < 120\,\text{GeV}$ range. A total of 7.5 million $Z \to \mu\mu$ data events are selected. The signal purity of the selected dimuon sample is larger than 99.5%. For the W-like $m_Z$ analysis, only one of the muons from the Z boson decay is considered to form the $(p_T^\mu, \eta^\mu)$ templates. The other muon is treated as a neutrino and, hence, is excluded from the $p_T^\text{miss}$ computation [32]. Considering the relative scale of $m_Z$ compared with $m_W$, events must satisfy $m_T > 45\,\text{GeV}$, where $m_T$ is calculated from the selected muon and the modified $p_T^\text{miss}$. To define statistically independent samples that mimic the W boson selection, the $Z \to \mu\mu$ events are split into two sets based on the event number, so that odd (even) events are used to analyze positive (negative) muons. Only the analyzed muon is required to match the object that triggered the event, which avoids the need to evaluate correlations in the triggering efficiency in events where both muons satisfy the trigger requirements. We analyze the two samples separately, such that all events are considered and no event is used more than once. More details on the data sample and event selection are given in Section A.1.

Monte Carlo (MC) generators are used to produce large samples of simulated events that are used to guide the analysis and to assess the consistency of the data with different hypotheses for the value of $m_W$. Simulated W and Z boson event samples are generated with MiNNLO$_\text{PS}$ [33, 34], interfaced with PYTHIA [35] for the parton shower and hadronization, and with PHOTOS++ [36, 37] for the final-state photon radiation. The Z boson event samples include all contributions to the dilepton final state, including contributions from virtual photons. We modify the MiNNLO$_\text{PS}$ predictions with two-dimensional binned corrections in the W or Z boson $p_T$ and rapidity obtained with SCETLIB [22, 23, 38], thereby achieving

N$^3$LL+NNLO accuracy and improving the description of the data. The CT18Z PDF set [39] at NNLO accuracy is used. The detector response is simulated using a detailed description of the CMS detector, implemented with the GEANT4 package [40]. The reconstruction algorithms are the same for simulated and data events. The simulated event samples, including those for the relevant background processes, are described in Section A.1.

The average number of pileup interactions in data is 25, with a tail extending up to 44. The simulated distributions of the number of pileup interactions and the position along the beam line of the pp collision producing the muon are corrected to match the measured distributions, so as to accurately capture their impact on the muon reconstruction efficiency. The muon trigger, reconstruction, identification, and isolation efficiencies predicted by the simulation are corrected to match those measured in data, as discussed in Section A.2. The simulated $p_T^{miss}$ and $m_T$ distributions are corrected using $Z \to \mu\mu$ events in data, as discussed in Section A.3.

The main backgrounds in the selected $W \to \mu\nu$ data sample result from events with nonprompt muons, primarily from decays of heavy-flavor hadrons, or with prompt muons, from $Z \to \mu\mu$ decays where one muon misses the detector acceptance. Smaller backgrounds include $W \to \tau\nu$ and $Z \to \tau\tau$ decays, with one or more $\tau$ leptons decaying to muons, as well as top quark and antiquark pair, single top quark, and diboson production. As discussed in Section A.4, the nonprompt-muon background is evaluated with the "extended ABCD" method [41], using sideband regions in data defined by inverting the $m_T$ selection, the muon isolation requirement, or both. The uncertainty in the estimated background yields is dominated by the nonprompt-muon background contribution, and contributes 3.2 MeV to the uncertainty in $m_W$.

# 4  High-precision muon momentum calibration

A precise calibration of the muon momentum measurement is a crucial component of the $m_W$ analysis. For the momentum range of the muons selected in this analysis, hits in the silicon tracker have much greater importance in the track curvature determination than those in the muon system. Therefore, and in order to limit the volume of the detector in which the experimental conditions must be precisely determined, we reconstruct the muon momentum exclusively using the silicon pixel and strip detectors, and exploit the muon system only for triggering and identification.

Since $m_W$ is measured from the $p_T^\mu$ spectrum, relative uncertainties in the $p_T^\mu$ scale translate directly into a corresponding $m_W$ relative uncertainty. The reconstruction and calibration of the momentum scale requires an exceptionally detailed understanding of the features that impact the propagation and measurement of charged particle tracks. In particular, the relative alignment of the tracking detector components, the magnetic field throughout the tracking volume, and the material distribution, which governs the energy loss and multiple scattering (small-angle deflections due to interactions with electrons or nuclei that lead to deviations from the ideal particle trajectory), must be precisely determined. The muon tracks are reconstructed using algorithms and conditions specifically developed for this analysis, including a magnetic field mapping and a material model with a higher precision than those used in the standard CMS reconstruction. The alignment procedure [30] used to determine the position and orientation of the silicon modules has been extended to include fine-granularity corrections for the magnetic field and energy loss. The correspondence between the measured track curvature and the muon momentum is calibrated using a sample of events in which the dimuon invariant mass is consistent with the well-established mass of the $J/\psi$ resonance [5]. We extract parameterized corrections in fine bins of $\eta^\mu$ and extrapolate across the relevant range of $p_T^\mu$ using a model that takes into account small offsets in the magnetic field, alignment, and tracker ma-

terial remaining after the initial correction procedure. We validate our results using samples of $Y(1S) \rightarrow \mu\mu$ and $Z \rightarrow \mu\mu$ events. The uncertainty in the procedure is evaluated from the deviations of the $\eta^\mu$-binned correction parameters from zero when applying the corrections derived from $J/\psi \rightarrow \mu\mu$ events to $Z \rightarrow \mu\mu$ events and constraining $m_Z$ to the value of Ref. [5].

Extrapolating corrections to the muon momentum resolution from the relatively low momentum range typical of muons from the $Y(1S)$ meson decay to the higher momentum range of muons from Z boson decays is more challenging than for the momentum scale calibration, because multiple scattering has a large impact on the muon momentum resolution and is highly momentum dependent. For this reason we correct the muon momentum resolution in simulation to match the measured resolution in data using both $J/\psi \rightarrow \mu\mu$ and $Z \rightarrow \mu\mu$ events. The uncertainty in this correction is 1.4 MeV. Additional details on the muon momentum scale and resolution calibrations are given in Section A.5, where Table A.1 lists the contributions of the muon momentum calibration to the uncertainty in $m_W$. The muon momentum calibration contributes 4.8 MeV to the $m_W$ uncertainty, or about 60 parts per million.

## 5    Theoretical corrections and uncertainties

We exploit state-of-the-art simulation tools to obtain precise predictions for the $p_T^\mu$ spectrum at $N^3LL+NNLO$ perturbative accuracy. The uncertainties in the predictions include contributions reflecting the limited knowledge of the PDFs, the missing higher-order perturbative corrections in the QCD and EW interactions, and the nonperturbative effects. The $p_T^W$ spectrum cannot be directly measured with high precision due to the limited $p_T^{miss}$ precision. Although the $p_T^Z$ spectrum is measured precisely, using it to infer the $p_T^W$ spectrum requires estimating theoretical uncertainties in the $p_T^W / p_T^Z$ ratio, which depend strongly on the assumed uncertainty correlation [42]. Therefore, we do not apply corrections derived from the measured $p_T^{\mu\mu}$ spectrum to the W boson simulation. Instead, corrections to the $p_T^W$ spectrum come from $W \rightarrow \mu\nu$ data events via the profiling procedure employed in the maximum likelihood fits used to extract results. This approach relies on the high accuracy of the theoretical predictions, novel techniques to model their uncertainties and correlations across phase space, and the large statistical power of the analyzed data sample.

The SCETLIB calculation parameterizes the dominant sources of uncertainty in the $p_T^V$ spectra due to perturbative and nonperturbative effects. Perturbative uncertainties are represented by the TNPs of Ref. [24], whose impact on the analysis is evaluated by varying their values. The calculations treat the quarks as massless. Possible modifications due to the true quark masses are effectively absorbed into the other sources of modeling uncertainty, as discussed in Section A.6. We have tested other alternatives for the $p_T^W$ modeling, at equivalent or higher perturbative orders, and confirmed that the variation in $m_W$ is within the uncertainty evaluated from our nominal prediction at $N^3LL+NNLO$ accuracy.

The relative fractions of the Z and W boson helicity states and their uncertainties due to missing higher-order perturbative corrections are evaluated at NNLO in QCD using MiNNLO$_{PS}$; we have verified their consistency with the fixed-order NNLO QCD predictions of DYTURBO [43] and MCFM [44]. Uncertainties due to the PDFs, including their impact on the W boson helicity states, are evaluated by propagating the Hessian eigenvectors of the CT18Z PDF set [45]. Their contribution to the uncertainty in $m_W$ is 4.4 MeV. We have repeated the $m_W$ measurement using seven alternative PDF sets. Additional details on these studies, corrections, and uncertainties are given in Sections A.6–A.9.

# 6 Measurement of the Z and W boson masses

The results are obtained from binned maximum likelihood fits in which systematic uncertainties are represented by nuisance parameters with Gaussian constraints [46]. We allow the systematic uncertainties to be constrained and the central values to be pulled, with respect to their initial values, through the profile likelihood function [5] used in the fits. Common sources of uncertainty are correlated across bins of the distribution. The uncertainty due to the size of the simulated samples is estimated via the Barlow–Beeston approach [47], as simplified by Conway [46], with the nominal statistical uncertainty scaled up by 25% to account for the effect of fluctuations in the alternate templates used to construct the systematic variations [48]. The coverage of this uncertainty has been verified by bootstrap resampling the simulated samples [49]. The parameter of interest, i.e., the mass of the W or Z boson ($m_V$), is an unconstrained parameter in the fit. The effect of different $m_V$ values on the distributions is derived from a continuous interpolation around the nominal value in the fit, set to the world-average experimental value of Ref. [50], and from variations of $m_V$ by $\pm 100\,\mathrm{MeV}$, evaluated from the full matrix-element-level calculation of the MiNNLO$_\mathrm{PS}$ simulation. We verified that the maximum likelihood fit correctly extracts the value of $m_W$ used in the simulation for twenty points within this range, such that any residual bias on the fitted $m_V$ values is smaller than $0.1\,\mathrm{MeV}$. The construction and minimization of the likelihood is implemented using the TensorFlow software package [51], in which the use of automatic differentiation [52] of gradients in the likelihood minimization allows the $m_W$ and W-like $m_Z$ likelihood fits to be computationally feasible and numerically stable, despite involving approximately 3000 bins and 4000 nuisance parameters.

## 6.1 Extraction of the Z boson mass from the dimuon mass spectrum

We extract $m_Z$ from a binned maximum likelihood fit to the dimuon mass distribution, in 25 bins of $m_{\mu\mu}$ and 14 bins of $\eta^\mu$ of the muon with the largest $|\eta^\mu|$. Compared with the world-average value, $m_Z^{\mathrm{PDG}} = 91\,188.0 \pm 2.0\,\mathrm{MeV}$ [5], dominated by measurements at the LEP collider, we obtain

$$m_Z^{\mu\mu} - m_Z^{\mathrm{PDG}} = -2.2 \pm 4.8\,\mathrm{MeV}. \tag{1}$$

The largest contribution to the uncertainty comes from the $p_T^\mu$ scale, $4.6\,\mathrm{MeV}$. The $m_Z^{\mathrm{PDG}}$ uncertainty [5] is also included, as described in Section A.5.

Figure 1 shows the measured and simulated $Z \rightarrow \mu\mu$ dimuon mass distributions, the latter reflecting the best fit values of nuisance parameters obtained from the maximum likelihood fit. The impact of a $4.8\,\mathrm{MeV}$ variation around the obtained $m_Z$ value is also shown, illustrating the precise understanding of the distribution that is achieved. The excellent consistency of our result with $m_Z^{\mathrm{PDG}}$ is a powerful validation of the muon reconstruction, momentum scale calibration, and corrections. Although $Z \rightarrow \mu\mu$ events are not used to determine the values of the parameterized muon momentum scale calibration, they are used, together with the $m_Z^{\mathrm{PDG}}$ value [5], to define the systematic uncertainties. Therefore, our $m_Z$ value is not a measurement that is independent of the experimental world average.

## 6.2 W-like measurement of the Z boson mass

The W-like $m_Z$ measurement mimics the $m_W$ measurement procedure. The $m_Z$ value is determined from a binned maximum likelihood fit to the $(p_T^\mu, \eta^\mu, q^\mu)$ distribution of the selected muons, splitting the data into two independent samples and validating the theory model with the helicity fit described in Section A.10. The result for the analysis configuration selecting positive muons in odd event-number events, compared with the experimental $m_Z$ average [5],
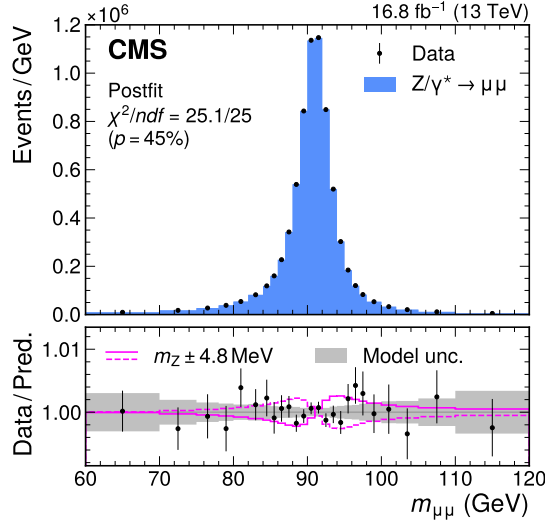
Figure 1: The Z boson mass measurement. Measured and simulated $Z \to \mu\mu$ dimuon mass distributions. The predicted $Z \to \mu\mu$ distribution is shown in blue. The small contributions of other processes are included but are not visible. The prediction reflects the best fit parameter values and uncertainties from the maximum likelihood fit. The bottom panel shows the ratio between the number of events observed in data, including variations in the predictions, and the total nominal prediction. The vertical bars represent the statistical uncertainties in the data. The total uncertainty in the prediction after the systematic uncertainty profiling procedure (gray band) and the effect of a $\pm4.8$ MeV variation of $m_Z$ (magenta lines) are also shown.

is

$$m_Z^{\text{W-like}} - m_Z^{\text{PDG}} = -6 \pm 7\,(\text{stat}) \pm 12\,(\text{syst}) = -6 \pm 14\,\text{MeV},$$

showing that the $m_Z^{\text{W-like}}$ value agrees with $m_Z^{\text{PDG}}$ (and with $m_Z^{\mu\mu}$). The configuration where the $Z \to \mu\mu$ events are selected with the alternative muon charge and event number polarity matching agrees with this result to within one standard deviation. The $m_Z$ values extracted in the helicity fit analysis configuration agree with this baseline result within the uncorrelated uncertainties of the two analyses, for both $Z \to \mu\mu$ event samples.

We validate the accuracy of the theory modeling and corresponding uncertainties by measuring the $p_T^Z$ directly in $Z \to \mu\mu$ events. Using the prediction and uncertainties for Z boson production described in Section 5, we perform a binned maximum likelihood fit of the two-dimension distribution of the dimuon $p_T$ and rapidity $(p_T^{\mu\mu}, y^{\mu\mu})$ to the observed $Z \to \mu\mu$ data. The consistency of the adjusted predictions and their uncertainties with the data is assessed with a goodness-of-fit test based on a saturated model, in which an unconstrained normalization parameter is introduced for each bin of the likelihood [53]. The $p$-value obtained from the comparison of the nominal and saturated likelihoods, 16%, affirms that the model and its uncertainty provide an accurate description of the data. The predicted $p_T^{\mu\mu}$ distribution, reflecting the best fit values of the nuisance parameters, is compared with the observed data in Fig. A.10.

The results of the $p_T^{\mu\mu}$ fit are not an input to the W-like $m_Z$ measurement. Rather, we independently determine values for the nuisance parameters describing the $p_T^Z$ modeling from the W-like $m_Z$ measurement and verify that they are consistent with those from the direct fit to $p_T^{\mu\mu}$. Figure 2 shows the generator-level $p_T^Z$ distribution, adjusted by the nuisance parameter values and uncertainties obtained from the two independent maximum likelihood fits. The result of these fits reflects corrections to the $p_T^{\mu\mu}$ predictions obtained directly from the maximum
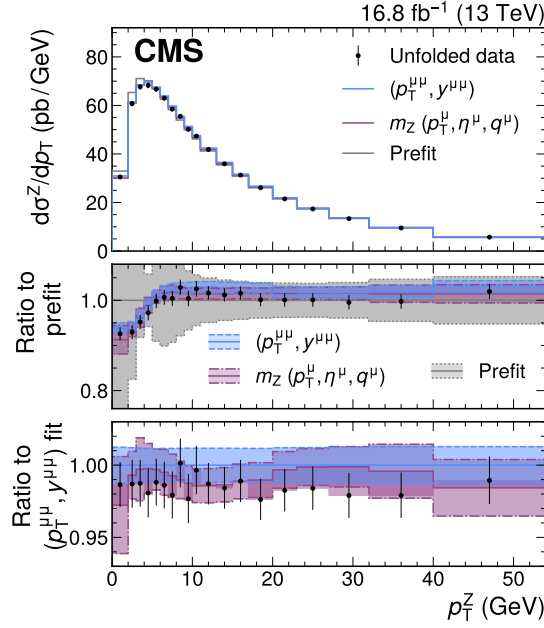
Figure 2: Validation of the theory model. Unfolded measured $p_T^Z$ distribution (points) compared with the generator-level SCETLIB+MINNLO$_{PS}$ predictions before (prefit, gray) and after adjusting the nuisance parameters to the best fit values obtained from the W-like $m_Z$ fit (magenta) or from the direct fit to the $p_T^{\mu\mu}$ distribution (blue). The center panel shows the ratio of the predictions and unfolded data to the prefit prediction. The uncertainty in the prefit prediction is shown by the shaded gray area. The bottom panel shows the ratio of the predictions and unfolded data to the prediction adjusted to the best fit values obtained from the fit to the $(p_T^{\mu\mu}, y^{\mu\mu})$ distribution. The uncertainties in the predictions after the maximum likelihood fits are shown in the shaded magenta and blue bands. The vertical bars represent the total uncertainty in the unfolded data.

likelihood fit to data. To test the accuracy of the adjusted predictions in describing our data, we account for effects of the detector response and resolution by "unfolding" our measurement to the generator level, as described in Section A.9. The consistency of the distributions obtained from the direct $p_T^{\mu\mu}$ fit and from the W-like $m_Z$ fit, as well as the consistency between each of them and the data, confirms the robustness of the predictions and of the uncertainty model, as well as the ability of the $(p_T^\mu, \eta^\mu)$ distribution to constrain the $p_T^V$ modeling in situ. This result supports adopting the same treatment for the $p_T^W$ distribution in the $m_W$ analysis, where $p_T^W$ cannot be precisely measured without theoretical input, and allows our $m_W$ measurement to be independent of the assumed correlation between $p_T^Z$ and $p_T^W$.

Section A.9 gives more details on the stability of our W-like Z boson mass measurement under different modeling assumptions and its consistency with the measured $p_T^{\mu\mu}$ distribution.

## 6.3   Measurement of the W boson mass

Having validated the analysis steps using the Z boson data, we proceed with the determination of the W boson mass. A binned maximum likelihood template fit is performed to the $(p_T^\mu, \eta^\mu, q^\mu)$ distribution, shown in Fig. A.16, and the observed $m_W$ value is

$$m_W = 80\,360.2 \pm 2.4\,(\text{stat}) \pm 9.6\,(\text{syst}) = 80\,360.2 \pm 9.9\,\text{MeV},$$

in agreement with the EW fit prediction, $m_W = 80\,353 \pm 6\,\text{MeV}$ [5], and with other experimental results, except the latest measurement reported by the CDF Collaboration [11]. The EW fit prediction is based on relationships between $m_W$ and other experimental observables, including the Z boson, Higgs boson, and top quark masses, the fine-structure constant, and the muon lifetime. The uncertainty in the prediction is due to missing higher-order terms in the perturbative calculation used to derive the predicted relationship between the experimental inputs and from uncertainties in the experimental inputs themselves. The two sources of uncertainty are of comparable size.
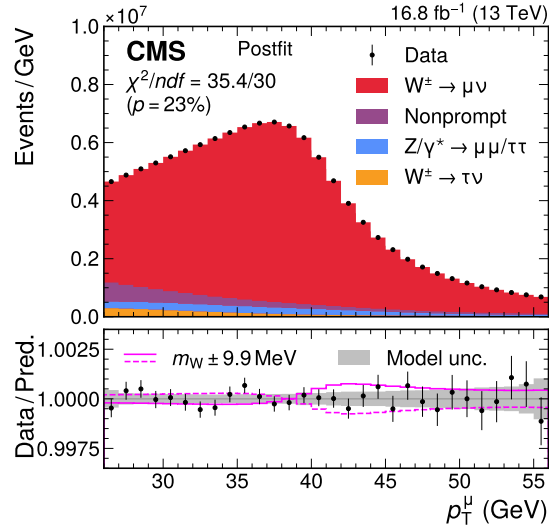


Figure 3: The W boson mass measurement. Measured and predicted $p_T^\mu$ distributions, showing the sensitivity to $m_W$ from the characteristic Jacobian peak at $\sim m_W/2$. The predicted $W \to \mu\nu$ contribution is shown in red, while the background contributions are shown in blue, purple, and yellow. Additional background contributions are included but not visible. The prediction is adjusted to the best fit values of the nuisance parameters and the measured value of $m_W$. The bottom panel shows the ratio between the number of events observed in data, including variations in the predictions, and the total nominal prediction. The vertical bars represent the statistical uncertainties in the data. A shift in the $m_W$ value shifts the peak of the distribution, as illustrated by the solid and dashed magenta lines, which show an increase or decrease of $m_W$ by 9.9 MeV. The total contribution of all theoretical and experimental uncertainties in the predictions, after the systematic uncertainty profiling in the maximum likelihood fit, is shown by the gray band.

Figure 3 shows the measured and simulated $p_T^\mu$ distributions, with the predictions reflecting the best fit values of the nuisance parameters and of $m_W$ extracted from the maximum likelihood fit to the $(p_T^\mu, \eta^\mu, q^\mu)$ distribution. The effect on the $p_T^\mu$ distribution of a 9.9 MeV variation in $m_W$ is shown to illustrate the degree to which the distribution and its uncertainties are controlled, enabling the high precision of the measurement. The main uncertainties in the $m_W$ measurement are due to the $p_T^\mu$ scale (4.8 MeV) and the PDF uncertainties (4.4 MeV). A detailed breakdown of the $m_W$ measurement uncertainty is provided in Table A.4 and alternative breakdowns are detailed in Section A.11. The robustness of the result with respect to the theory model is tested further by performing the $m_W$ measurement with the helicity fit configuration, as discussed in Section A.10. The result, $80\,360.8 \pm 15.2\,\text{MeV}$, is consistent with the nominal value and is stable against variations in the constraints imposed on the predicted helicity cross sections.

# 7 Discussion

In this paper we report the first W boson mass measurement by the CMS Collaboration at the CERN LHC. The result is significantly more precise than previous LHC measurements. The W boson mass is extracted from a sample of 117 million selected $W \rightarrow \mu\nu$ events, collected in 2016 at the proton-proton collision energy of 13 TeV, via a highly granular binned maximum likelihood fit to the three-dimensional distribution of the muon $p_T^\mu$, $\eta^\mu$, and electric charge. Novel experimental techniques have been used, together with state-of-the-art theoretical models, to improve the measurement accuracy. The muon momentum calibration, based on $J/\psi \rightarrow \mu\mu$ decays, as well as the data analysis methods and the treatment of the theory calculations used in the $m_W$ measurement have been extensively validated by extracting $m_Z$ and $p_T^Z$ both from a direct $Z \rightarrow \mu\mu$ dimuon analysis and from a W-like analysis of the Z boson data.
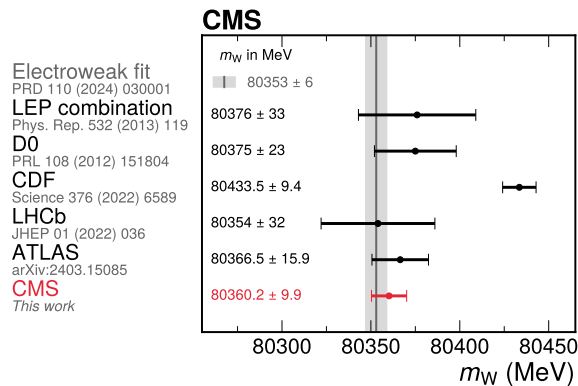


Figure 4: Comparison with other experiments and the EW fit prediction. The $m_W$ measurement from this analysis (in red) is compared with the combined measurement of experiments at LEP [54], and with the measurements performed by the D0 [55], CDF [11], LHCb [9], and ATLAS [10] experiments. The global EW fit prediction [5] is represented by the gray vertical band, with the shaded band showing its uncertainty.

As shown in Fig. 4, the measured value, $m_W = 80\,360.2 \pm 9.9$ MeV, agrees with the standard model expectation from the electroweak fit and is in disagreement with the measurement reported by the CDF Collaboration. Our result has similar precision to the CDF Collaboration measurement and is significantly more precise than all other measurements. The dominant sources of uncertainty are the muon momentum calibration and the parton distribution functions. Uncertainties in the modeling of W boson production are subdominant due to novel approaches used to parameterize and constrain the predictions and their corresponding uncertainties in situ with the data. This result constitutes a significant step towards achieving an experimental measurement of $m_W$ with a precision matching that of the EW fit. Together with other recent measurements performed by the CMS Collaboration, including the top quark mass [56] and the effective electroweak mixing angle [57], this work demonstrates the power of the CMS detector and of the LHC as instruments for precision measurements of the parameters of the standard model.

# A  Details of the analysis methods

## A.1  Details regarding the event samples and selection criteria

We simulate W and Z boson production at NNLO in QCD using the MiNNLO$_\text{PS}$ Wj and Zj [33, 34] (rev. 3900) processes in POWHEG-BOX-V2 [58–60], interfaced with PYTHIA 8.240 [35] for the parton shower and hadronization, and with PHOTOS++ 3.61 [36, 37] for final-state photon radiation. We use the CP5 underlying event tune [61], with the hard primordial-$k_\text{T}$ parameter set to 2.225 GeV, obtained from a dedicated optimization using the $p_\text{T}^{\mu\mu}$ data of Ref. [62]. The $(G_\mu, m_\text{W}, m_\text{Z})$ and $(G_\mu, \sin^2\theta_\text{eff}, m_\text{Z})$ EW input schemes are used for W and Z boson production, respectively. The CT18Z PDF set [39] at NNLO accuracy was chosen for the nominal analysis, before unblinding the result, given its good description of our W and Z data and because the expected shifts in $m_\text{W}$ from using other modern PDF sets are within its uncertainties. Additional NNLO PDF sets are studied using event-level weights in the POWHEG MiNNLO$_\text{PS}$ sample: NNPDF3.1 [63], NNPDF4.0 [64], CT18 [39], MSHT20 [65], and PDF4LHC21 [66]. We also consider the MSHT20aN3LO approximate N$^3$LO PDF set [67]. The POWHEG MiNNLO$_\text{PS}$ generator is also used to simulate events with W or Z bosons decaying to $\tau$ leptons, with the same theory corrections on the boson production kinematic distributions as those applied to the samples with muonic decays. To ensure that the MC sample size is not a significant source of uncertainty in the measurement, simulated samples of more than 4 billion (400 million) W (Z) boson production events have been produced. The EW production of lepton pairs or of a W boson in association with a quark through photon-photon or photon-quark scattering is simulated at LO using PYTHIA 8.240 [68]. Top quark and diboson production are simulated at NLO QCD accuracy using MADGRAPH5_aMC@NLO v2.6.5 [69] and POWHEG-BOX-V2, respectively, interfaced with PYTHIA 8.240 for the parton shower and hadronization. Quarkonia production is simulated using PYTHIA 8 interfaced with PHOTOS++ v3.61 for final-state photon radiation. Single-muon events have been simulated for additional validation of the muon reconstruction and calibration.

The selected muons must have a reconstructed track in both the silicon tracker and the muon detectors, with a consistent track fit for hits in both detector subsystems, and pass additional quality criteria to ensure a high purity of the selected events. We use the "medium" identification working point [17], whose efficiency is better than 98% for signal muons. The muons must have a transverse impact parameter smaller than 500 $\mu$m with respect to the beam line and be isolated from hadronic activity in the detector. The muon isolation is defined as the pileup-corrected ratio between $p_\text{T}^\mu$ and the sum of the $p_\text{T}$ of all other reconstructed physics objects within a cone centered around the muon [18]. The isolation of selected muons must be smaller than 15%, using a cone of radius $\sqrt{(\Delta\phi)^2 + (\Delta\eta)^2} = 0.4$. Only charged particles within 2 mm of the muon track along the beam axis are considered in the isolation sum. The distance is evaluated between the points of closest approach to the beam line for each track. The same criteria are used to select charged particles used in the $p_\text{T}^\text{miss}$ calculation. Our definition differs from the standard CMS approach, where charged particles in the isolation and $p_\text{T}^\text{miss}$ sums are defined with respect to the vertex that maximizes the sum of $p_\text{T}^2$ of the associated physics objects [70]. This change of definition is needed to minimize the rate at which the wrong vertex is chosen, which is negligible in Z $\to \mu\mu$ events but, with the standard CMS algorithm, ranges from 1 to 5% for W $\to \mu\nu$ events, depending on $p_\text{T}^\text{W}$. Indeed, to ensure the validity of the isolation and $p_\text{T}^\text{miss}$ corrections measured with Z $\to \mu\mu$ events and applied to W $\to \mu\nu$ events (as described in Sections A.2 and A.3) it is important to make sure that there are no differences in their dependence on the vertex selection.

Events are rejected if they contain electrons with $p_\text{T} > 10$ GeV satisfying the identification

criteria of the "veto" working point (which has 95% efficiency for genuine electrons [18]) or additional muons of $p_T > 15\,\text{GeV}$ matching the "loose" criteria (more than 99% efficient for real muons [17]).

## A.2   Details regarding the efficiency corrections

The $m_W$ measurement is based on a fit to the measured $(p_T^\mu, \eta^\mu, q^\mu)$ distribution using simulated templates for the signal and most background processes. Therefore, it is important that the simulation can accurately reproduce the efficiency of the event selection in the $(p_T, \eta)$ bins used in the analysis. Corrections to the simulated muon efficiencies are determined from data with the tag-and-probe (T&P) method [71], using events from the same $Z \to \mu\mu$ sample that we use in the analysis, except that we apply a looser event selection.

The efficiencies are measured differentially in $(p_T, \eta)$ for different stages of the muon selection, factorized as: reconstruction of a standalone track in the muon chambers; matching of a standalone muon with a track in the tracker to form a global muon candidate (tracking); impact parameter and identification quality criteria of the global muon track; trigger selection; muon isolation. Misalignment or other effects in the reconstruction of tracks in the muon chambers, which are used for triggering and identification purposes, can result in charge dependent biases in the measured efficiencies. To properly account for them, efficiencies are measured separately for each muon charge except for the isolation step, for which the charge asymmetry is found to be negligible. The muon isolation is sensitive to the angular distance between the muon and the sum of the measured charged and neutral hadrons in the event, referred to as the hadronic recoil. The distribution of the recoil is different between W and Z boson production events, leading to a bias in the muon isolation efficiency measured using Z boson decays. For a given $p_T^Z$ value, the bias is larger for low $p_T^\mu$, when the muon is more likely produced in the direction opposite to that of the Z boson $p_T$ and in the vicinity of the recoil. The trigger efficiencies are also affected because of the isolation requirement applied at the trigger level. To account for this effect, the trigger and isolation efficiencies are measured triple-differentially in the muon $(p_T, \eta)$ and in the projection of the Z boson recoil along the $p_T^\mu$ direction, $u_T$. The corrections are applied to $W \to \mu\nu$ events using the W boson recoil, after correcting its distribution as described in Section A.3.

The efficiencies are evaluated in the measured and simulated event samples, and their ratios are used as scale factors (SFs) to reweight the simulated events in $(p_T, \eta)$ bins (and $u_T$ bins, where appropriate). The granularity in $\eta^\mu$ corresponds to the 48 bins used in the analysis. The statistical uncertainty in the SFs originates from the limited sample of measured and simulated $Z \to \mu\mu$ events in the T&P estimate, and systematic uncertainties stem from the modeling of the $Z \to \mu\mu$ mass distributions with signal and background components when extracting the efficiencies in the measured event sample. We evaluate these systematic uncertainties by repeating the efficiency measurements in the data sample after varying the signal or background models. To mitigate the effects of statistical fluctuations and discrete bin edges, the SFs are smoothed as a function of $p_T^\mu$, or of $u_T$-$p_T^\mu$, using a polynomial interpolation. No smoothing is performed versus $\eta^\mu$ because physical boundaries in the detector might produce genuine discontinuities in the $\eta^\mu$ dependence of the efficiency. Instead, a smooth dependence on $p_T^\mu$ is expected in the momentum range of interest. The smoothing simplifies the treatment of the SF statistical uncertainties in the analysis fit and also leads to reduced uncertainties in $m_W$ by imposing that the measured SFs are correlated across the $p_T^\mu$ or $u_T$-$p_T^\mu$ bins. We have verified that no bias is induced in the extracted $m_W$ value by the smoothing procedure, within the corresponding uncertainties.

The statistical uncertainties in the SFs are obtained from the eigenvectors of the covariance matrix of the fit determining the smoothing function parameters for the nominal SFs in each $\eta^\mu$ bin, for each efficiency step (and charge, where appropriate), leading to 2784 independent nuisance parameters. The systematic uncertainties in the SFs are estimated as the difference between the smoothed values for the nominal SFs and the alternative ones from the variation of the signal or background models. Because the same signal and background models, and variations thereof, are employed for all T&P bins, each source of systematic uncertainty is treated as fully correlated across all bins. However, the SFs for the nominal and alternative T&P models are obtained by fitting the same data, and are both affected by large statistical uncertainties because of the fine granularity versus $\eta^\mu$. Therefore, uncorrelated variations for each of the $\eta^\mu$ bins are also included, with the same magnitude as the correlated uncertainty in each bin. Separate uncertainties are assigned for each step, for a total of 343 nuisance parameters, treated as correlated between muon charges. The statistical and systematic components of the SF uncertainties, after the smoothing, have a similar contribution to the uncertainty in $m_W$, and their combined effect is 3.0 MeV.

Dedicated SFs and uncertainties are derived for the muon veto selection employed in the single-muon analysis. These are used to correct the simulated yields of the Z boson background process in events where the second prompt muon falls inside the analysis $(p_T^\mu, \eta^\mu)$ acceptance window but fails the reconstruction or identification criteria of the veto. This component of the $Z \to \mu\mu$ background is characterized by a $p_T^\mu$ distribution similar to that of the muons from W decays, but peaking at larger values of $p_T^\mu$. Moreover, because of the high veto efficiency, close to unity in many bins, small variations between data and simulation can result in relatively large corrections for the probability to fail the veto. To avoid biases in the measured $m_W$ because of $Z \to \mu\mu$ background variations induced by these corrections, dedicated veto SFs and corresponding uncertainties are evaluated. These are measured and smoothed in the same way as the others, but applied as a function of the $(p_T, \eta)$ of the second generator-level muon (evaluated after final-state radiation), taken as a proxy for the nonreconstructed muon. Veto SFs are computed as the product of three independent terms, accounting for muon tracking, reconstruction, and loose identification, further split by charge. These SFs are measured for $p_T^\mu > 15$ GeV, consistently with the lower $p_T^\mu$ threshold used in the veto selection. Uncertainties are defined using the same approach as detailed before and are encoded in a total of 384 (147) nuisance parameters for the statistical (systematic) components. These nuisance parameters are treated as uncorrelated with respect to those associated to the other efficiency steps. Because the veto selection strongly suppresses the Z boson background affected by these SFs, their contribution to the uncertainty in $m_W$ is smaller than 0.5 MeV. The nominal muon veto restricts the selection to "global muons," which have a high-quality track in both the tracker and muon detectors. An alternative definition has also been tested, with the muon inner track not required to be matched to a track reconstructed in the muon detectors. This looser selection has higher efficiency for prompt muons and, therefore, provides better rejection of the $Z \to \mu\mu$ background, at the cost of larger systematic uncertainties in the measured veto SFs because of the combination of different categories of reconstructed muons. Dedicated tests using pseudo-data generated with either veto selection have been carried out, showing that the measured $m_W$ values agree within less than 0.1 MeV between the two veto selections and that the residual bias in $m_W$ is covered by the veto SF uncertainties.

Further corrections and corresponding uncertainties are applied to the simulated events. Partial mistiming of signals in the muon detectors led to the incorrect assignment of the triggered event to the previous proton bunch crossing for a small fraction of events [14]. This is known as "prefiring", and caused a reduction in the trigger efficiency. A correction for this effect is

determined in bins of $\eta^\mu$ and $p_T^\mu$ [72]. The correction increases with $\eta^\mu$ and varies between 0.5 and 2%. A similar issue originating from the prefiring of the electromagnetic calorimeter triggers affects the analysis through hadronic jets containing photons or electrons not rejected by the veto. The total contribution of the prefiring to the uncertainty in $m_W$ is about 0.7 MeV.

The quality of the experimental corrections applied to the simulated events is validated using $Z \rightarrow \mu\mu$ events, which offer a pure sample of prompt muons, comparing the distribution of the selected muon $\eta^\mu$ with the measured one, for each muon charge, as shown in Fig. A.1. The agreement between measured and simulated data is within 2% in all bins, and the difference is smaller than the systematic uncertainty.
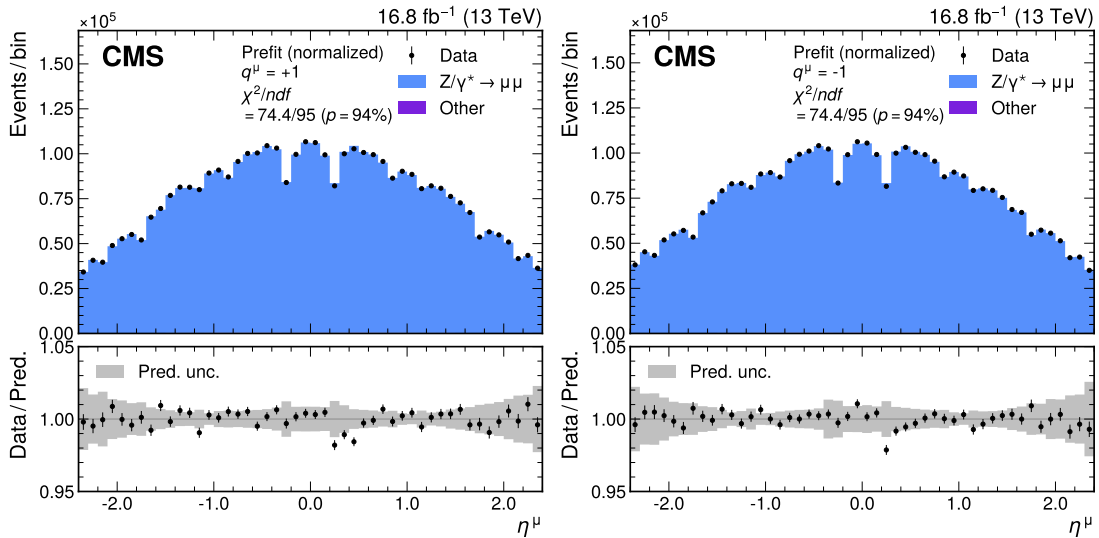


Figure A.1: Measured and predicted $\eta^\mu$ distributions in $Z \rightarrow \mu\mu$ events with the W-like Z boson selection for positively (left) and negatively (right) charged muons. The total uncertainties (statistical and systematic) are represented by the gray bands and the normalization of the simulated spectrum is scaled to the measured distribution, to better illustrate the level of agreement between the two. The vertical bars represent the statistical uncertainties in the data. The bottom panel shows the ratio of the number of events observed in data and of variations in the predictions to that of the total nominal prediction.

## A.3   Hadronic recoil calibration

To further improve the modeling of $p_T^{\mathrm{miss}}$ and $m_T$ in the simulated events, hadronic recoil corrections are derived using measured $Z \rightarrow \mu\mu$ events. Templates of the parallel and perpendicular components of the hadronic recoil (which balances the $p_T^Z$) along the Z boson momentum are parameterized as a function of the reconstructed $p_T^{\mu\mu}$, both in the simulated and measured events. For each event, a new value of $p_T^{\mathrm{miss}}$ is computed using an inverse cumulative distribution function transformation of the function mapping the simulated templates to data. The corrections derived from $Z \rightarrow \mu\mu$ events are applied to simulated $W \rightarrow \mu\nu$ events by using the generator-level $p_T^W$ to evaluate the corrections parameterized in $p_T^{\mu\mu}$. Differences between the W and Z recoil modeling are accounted for as a systematic uncertainty. Statistical uncertainties of the template parameterization are taken into account, although they have a negligible impact on our $p_T^\mu$-based $m_W$ measurement. Figure A.2 shows the recoil-corrected transverse mass distribution for $Z \rightarrow \mu\mu$ and $W \rightarrow \mu\nu$ events. Apart from a slight disagreement in normalization between the measured and simulated distributions (unrelated to the recoil and accounted for by other uncertainties), the scale and resolution are corrected with subpercent precision.
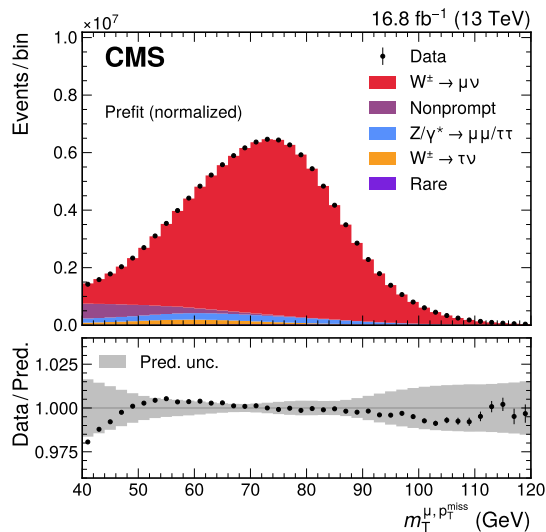
Figure A.2: Measured and predicted $m_T$ distributions in $W \rightarrow \mu\nu$ events, after calibrating the hadronic recoil. The predictions are those prior to the fit to data. The total uncertainties (statistical and systematic) are represented by the gray band and the normalization of the simulated spectrum is scaled to the measured distribution to better illustrate their agreement. The vertical bars represent the statistical uncertainties in the data. The bottom panel shows the ratio of the number of events observed in data and of variations in the predictions to that of the total nominal prediction.

The uncertainty in the corrections is evaluated from the statistical uncertainty of the fits that parameterize the correction of the simulation to the data. Their impact on $m_W$ is assessed by varying the correction parameters according to the eigenvectors of the fit covariance matrix. We have verified that their contribution to the uncertainty in $m_W$ is below 0.3 MeV. Because these variations are computationally expensive to evaluate, and their contribution to the $m_W$ uncertainty is negligible, they are not included in the nominal fit configuration.

## A.4 Nonprompt-muon background determination

The nonprompt-muon background consists primarily of events where muons originate from decays of heavy-flavor hadrons (which have sizable lifetimes) rather than from the collision point. Despite the large suppression applied by the muon selection criteria, a significant contribution from this background remains in the W boson selection. We evaluate it using data from sideband regions that are defined by inverting the $m_T$ selection, the muon isolation requirement, or both. To account for correlations between the isolation and the $m_T$ sideband regions, the "extended ABCD method" proposed in Ref. [41] is used. In this method, the low-$m_T$ sideband region is divided into two regions with $m_T < 20$ GeV or $20 < m_T < 40$ GeV, each one further split into events passing or failing the muon isolation criterion, such that the signal region is complemented by five sideband regions of isolation and $m_T$, compared with the typical three of the classic ABCD method. In the sideband regions, the nonprompt-muon component is evaluated by subtracting from data the contribution of processes with prompt muons, estimated from simulations. For each bin of $p_T^\mu$, $\eta^\mu$, and charge, the low-$m_T$ regions are used to obtain a transfer factor that is then applied to nonprompt-muon events that satisfy the $m_T$ selection but fail the isolation requirement, to obtain an estimate of the nonprompt-muon background in the signal region. To suppress statistical fluctuations, the nonprompt-muon background contribution in each sideband region is smoothed in $p_T^\mu$ with an exponential of a third-order Chebyshev polynomial. The statistical uncertainties of the data are accounted for

by propagating the uncertainties in the smoothing function parameters through the analysis. This procedure results in 384 variations, reflecting the four coefficients of the smoothing polynomials, the two charges, and the 48 $\eta^\mu$ bins. The prompt-muon contamination in the sideband regions is modeled with simulated events, with all the corrections applied, as for the signal region, including the appropriate combination of SFs for events that fail the isolation requirement in the nonisolated sideband regions. All experimental and theoretical systematic uncertainties in the prompt-muon contamination are propagated to the sideband regions by repeating the subtraction of the prompt component and the determination of the smoothing parameters in the sideband regions for each variation. In this way, uncertainties stemming from experimental or theoretical sources are also assigned to the nonprompt-muon background, and the correct correlation structure between prompt- and nonprompt-muon events is consistently taken into account in the uncertainty model.
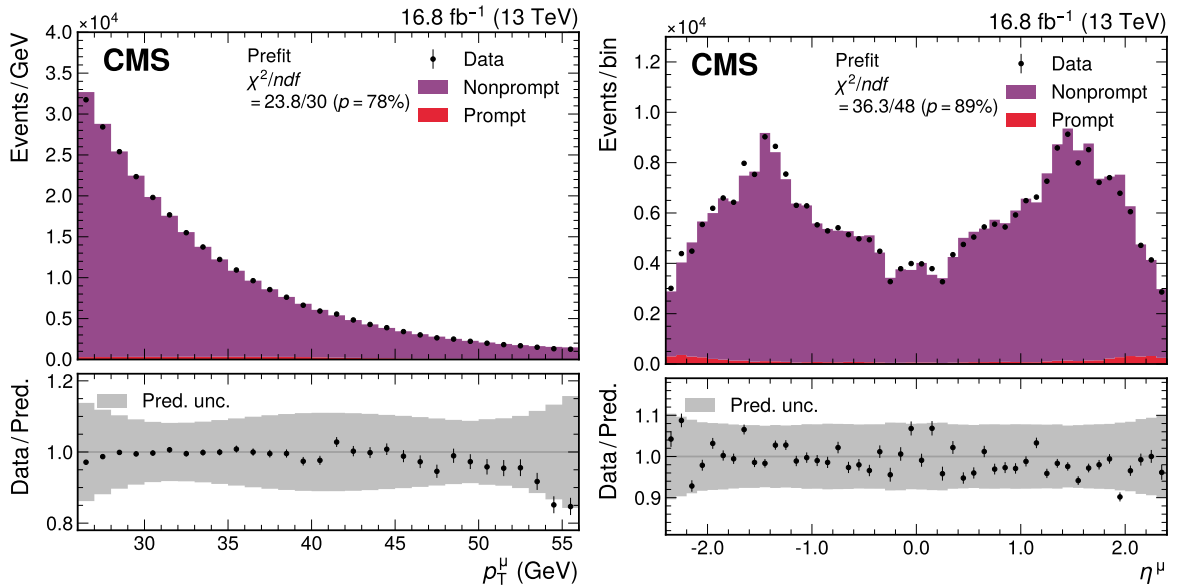


Figure A.3: The observed data and the prediction of the extended ABCD method before the maximum likelihood fit, for the $p_T^\mu$ (left) and $\eta^\mu$ (right) distributions, in a region enriched in events with nonprompt muons obtained by selecting muons compatible with being produced in a secondary vertex. Small contributions from events with a prompt muon, evaluated using simulated samples, are shown by the red histogram. The total uncertainties (statistical and systematic) are represented by the gray bands. The vertical bars represent the statistical uncertainties in the data. The bottom panel shows the ratio of the number of events observed in data and of variations in the predictions to that of the total nominal prediction.

This procedure was validated using a simulated sample of nonprompt-muon events by comparing the MC prediction in the W boson signal region with the prediction obtained from the extended ABCD method. The extended ABCD method overestimates the number of nonprompt-muon events in the signal region. A normalization correction factor of 0.85 is assessed from simulation and applied to the final estimation to correct for this overestimation. We account for residual differences in the shape of the $p_T^\mu$ distribution by varying the coefficients of the smoothing polynomial. These two additional variations are fully correlated across $\eta^\mu$ and charge bins. The method was validated using a data sample enriched in events with nonprompt muons originating from a secondary vertex. As shown in Fig. A.3, the measured and predicted nonprompt-muon events agree within uncertainties, and the agreement in the total number of events is within 2% in this region, confirming the aforementioned correction factor. A normalization uncertainty of 5% is assigned to the nonprompt-muon prediction to cover this

difference and possible differences between the control and signal regions. The uncertainty model is tested by performing a fit to the $(p_T^\mu, \eta^\mu, q^\mu)$ distributions, leading to a $p$-value of 98% and good agreement between data and prediction.

The total uncertainty in $m_W$ from the nonprompt-muon background is estimated to be 3.2 MeV, a value that includes the normalization uncertainty and systematic variations of the coefficients (2.5 MeV) and the statistical uncertainty of the smoothing function coefficients and their variations (1.9 MeV). Additional $m_W$ uncertainties result from variations of the predicted nonprompt-muon background due to experimental and theoretical effects, which modify the prompt-muon contamination that is subtracted from data in the sideband regions. They are accounted for as part of the corresponding experimental and theoretical uncertainties in $m_W$ from the respective sources.

## A.5    Details regarding the muon momentum calibration

The muon tracks are first reconstructed using a standard pattern recognition and Kalman filter track fit [19]. To improve the accuracy of the track parameter determination, the tracks are then refitted using a continuous variable helix (CVH) fit, a global $\chi^2$ fit that extends the generalized broken-line fit [73, 74] to incorporate continuous energy loss and multiple scattering from finite material elements. The detailed material model of the CMS detector used for our simulation is based on the initial design of the tracker material and support structures as well as in situ measurements using collision data, such as Ref. [75]. This model is incorporated into the track fit using the GEANT4e propagator [40, 76, 77]. To model the magnetic field, we use a parameterization of the detailed three-dimensional solenoidal field map [78] rather than the less accurate, but computationally faster, finite-element model used in the standard reconstruction. The starting point for the alignment corresponds to what is used in the standard CMS reconstruction [30, 79]. As compared with the standard track fit, additional quality criteria are used to select pixel hits, and a refined parameterization of the local hit position is used for the trapezoidal strip modules in the endcaps of the strip detector. To ensure an accurate modeling of track hit positions in the simulation, the numerical precision of the helix-surface intersection in GEANT4 has been increased with respect to the standard CMS simulation.

Although the models used to describe the magnetic field, the material distribution, and the detector alignment are the most accurate currently available, a few sources of potential biases remain. The magnetic field model is based on measurements made in the ground-level assembly hall rather than in the cavern and does not account for differences in the field induced by material in the detector and surroundings. The simulation geometry underlying the material model might not provide a perfect description of the real detector and there are inaccuracies in the Gaussian model used to incorporate material effects. Finally, the alignment is affected by small residual biases in the alignment procedure and by so-called "weak modes" (misalignment patterns, including global translations, twists, and radial expansions, that bias the parameter extraction from the track but do not impact the overall $\chi^2$ of the track fits [79]). To correct for these biases, we developed a generalized correction procedure that extends the standard alignment procedure. The alignment degrees of freedom are parameterized by the three translation and three rotation degrees of freedom per tracker module, albeit without extra parameters for module deformation or residual time dependence. The parameterization is extended with additional parameters to correct the $z$ component of the magnetic field and the energy loss from material in the vicinity of each module. The correction parameters are derived from a sample of $J/\psi \to \mu\mu$ decays using the CVH fit, imposing the additional constraints that the muons are produced from a common vertex and that the muon pair has a mass consistent with that of the $J/\psi$ meson. These are needed to constrain weak modes in the alignment,

magnetic field, and energy loss parameters.

The correction procedure is effective in absorbing local biases in the magnetic field, energy loss, and alignment, but remains subject to weak modes, as well as to residual biases resulting from limitations in the Gaussian J/$\psi$ meson mass constraint. Convolution effects from the finite detector resolution and for final-state radiation are only accounted for in an approximate manner, and background contributions are not considered. To correct for these potential biases, residual corrections are derived from fits to the J/$\psi \to \mu\mu$ dimuon mass distribution, in two steps. In the first step, we extract correction factors finely binned in a four-dimensional space constructed from the $p_T^\mu$ and $\eta^\mu$ of the two muons. In these fits, the signal model is based on templates from simulation, convoluted with a Gaussian whose mean and standard deviation account for the residual scale and resolution difference, whereas the combinatorial background is represented by an exponential function. In the second step we extract calibration factors for each individual muon by minimizing a $\chi^2$ that translates the J/$\psi$ meson mass correction factors in all four-dimensional bins of $p_T^\mu$ and $\eta^\mu$ of the positively and negatively charged muons, to parameterize corrections for each muon as a function of $\eta^\mu$ and charge.

The residual corrections to the muon momenta are parameterized as a function of the curvature, $k \equiv 1/p_T$, as

$$\frac{\delta k}{k} = A_{i\eta} - \epsilon_{i\eta}\,k + q\,M_{i\eta}/k. \tag{2}$$

The $i\eta$ subscript indicates the corresponding $\eta$ bin of the correction parameters, which are independent for the 48 $\eta$ bins of width 0.1. The $A_{i\eta}$ term corresponds to a small adjustment of the magnetic field. The $\epsilon_{i\eta}$ term is the first one in a Taylor series expansion for the effect of mismodeling the energy loss between the interaction point and the first hit measurement. The $M_{i\eta}$ term expresses the bias in the track sagitta resulting from a misalignment of the tracker in the plane transverse to the magnetic field. The expression captures the leading behavior once local biases in the magnetic field, material, and alignment are corrected. In the presence of sufficiently large local biases, additional terms would appear with a more complicated functional form. Using MC simulation, we have validated that residual biases are well described by this functional form, after performing the track refit and applying the generalized global corrections. The corrections are then applied by shifting the reconstructed curvature of the measured muons.

To avoid extrapolating the muon momentum resolution corrections from the relatively low momentum values typical of muons from J/$\psi$ decays, we calibrate the muon momentum resolution using both J/$\psi \to \mu\mu$ and Z $\to \mu\mu$ events. The resolution corrections are derived from fits to the J/$\psi \to \mu\mu$ and Z $\to \mu\mu$ dimuon mass distributions, binned in the $p_T^\mu$ and $\eta^\mu$ of the positively and negatively charged muon as for the scale corrections, and after correcting the momentum scale using the calibration parameters previously extracted from the J/$\psi$ sample. The resolution is parameterized as a function of the curvature as

$$\frac{\sigma_k^2}{k^2} = a_{i\eta}^2 + \frac{c_{i\eta}^2}{k^2} + \frac{b_{i\eta}^2}{1 + d_{i\eta}^2 k^2}, \tag{3}$$

where the parameters $a_{i\eta}$, $c_{i\eta}$, $b_{i\eta}$, and $d_{i\eta}$ parameterize the contributions to the curvature resolution from multiple scattering, hit resolution, and the correlations between them induced by the track fit. These parameters are computed in 24 $\eta$ bins of width 0.2 for each of the four terms, separately for data and simulation, and are applied by smearing the reconstructed curvature of the simulated muons through a Gaussian distribution with the width corresponding to the difference in quadrature between data and simulation.
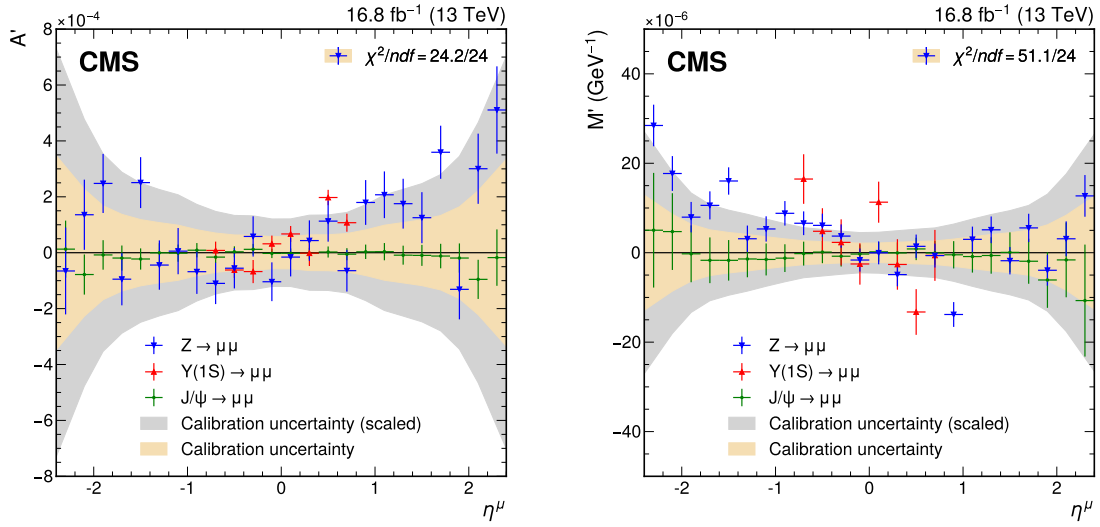
Figure A.4: Charge-independent ($A'$, left) and charge-dependent ($M'$, right) residual scale differences from using $J/\psi \to \mu\mu$, $\Upsilon(1S) \to \mu\mu$, and $Z \to \mu\mu$ events. The charge-independent comparison probes a magnetic-field-like difference, whereas the charge-dependent comparison reflects a misalignment-like term. The points with error bars represent the scale parameters and statistical uncertainties associated with the closure test performed with $J/\psi \to \mu\mu$ (green), $\Upsilon(1S) \to \mu\mu$ (red), and $Z \to \mu\mu$ (blue) events. The yellow band represents the corresponding statistical uncertainty in the calibration parameters derived from the $J/\psi$ calibration sample. The filled gray band shows this uncertainty scaled by a factor of 2.1, as described in the text. The $\chi^2$ values correspond to the compatibility of the scale parameters with zero for the closure test performed with $Z \to \mu\mu$ events and take into account the statistical uncertainties for these parameters, as well as for the calibration parameters derived from the $J/\psi$ sample, without additional scaling. The calibration parameter uncertainties are fully uncorrelated from the $Z$ and $\Upsilon(1S)$ closure test uncertainties, but very strongly correlated with the $J/\psi$ closure uncertainties, since they use the same data.

The calibration is validated using $J/\psi \to \mu\mu$, $\Upsilon(1S) \to \mu\mu$, and $Z \to \mu\mu$ events, by computing the residual muon momentum scale difference between the measured and simulated distributions, after applying all corrections, following the same two-step procedure used to derive the calibration factors. The residual scale differences between the event samples are obtained in 24 bins of $\eta^\mu$ following the parameterization of Eq. (2) with $\epsilon_{i\eta} = 0$. The resulting closure parameters, corresponding to a charge-independent magnetic-field-like residual ($A'$) and a charge-dependent alignment-like residual ($M'$), are shown in Fig. A.4. The $\chi^2$ compatibility test for the $J/\psi \to \mu\mu$ calibration applied to $Z \to \mu\mu$ events demonstrates that there is consistency within the statistical uncertainties for the charge-independent residuals. A small inconsistency for the charge-dependent residuals is seen, indicating a systematic uncertainty source. Given the momentum range relevant for $W \to \mu\nu$ events, the magnetic field and alignment effects are dominant with respect to those reflecting energy loss. The $\Upsilon(1S) \to \mu\mu$ events are only used to validate the calibration in the central region of the detector, where the dimuon mass resolution allows us to select a high purity sample of muons from the $\Upsilon(1S)$ meson decay. The small deviations from zero in the $J/\psi \to \mu\mu$ events are due to the larger $\eta^\mu$ bin sizes used for the validation step and from small $p_T^\mu$ bin migrations after applying the initial corrections in the $A'$ and $M'$ parameter extraction. The differences are small compared with the statistical uncertainty in the calibration procedure.

The uncertainties propagated to the analysis include the statistical uncertainties in the calibration parameters extracted from the J/$\psi$ sample, with statistical correlations taken into account, as well as the statistical uncertainties in the residual nonclosure between the J/$\psi$ and the Z samples and the systematic uncertainty associated with the reference measurement of the Z boson mass [5]. Although these uncertainties account for the limited size of the measured and simulated event samples in the J/$\psi$ calibration procedure and closure tests, as well as for the uncertainty in the world-average Z boson mass, other systematic effects might be present, related to weak modes with different sensitivity in J/$\psi \to \mu\mu$ and $\Upsilon(1S) \to \mu\mu$ events, trigger biases, or other sources. Remaining systematic effects that are not explicitly accounted for are assessed from the closure test between the J/$\psi$ calibration and the momentum scale from the Z sample. The statistical compatibility of this test is assessed for different $\eta^\mu$ binning choices and considering several possible correlated patterns of biases. To cover all possible biases with a reduced $\chi^2$ smaller than unity, the statistical uncertainty in the J/$\psi$ calibration parameters is scaled by a factor of 2.1, as shown in Fig. A.4.

For the momentum resolution, the relative agreement between the measured and simulated samples, especially in the tails of the momentum response distribution, is affected by a different pixel hits efficiency after the tighter quality requirements imposed in the CVH fit. To account for this, a systematic uncertainty is evaluated by reweighting the simulated pixel hit multiplicity distribution to match data differentially in $\eta^\mu$ and taking the full difference as an uncertainty. Since the nominal resolution corrections are also affected by this issue, we assign a systematic uncertainty to cover the residual disagreement. This uncertainty is expressed in terms of the statistical uncertainty of the resolution correction parameters, which are scaled by a factor of 10 to cover the observed differences. Because the statistical uncertainty in the resolution correction is small, and because the $m_\mathrm{W}$ measurement is not sensitive to small changes in the resolution, these scaled resolution uncertainties only contribute 1.4 MeV to the uncertainty in $m_\mathrm{W}$.

The uncertainties in $p_\mathrm{T}^\mu$ from the momentum scale and resolution calibrations are several orders of magnitude smaller than the $p_\mathrm{T}^\mu$ bin width of our likelihood function. If the uncertainty in the $(p_\mathrm{T}^\mu, \eta^\mu, q^\mu)$ distribution is evaluated directly from event-level variations of $p_\mathrm{T}^\mu$, significant fluctuations are introduced into the uncertainty templates due to the low probability of bin migration. To avoid introducing these statistical fluctuations into the nuisance parameters of the likelihood, the scale and resolution uncertainties are propagated as event weights that exploit the momentum response distributions in the simulation to estimate the relative contributions of an event across bins of the distribution. The resulting scale and resolution uncertainties have also been validated by applying the difference in scale between the J/$\psi \to \mu\mu$ and Z $\to \mu\mu$ events to the W boson simulation to build a biased prediction that is tested as pseudo-data in the fit. The resulting shift in $m_\mathrm{W}$ from this procedure is covered by the corresponding calibration uncertainties. The breakdown of muon momentum calibration uncertainties is shown in Table A.1. The total contribution of the muon momentum calibration to the $m_\mathrm{W}$ uncertainty is 4.8 MeV. Figure A.5 shows the Z $\to \mu\mu$ dimuon mass distributions after correcting the muon momentum scale by the calibration parameters extracted from fits to the J/$\psi$ events.

## A.6   Modeling of the W and Z boson transverse momentum distributions

To achieve the best accuracy in modeling the $p_\mathrm{T}^\mathrm{V}$ spectra, we correct the generator-level $p_\mathrm{T}^\mathrm{V}$ and $y^\mathrm{V}$ distributions in M$\textsc{i}$NNLO$_\textsc{ps}$ to state-of-the-art calculations in QCD, including the resummation of logarithmically-enhanced contributions at small $p_\mathrm{T}^\mathrm{V}$ and a model for nonperturbative effects also at small $p_\mathrm{T}^\mathrm{V}$. We use the SCET$\textsc{lib}$ code [22, 23, 38], which performs $p_\mathrm{T}^\mathrm{V}$ resummation

Table A.1: Breakdown of muon momentum calibration uncertainties.

| Source of uncertainty | Nuisance parameters | Uncertainty in $m_W$ (MeV) |
|---|---|---|
| J/$\psi$ calibration stat. (scaled $\times$2.1) | 144 | 3.7 |
| Z closure stat. | 48 | 1.0 |
| Z closure (LEP measurement) | 1 | 1.7 |
| Resolution stat. (scaled $\times$10) | 72 | 1.4 |
| Pixel multiplicity | 49 | 0.7 |
| Total | 314 | 4.8 |
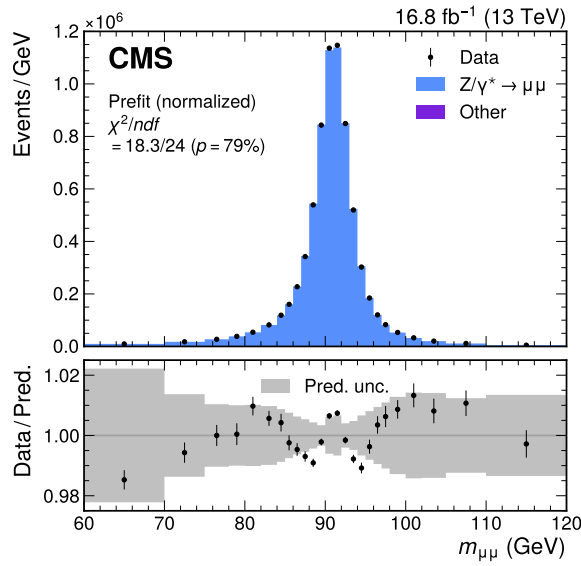


Figure A.5: Measured and simulated Z $\to \mu\mu$ dimuon mass distributions, after applying the muon momentum scale and resolution corrections. The simulated predictions and uncertainties are scaled to match the number of observed data events. The vertical bars represent the statistical uncertainties in the data. The bottom panel shows the ratio of the number of events observed in data and of variations in the predictions to that of the total nominal prediction.

as formulated using soft-collinear effective theory (SCET) [80–82], using deterministic numerical integration routines to provide predictions with high numerical accuracy. The resummed predictions from SCETLIB are matched to the fixed-order calculation from DYTURBO [43], at $O(\alpha_s^2)$ in the QCD coupling constant $\alpha_s$, to achieve N$^3$LL+NNLO accuracy. The correction is derived from the ratio of the SCETLIB+DYTURBO and MiNNLO$_{PS}$ predictions (after the parton shower but before final-state photon radiation) in the full phase space of the decay lepton kinematics. The corrections are binned in 1 GeV bins of $p_T^V$, up to 100 GeV, and 0.25 wide bins in the $|y^V| < 5.0$ range. They are applied to the MiNNLO$_{PS}$ simulation by sampling the binned corrections per event with the generator-level $|y^V|$ and $p_T^V$ to obtain event-level weights that are propagated through the full experimental analysis. This procedure allows us to maintain the statistical power of the MiNNLO$_{PS}$ MC sample while improving its accuracy at small $p_T^V$. After the correction, the dependence of the $p_T^V$ distribution on the parton shower and tune is negligible. We have compared the predictions using SCETLIB+DYTURBO with those using DYTURBO v1.4.0 [43, 83], MATRIX+RADISH v1.0.0 [42, 84], and CuTe-MCFM v10.2 [44, 85], at equivalent or higher perturbative order. After propagating those predictions through the analysis as binned corrections in $p_T^V$, we find that the expected shifts in $m_W$ are within the

SCETLIB+DYTURBO uncertainties.
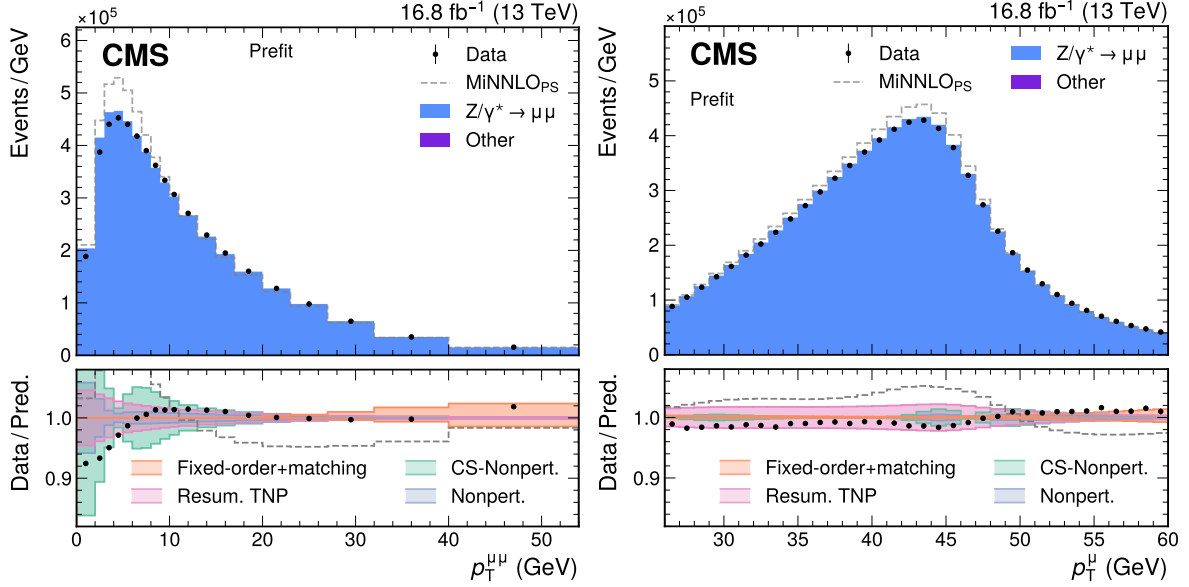


Figure A.6:  Measured and simulated $p_T^{\mu\mu}$ (left) and $p_T^{\mu}$ (right) distributions in selected $Z \to \mu\mu$ events.  The standalone uncorrected MINNLO$_{PS}$ predictions are shown by the dashed gray line.  The nominal predictions (blue) correct the POWHEG MINNLO$_{PS}$ $p_T^V$ with SCETLIB+DYTURBO at N$^3$LL+NNLO, as described in the text.  The vertical bars represent the statistical uncertainties in the data.  The bottom panel shows the ratio of the number of events observed in data to that of the total nominal prediction, as well as the relative impact of variations of the predictions.  Different sources of uncertainty are shown as solid bands in the lower panel: the fixed-order uncertainty and the uncertainty in the resummation and fixed-order matching (orange), resummed prediction using TNPs (pink), the Collins–Soper (CS) kernel nonperturbative uncertainty (green), and other nonperturbative uncertainties (light blue).  Additional sources of experimental and theoretical uncertainty that impact the agreement with the data are not shown.

As illustrated in Fig. A.6, the SCETLIB+DYTURBO correction substantially improves the description of $p_T^{\mu\mu}$ and $p_T^{\mu}$ data in selected $Z \to \mu\mu$ events when compared with the standalone MINNLO$_{PS}$ predictions. Uncertainties in the $p_T^W$ prediction, particularly those impacting the low-$p_T^W$ region, can shift the Jacobian peak of the $p_T^{\mu}$ distribution in a way similar to a variation of $m_W$. Therefore, the sensitivity of the analysis to $m_W$ critically relies on differentiating the uncertainty in $p_T^W$ and its impact on the $p_T^{\mu}$ distribution from $m_W$ variations. As can be appreciated from Fig. A.6, different sources of uncertainty contribute predominantly to different $p_T^V$ regions. The nonperturbative uncertainty is most pronounced at low $p_T^V$. Uncertainties in the resummation calculation and in the matching of the resummed and fixed-order calculations are relevant up to $p_T^V \approx 40\,\text{GeV}$. The nonperturbative and resummation uncertainties have the largest impact on the $p_T^{\mu}$ distribution around the Jacobian peak region that is sensitive to the $m_W$ value. Consequently, their contributions have an important impact on the measurement of $m_W$. The perturbative uncertainties in fixed-order QCD, which are dominant at high $p_T^V$, have a small impact on $p_T^{\mu}$ in the region sensitive to $m_W$. The uncertainties are estimated by varying the relevant parameters of the SCETLIB+DYTURBO calculation to obtain alternative predictions that are propagated through the full experimental analysis via event-level weights.

Perturbative uncertainties in the resummed predictions are evaluated using the TNP approach recently proposed in Ref. [24], which exploits the known all-order perturbative structure of the resummed calculation and is implemented in SCETLIB. In the SCET formalism used here, there are three perturbative ingredients in the $p_T^V$ resummation: the "hard function" that describes the hard virtual corrections for W and Z production, the "proton beam functions" that extend the PDFs to include collinear radiation, and the "soft function" describing soft radiation. All these functions share a system of renormalization group equations whose solution yields the all-order resummation of logarithms of $p_T^V/m_V$. In the TNP approach, the minimal independent set of ingredients that would be needed at the next perturbative order are identified and parameterized in terms of common nuisance parameters. Specifically, there are six sources of TNPs: the three fixed-order boundary conditions of each of the hard (H), soft (S), and beam (B) functions, and three anomalous dimensions governing their renormalization group evolution, namely the cusp anomalous dimension ($\Gamma_{cusp}$) and the virtuality and rapidity noncusp anomalous dimensions ($\gamma_\mu$ and $\gamma_\nu$). The TNPs of the hard and soft functions and the three anomalous dimensions are numerical constants. As such, they are propagated as scalar variations around their known values. The beam functions (BF) comprise five one-dimensional functions of the Bjorken-$x$ for the different partonic splitting channels. The qqV and qg BF contain the dominant quark to quark ($q \rightarrow q$) and gluon to quark ($g \rightarrow q$) channels, while the others ($q\bar{q}V$, qqS qq$\Delta$S) correspond to specific nondiagonal $q \rightarrow q'$ contributions that are present at higher orders [38]. We use their known functional shape and treat their normalization as a scalar TNP for each partonic channel. The TNPs have a true, but unknown, value that can be varied according to their expected typical magnitude. As a result, the TNP approach provides a robust prediction for the correlation of the uncertainties due to the missing higher orders across $p_T^V$, $y^V$, and $m_V$, which can be consistently used in the profile maximum likelihood fit used to extract $m_W$. Figure A.7 shows the impact of the ten TNPs, propagated through the analysis via the event-weighting procedure, on the $p_T^\mu$ spectrum in $W \rightarrow \mu\nu$ events.
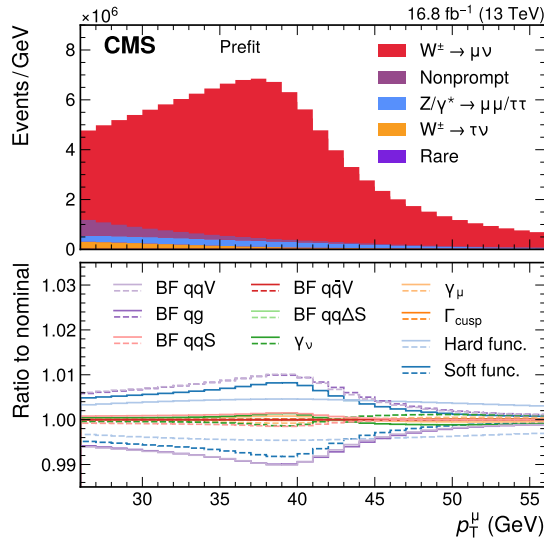


Figure A.7: The predicted $p_T^\mu$ distribution for selected $W \rightarrow \mu\nu$ events, before the maximum likelihood fit. The lower panel shows the ratio of the ten TNP variations described in the text to the nominal prediction, illustrating their impact on the spectrum.

The SCETLIB program implements different configurations for the TNPs, in terms of the logarithmic accuracy of the prediction and the perturbative order at which the TNPs are included. We use the $N^{3+0}LL$ scheme, where the prediction has $N^3LL$ accuracy and the TNPs represent-

ing the unknown higher-order corrections are estimated from multiplicative variations of the same $N^3LL$ terms. We also consider two alternate schemes, $N^{3+1}LL$ and $N^{4+0}LL$. The $N^{3+1}LL$ scheme implements the full $N^4LL$ perturbative structure, combining the known values for the parameters up to $N^3LL$ with best estimates of the higher-order terms and their variations to define the TNP variations. The $N^{4+0}LL$ scheme follows the same approach as the $N^{3+0}LL$, but is based on the $N^4LL$ calculation. We have verified that using the $N^{3+1}LL$ or the $N^{4+0}LL$ schemes has a negligible impact on the results with respect to the nominal $N^{3+0}LL$ scheme. As discussed in Sections A.9 and A.11, we validate the robustness of this approach against the measured $p_T^{\mu\mu}$ distribution and the W-like measurement of $m_Z$, where the impact of the $p_T^Z$ modeling uncertainty is treated in the same way.

The perturbative uncertainty in the fixed-order matching correction of the unpolarized calculation is assessed from 7-point variations of the factorization and renormalization scales, $\mu_R$ and $\mu_F$, in the DYTURBO calculation. The uncertainty is treated as a correlated nuisance parameter for the different W (and Z) boson decay channels, and between $W^+$ and $W^-$ boson production, but uncorrelated between W and Z boson production. An uncertainty due to the matching procedure is evaluated by varying the midpoint of the transition between the resummation and the fixed-order regime from the nominal value of $0.5\,m_V$ to $0.35\,m_V$ and $0.75\,m_V$.

Nonperturbative effects, such as the residual transverse motion of the partons inside the proton, impact the $p_T^V$ distribution. These effects are expected to scale as $(\Lambda_{QCD}/p_T^V)^2$ [86], where $\Lambda_{QCD} \approx 200\,\text{MeV}$ is the QCD vacuum expectation value. As such, their impact is dominant at low $p_T^V$ and less relevant for $p_T^V \gtrsim 10\,\text{GeV}$. The predictions considered here implement phenomenological models that require tuning to data to describe these nonperturbative effects. Two sources of nonperturbative effects impact $p_T^V$. First, there can be nonperturbative corrections to the CS rapidity anomalous dimension [86], which are universal for W and Z boson production. Second, there are nonperturbative contributions to the beam (and soft) functions, which account for the "intrinsic $k_T$" of the partons inside the protons, that are not universal as they can depend on the flavor and Bjorken-$x$ of the interacting parton. As shown in Ref. [87], the leading nonuniversal dependence can be captured by a single effective model function that only depends on the vector boson rapidity for each given vector boson type, besides the helicity cross section and the collision center-of-mass energy. The SCETLIB program implements a corresponding nonperturbative model for both these sources [23], where the model parameters effectively determine the first two powers in an expansion in $(\Lambda_{QCD}/p_T^V)^2$ together with a parameter that determines the overall asymptotic behavior for $p_T^V \to 0$. For the intrinsic $k_T$, the effective model amounts to a (rapidity-dependent) Gaussian smearing in the Fourier conjugate of $p_T^V$.

In our analysis, the parameters of the SCETLIB model are loosely constrained around nominal values that correspond to minimal nonperturbative smearing. The CS anomalous rapidity parameters are correlated between Z and W boson production, whereas the Gaussian smearing terms are uncorrelated between the two. Their best fit values are extracted from the maximum likelihood fits to the measured distributions. The values obtained from a direct maximum likelihood fit to the $p_T^{\mu\mu}$ distribution are consistent with those resulting from the W-like fit to the $p_T^\mu$ distribution in $Z \to \mu\mu$ events.

The SCETLIB+DYTURBO and MiNNLO$_{PS}$ calculations are performed in a fixed-flavor scheme with massless quarks. Calculations with b and c quark masses have not been performed at a comparable perturbative accuracy. The impact of quark masses is expected to be mostly at the scale of the b and c masses. Their impact is partially estimated by varying the heavy-quark

thresholds using charm and bottom quark mass variations of the MSHT20 PDF set [88]. In addition, the loose initial constraints of our nonperturbative uncertainty model provide flexibility to cover such sources of uncertainty at low $p_T^V$. Quark mass effects are expected to differ between W and Z production because of the different flavor contributions to their production. This difference is captured by the variations of the PDF threshold and by our independent treatment of nonperturbative uncertainties between Z and W production. The sufficiency of our model to capture these effects is confirmed by the likelihood fits to data discussed in Section A.9.

The total impact on $m_W$ from the perturbative, nonperturbative, and quark mass threshold uncertainties is 2.0 MeV, the three components yielding comparable contributions. A summary of nuisance parameters in the maximum likelihood fit that represent these uncertainties is given in Table A.5. Section A.9 further discusses the validation of the model and its uncertainty.

## A.7 Modeling of the angular distributions in W and Z boson leptonic decays

The differential cross section for the production and decay of the spin-1 W and Z bosons can be decomposed in terms of spherical harmonics into nine helicity-dependent states [26],

$$\frac{d\sigma}{dp_T^2 \, dm \, dy \, d\cos\theta^* \, d\phi^*} = \frac{3}{16\pi} \frac{d\sigma^{U+L}}{dp_T^2 \, dm \, dy} \left[ (1 + \cos^2\theta^*) + \sum_{i=0}^{7} A_i(p_T, m, y) P_i(\cos\theta^*, \phi^*) \right]. \quad (4)$$

We choose the CS reference frame [89], where $\cos\theta^*$ and $\phi^*$ correspond to the polar and azimuthal angles of the muon emitted in the W boson decay. The angular coefficients $A_i$ depend on the boson charge, rapidity $y^V$, $p_T^V$, and $m_V$. Combined with the unpolarized cross section $\sigma^{U+L}$, they describe the relationship between the boson production and the kinematic distributions of the decay muons. The $P_i$ spherical harmonics describe the kinematic distributions of the daughter muon, which depend on the properties of the W or Z boson.

The nominal predictions for the angular distributions, from MINNLO$_{PS}$, are NNLO accurate in QCD. Uncertainties in the predicted angular coefficients impact the $p_T^\mu$ and $\eta^\mu$ distributions by modifying the polarization of the W boson. Uncertainties in the angular coefficients are assessed by varying $\mu_R$ and $\mu_F$ in the MINNLO$_{PS}$ predictions. The correlations of higher-order corrections across phase space and processes are not well known. Therefore, we consider these variations uncorrelated among the $A_i$ coefficients and in ten $p_T^V$ bins, but correlated across $y^V$, and between $W^+$, $W^-$, and Z.

We have verified that the MINNLO$_{PS}$ predictions and uncertainties for the angular coefficients are consistent with NNLO fixed order calculations, and that the $A_i$ coefficients predicted at N$^3$LL, assessed with both SCETLIB and DYTURBO, are consistent with the MINNLO$_{PS}$ predictions within the assigned uncertainties. The isotropic smearing of the colliding partons due to the intrinsic $k_T$ model of PYTHIA induces a modest change to the angular coefficients, in particular $A_1$ and $A_3$ at low W or Z boson transverse momentum. The full difference between the angular coefficients before and after the PYTHIA 8 shower and intrinsic $k_T$ is taken as an additional systematic uncertainty, fully correlated across angular coefficients, phase space, and W and Z boson production. The total uncertainty in $m_W$ due to the uncertainty in the predicted angular coefficients is 3.2 MeV, with the largest contributions coming from $A_0$, $A_2$, and $A_4$.

## A.8 Parton distribution functions

Figure A.8 shows the $\eta^\mu$ distribution for $W^+$ and $W^-$ boson events, compared with the predictions obtained with the CT18Z PDF set and its uncertainties, as well as with the central

predictions for several other PDF sets. The consistency among the five PDF sets and the observed data is determined by performing likelihood fits to these distributions for each PDF set under consideration. Fits are performed including all the uncertainties of the nominal $m_W$ fit, as well as removing the PDF+$\alpha_s$ or the theory uncertainties. The impact of $\alpha_s$ is evaluated from alternative PDF fits with $\alpha_s$ shifted by $\pm0.015$ from its nominal value of 0.118. The change of $\alpha_s$ is propagated through the matrix element calculation in MiNNLO$_{PS}$ and the SCETlib+DYTurbo corrections. The corresponding saturated likelihood goodness-of-fit values are reported in Table A.2.
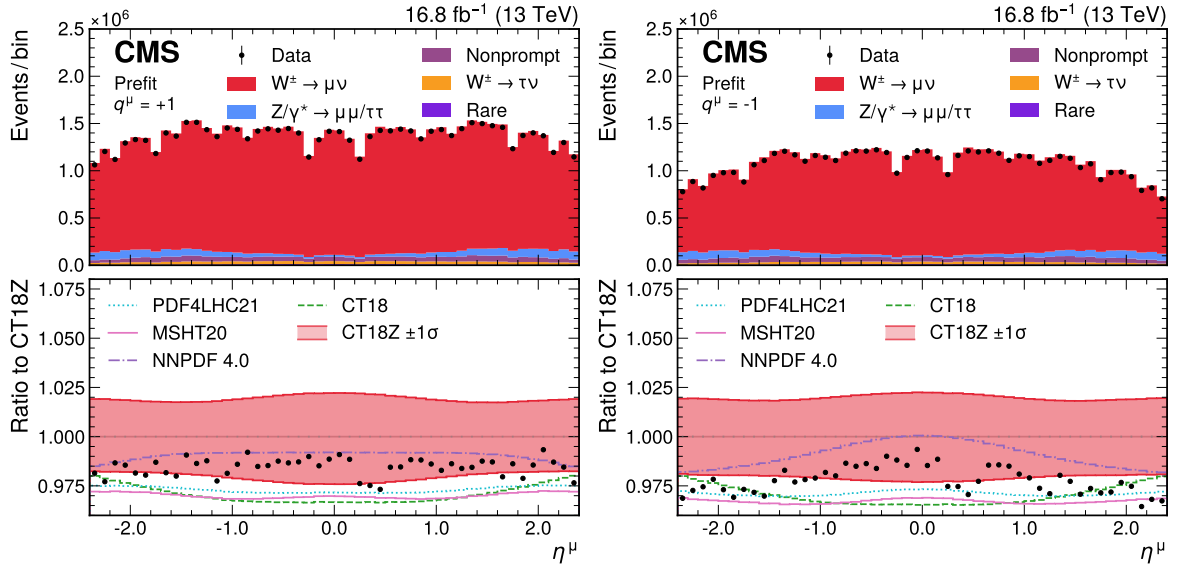


Figure A.8: Measured and predicted $\eta^\mu$ distributions for positively (left) and negatively (right) charged muons. The nominal prediction, obtained with the CT18Z PDF set, is shown in filled light red. The uncertainty, evaluated as the sum of the eigenvector variation sets, is represented by the filled band in the lower panel. The predictions using the PDF4LHC21, MSHT20, NNPDF4.0, and CT18 sets are also shown (without uncertainty bands). The vertical bars represent the statistical uncertainties in the data. The bottom panel shows the ratio of the number of events observed in data and of variations in the predictions to that of the nominal prediction.

To test the dependence of the result on the choice of PDF set, we performed the $m_W$ measurement with the NNPDF3.1 [63], NNPDF4.0 [64], CT18 [39], MSHT20 [65], and PDF4LHC21 [66] sets at NNLO, and the approximate N$^3$LO set MSHT20aN3LO [67]. To assess the consistency of the PDF sets we perform studies where the MC simulation for the W and Z boson production, and the corresponding PDF uncertainties, are obtained from a given PDF set while another PDF set provides pseudodata. We then evaluate if the $m_W$ value extracted from the fit lies within the uncertainty predicted by the PDF set under test. In the case of the CT18Z, CT18, and PDF4LHC PDF sets, their uncertainty covers the $m_W$ value extracted with all other PDF sets. This does not happen for the remaining PDF sets and, hence, we test the impact of increasing their PDF uncertainty by scaling all eigenvectors by a constant value until the difference in the extracted $m_W$ is within the postfit $\sigma_{PDF}$. The scale factors determined with this procedure are reported in Table A.3, which also shows that the total $m_W$ (unscaled) uncertainty due to the alternative PDF sets ranges from 2.4 to 4.6 MeV. Results for each PDF set, obtained with and without the scaling factors, are reported in Section 6. The scaling of the PDF uncertainty has only a moderate impact on the total $m_W$ uncertainty and leads to a better consistency between the measured $m_W$ values for different PDF sets. Given its agreement with data, relatively large uncertainty, and consistency with the other PDF sets, we select the CT18Z PDF set for the nominal prediction.

Table A.2: Goodness-of-fit test statistic for different PDF sets when fitting simultaneously the $\eta^\mu$ distributions for selected $W^+$ ($W^-$) events and the $y^{\mu\mu}$ distribution for $Z \to \mu\mu$ events. The saturated likelihood ratios, which are expected to follow a $\chi^2$ distribution with ndf degrees of freedom if the model is an accurate representation of the data, and the associated $p$-value are both shown. The fit is performed in the nominal configuration with all uncertainties (left column), nominal configuration without PDF and $\alpha_s$ uncertainties (middle column), and nominal configuration without theory uncertainties (right column).

| PDF set | Nominal fit | | Without PDF+$\alpha_s$ unc. | | Without theory unc. | |
|---|---|---|---|---|---|---|
| | $\chi^2$/ndf | $p$-val. (%) | $\chi^2$/ndf | $p$-val. (%) | $\chi^2$/ndf | $p$-val. (%) |
| CT18Z | 100.7/116 | 84 | 125.3/116 | 26 | 103.8/116 | 78 |
| CT18 | 100.7/116 | 84 | 153.2/116 | 1.0 | 105.7/116 | 74 |
| PDF4LHC21 | 97.7/116 | 89 | 105.5/116 | 75 | 104.1/116 | 78 |
| MSHT20 | 97.0/116 | 90 | 107.4/116 | 70 | 98.8/116 | 87 |
| MSHT20aN3LO | 99.0/116 | 87 | 122.8/116 | 31 | 101.9/116 | 82 |
| NNPDF3.1 | 99.1/116 | 87 | 105.5/116 | 75 | 115.0/116 | 51 |
| NNPDF4.0 | 99.7/116 | 86 | 104.3/116 | 77 | 116.7/116 | 46 |

The PDF uncertainty in $m_W$ from the CT18Z set is 4.4 MeV.

Table A.3: Prefit uncertainty scaling factors required to cover the central predictions of the considered PDF sets and postfit impact on $m_W$, with and without scaled PDF uncertainties.

| PDF set | Scale factor | Impact on $m_W$ (MeV) | |
|---|---|---|---|
| | | Original $\sigma_{\mathrm{PDF}}$ | Scaled $\sigma_{\mathrm{PDF}}$ |
| CT18Z | — | 4.4 | |
| CT18 | — | 4.6 | |
| PDF4LHC21 | — | 4.1 | |
| MSHT20 | 1.5 | 4.3 | 5.1 |
| MSHT20aN3LO | 1.5 | 4.2 | 4.9 |
| NNPDF3.1 | 3.0 | 3.2 | 5.3 |
| NNPDF4.0 | 5.0 | 2.4 | 6.0 |

## A.9 Impact of missing higher-order electroweak corrections

By interfacing MINNLO$_{\mathrm{PS}}$ with PHOTOS++, QED final-state radiation (FSR) is considered at leading logarithmic (LL) accuracy, including matrix-element corrections and the effect of lepton pair production. Uncertainties in the QED FSR modeling are evaluated by propagating the differences in the post-FSR dimuon mass and $p_T^\mu$ distributions, by switching off the PHOTOS++ matrix-element corrections and comparing to a prediction from HORACE v3.2 [90, 91], where the QED FSR is modeled at leading logarithmic (LL) accuracy in the collinear approximation. The impact on $m_W$ is smaller than 0.3 MeV.

The QED initial-state radiation (ISR) is modeled by the PYTHIA 8 parton shower at LL accuracy. The uncertainty is evaluated by comparing to a sample with ISR photon radiation switched off. The modifications on the $p_T^V$ and $y^V$ distributions are propagated through the analysis and found to have a negligible impact on $m_W$. Besides the photonic corrections, we consider the impact of EW virtual corrections.

For the neutral-current Drell–Yan process, the separation between weak and photonic corrections can be performed in a gauge-invariant way. The virtual EW corrections are calculated at NLO with the Z_ew process in the POWHEG-BOX-V2 (rev. 3900) program [92, 93] including

universal higher-order (HO) corrections. The ratios between the NLO+HO EW and LO EW predictions of the Z boson mass, and of the rapidity and $\cos\theta^*$ distributions, are used to define a systematic variation to the nominal MiNNLO$_{PS}$ prediction.

For W boson production, the splitting into virtual and photonic corrections is not gauge invariant and is, hence, ambiguous. Nonetheless, it is possible to separate the two contributions, to reproduce the QED FSR given by PHOTOS++. This separation is implemented in Rene-SANCe 1.3.11 [94], and the uncertainty in weak virtual corrections is defined as the ratios between the NLO+HO EW and LO EW predictions of the W boson mass, and of the rapidity and $\cos\theta^*$ distributions. We cross-checked that the full NLO EW corrections (QED plus weak) agree at the 0.3% level between the POWHEG-BOX-V2 [95] and the ReneSANCe programs, also confirming previous benchmarks [96]. The uncertainty from the virtual EW corrections has an impact on $m_W$ of 1.9 MeV.

In order to validate the uncertainties in our theoretical predictions and to quantify the sensitivity of our result to alternative $p_T^V$ modeling approaches, we performed several additional checks to demonstrate the stability of the results when modifying the treatment of theoretical predictions and their uncertainties in the analysis. To facilitate this, we correct our dimuon data sample for the effect of the detector response by "unfolding" the two-dimensional $(p_T^{\mu\mu}, y^{\mu\mu})$ distribution, extending the study reported in Ref. [62]. The $Z/\gamma^* \to \mu\mu$ production cross section is extracted inclusively in the kinematics of the decay muons, defined before final-state photon radiation, and for $60 < m_Z < 120$ GeV, $p_T^Z < 54$ GeV, and $|y^Z| < 2.5$. The unfolding is performed via a maximum likelihood fit to the two-dimensional distribution of $(p_T^{\mu\mu}, y^{\mu\mu})$ without regularization. The unfolded $p_T^Z$ and $|y^Z|$ distributions, shown in Fig. A.9, are obtained by integrating over the other dimension of the measured two-dimensional distribution.
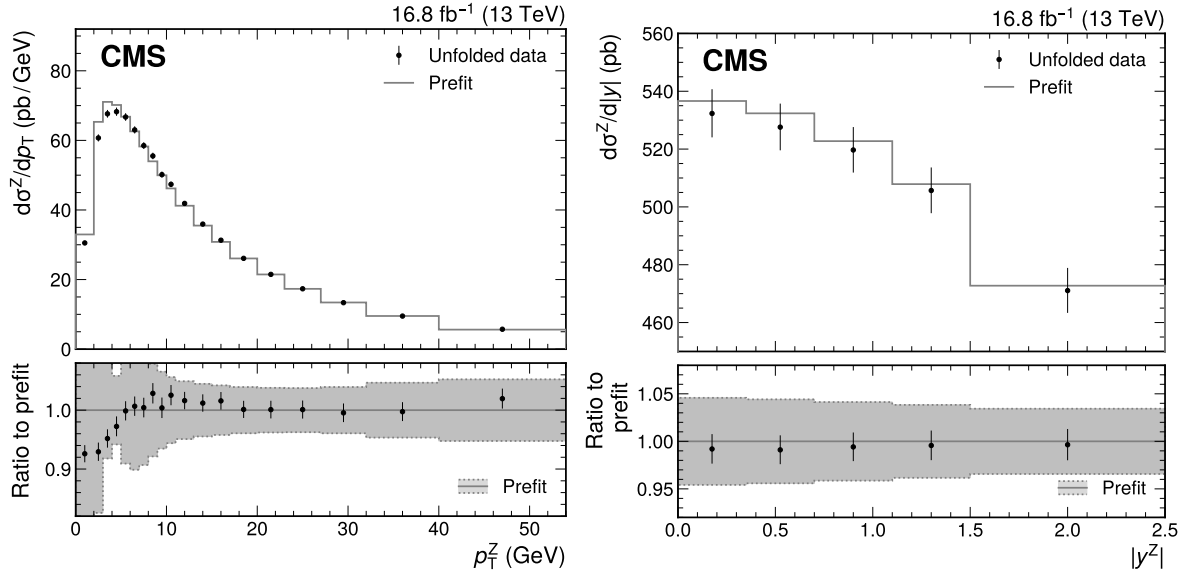


Figure A.9: Unfolded differential cross sections as functions of $p_T^Z$ (left) and $|y^Z|$ (right) compared with the prefit prediction from SCETLIB+DYTURBO. The results are obtained with the selection $|y^Z| < 2.5$ and $p_T^Z < 54$ GeV. The vertical bars represent the statistical uncertainties in the data. The bottom panel shows the ratio of the unfolded data to the SCETLIB+DYTURBO prediction.

Figure A.10 compares the $p_T^{\mu\mu}$ distribution measured in the full phase space of the decay leptons with the prediction of our nominal model of MiNNLO$_{PS}$ corrected to SCETLIB+DYTURBO at
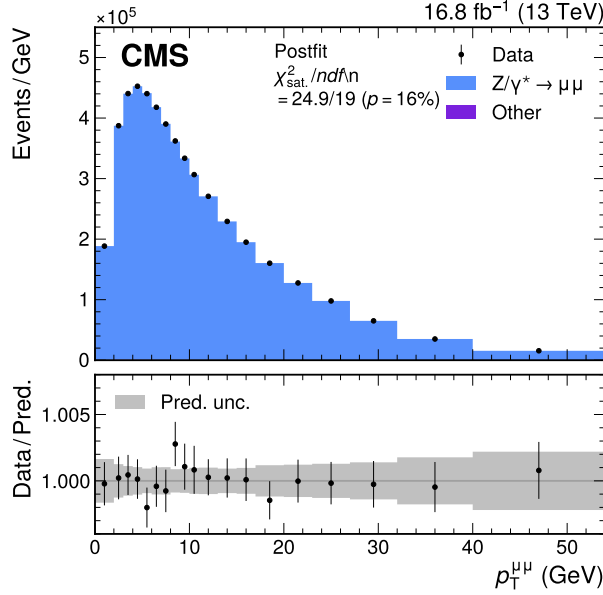
Figure A.10: Measured and simulated $p_T^{\mu\mu}$ distributions in selected $Z \to \mu\mu$ events, with the normalization and uncertainties of the prediction set to the postfit values. The gray band represents the total systematic uncertainty. The vertical bars represent the statistical uncertainties in the data. The bottom panel shows the ratio between the number of events observed in data, including variations in the predictions, and the nominal prediction.

$N^3LL+NNLO$, with $N^{3+0}LL$ TNPs. The predictions of SCETLIB+DYTURBO reflect the best fit values of the nuisance parameters obtained from the maximum likelihood fit. The ability of this model to describe the $p_T^{\mu\mu}$ distribution is a fundamental step towards using it in the W-like $m_Z$ and $m_W$ analyses. In particular, we find that the observed data have a 16% probability of being described as well as, or worse than, they are by the model, a level of agreement that validates the model and its uncertainties.

We have repeated the W-like $m_Z$ and $m_W$ measurements using predictions from SCETLIB at different orders of accuracy, matched to DYTURBO, as well as different approaches to incorporate the TNPs. When using $N^{3+1}LL$ and $N^{4+0}LL$ predictions and uncertainties, the measured value of $m_W$ is shifted by less than 0.5 MeV, to be compared with the 2.0 MeV of total $p_T^W$-modeling uncertainty of the nominal result. Although the approximate $N^4LL$ predictions [23] give slightly reduced $p_T^W$ uncertainties, the difference in the total uncertainty in $m_W$ is negligible when compared with the nominal result.

We have further assessed the impact of incorporating the $Z \to \mu\mu$ data in our model. For the W-like $m_Z$ measurement, the nominal prediction is corrected to the unfolded $p_T^Z$ distribution shown in Fig 2. The value of $m_Z$ extracted from this configuration differs by $-1.8$ MeV with respect to the nominal result, within the 1.8 MeV uncertainty due to the $p_T^Z$ modeling. The stability of these results, and their consistency with the independently measured value of $m_Z$, supports the use of the SCETLIB+DYTURBO prediction and its uncertainties.

We also test the impact of adjusting the $p_T^W$ distribution from the measured $p_T^Z$ distribution. For this comparison, we apply a correction to the $p_T^W$ distribution derived from the ratio of our $p_T^{\mu\mu}$ data to the $p_T^Z$ prediction from SCETLIB+DYTURBO. However, because of the differences between W and Z boson production, we do not consider this procedure to be an acceptable approach for the nominal result. The resulting shift in $m_W$ with respect to the nominal analysis

is smaller than $0.5\,\mathrm{MeV}$ and the change in the total uncertainty is negligible. This result is expected, given the excellent agreement found in the nominal analysis between the $p_\mathrm{T}^{\mu\mu}$ data and prediction, after the maximum likelihood fit.

Finally, we test a simultaneous fit to the $(p_\mathrm{T}^\mu, \eta^\mu, q^\mu)$ distribution in $W \to \mu\nu$ events and the $(p_\mathrm{T}^{\mu\mu}, y^{\mu\mu})$ distribution in $Z \to \mu\mu$ events. The TNPs are correlated across the W and Z boson processes, whereas uncertainties in the matching contributions and angular coefficients are left uncorrelated between the different processes. For the nonperturbative model, the Gaussian smearing parameters are considered independent for W and Z, whereas the CS anomalous rapidity is correlated. The $m_\mathrm{W}$ value extracted in this fit is shifted by $+0.6\,\mathrm{MeV}$ compared with the nominal result. The total uncertainty is moderately reduced because of additional constraints on theory and experimental uncertainties that are correlated across the W and Z processes. Figure A.11 presents a summary of these results, shown as a comparison to the nominal result and its uncertainty.
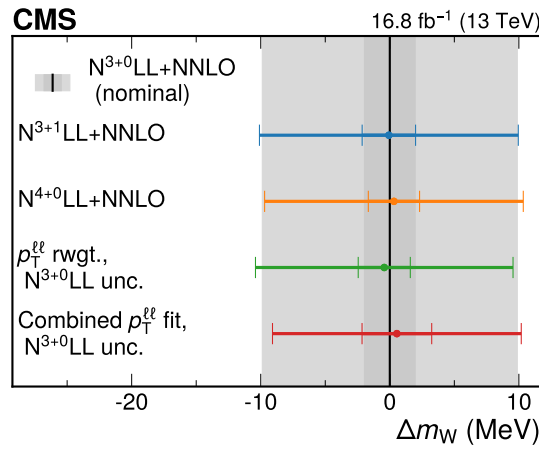


Figure A.11: Comparison of the nominal result and its theory uncertainty, using SCETLIB+DYTURBO at $N^3LL+NNLO$, with the difference in $m_\mathrm{W}$ measured when using alternative approaches to the $p_\mathrm{T}^W$ modeling and its uncertainty. The results from alternative approaches to the $p_\mathrm{T}^W$ modeling and uncertainty are shown as points. The solid black line represents the nominal result, the inner shaded gray band shows the $p_\mathrm{T}^W$ modeling uncertainty, and the outer shaded gray band shows the total uncertainty in the nominal result. The $p_\mathrm{T}^W$ modeling uncertainties are shown as the inner bars while the outer bars denote the total uncertainty.

The impact of including the $p_\mathrm{T}^{\mu\mu}$ data in the fit is illustrated in Fig. A.12, which compares the generator-level $p_\mathrm{T}^W$ spectrum modified by the best fit values of nuisance parameters for the two fits. The consistency of the two results supports the conclusion that the $p_\mathrm{T}^{\mu\mu}$ measurement is not required as an input to describe the $p_\mathrm{T}^W$ distribution, with the added benefit of a reduced model dependence of the result. In fact, the loose assumptions about the correlation of the nonperturbative parameters between W and Z boson production limit the impact of including the $p_\mathrm{T}^{\mu\mu}$ data.

## A.10   Helicity fit

While the theoretical model and uncertainties described in Section 5 reflect our best knowledge of QCD and of the proton structure, approximations of this model or the presence of new physics motivates the extraction of $m_\mathrm{W}$ using a parallel approach with a reduced model depen-
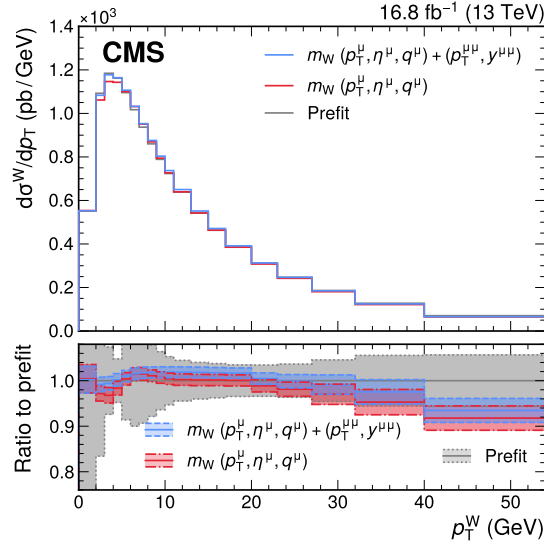
Figure A.12: The generator-level $p_T^W$ distribution, with three instances of the prediction and their uncertainty: before the maximum likelihood fit ("prefit"), and reflecting the results of the two fits described in the text. The distribution and uncertainties obtained from the combined $(p_T^\mu, \eta^\mu, q^\mu)$ and $(p_T^{\mu\mu}, y^{\mu\mu})$ fit is shown in red, whereas the purple band shows the distribution obtained from the nominal $(p_T^\mu, \eta^\mu, q^\mu)$ fit. The generator-level distribution predicted by SCETLIB+DYTURBO before incorporating in situ constraints is shown in gray. The ratio of the postfit predictions to the prefit prediction (in gray), as well as their uncertainties, are shown by the shaded bands in the lower panel.

dence, which we call "helicity fit". With this technique we extract, from a likelihood fit to the $(p_T^\mu, \eta^\mu, q^\mu)$ distribution, not only the mass of the W boson but also, simultaneously, its polarization and the $p_T^W$ and $y^W$ spectra. At the core of this alternative analysis is the observation that $m_W$ variations induce a uniform scaling of the $p_T^\mu$ spectrum, whereas changes in the W boson polarization or in the $(p_T^W, y^W)$ double-differential cross sections lead to a nonuniform sculpting of the $p_T^\mu$ and $\eta^\mu$ spectra. We implement variations in the W boson polarization and in the $(p_T^W, y^W)$ distribution as a set of independent nuisance parameters in the signal likelihood function that is used to fit the measured $(p_T^\mu, \eta^\mu, q^\mu)$ distribution. The W boson polarization enters into our analysis procedure through the helicity decomposition of Eq. (4). We use helicity cross sections, $\sigma_i$, which correspond to the product of the angular coefficients $A_i$ and the unpolarized cross section, and we neglect the terms with $i > 4$, predicted to be zero in first approximation and having no effect on our measurement (given that we integrate over the $\phi^*$ angle in Eq. (4)).

For each muon charge, the analysis covers the $p_T^V$ vs. $y^V$ plane with nuisance parameters that represent variations of the production cross section, separately for 7 bins in $y^V$ (within $|y^V| < 3$) times 8 bins in $p_T^V$ (for $p_T^V < 60$ GeV), plus 16 overflow bins. The five $\sigma_i$ helicity cross sections (with $i = 0$–4) plus the unpolarized cross section ($\sigma^{U+L}$) are defined for each of those 144 bins, leading to a total of 864 nuisance parameters. We propagate variations in the helicity amplitudes, which depend on the unobserved $p_T^W$ and $y^W$, into a multitude of $(p_T^\mu, \eta^\mu, q^\mu)$ distributions, obtained by reweighting the simulated events. For each individual variation, the sum of all contributions is recomputed to get a new prediction for the $(p_T^\mu, \eta^\mu, q^\mu)$ distribution. The nuisance parameters are constrained around the theoretical predictions with uncertainties that are relaxed with respect to their theoretical values, used for the nominal result. The $\sigma^{U+L}$

and $\sigma_4$ parameters have very loose initial constraints, of $\pm 50\%$ and $\pm 100\%$ of the predicted cross sections, respectively. The initial uncertainties in the four other helicity terms, for which the fit has limited constraining power, are defined by the spread of theory predictions (reflecting missing higher orders) and by uncertainties covering several different PDF sets. To ensure coverage of all possible correlated variations allowed by the theory model used in the baseline analysis, in addition to the explicit helicity cross section variations we also retain the PDF and missing higher-order uncertainties, as well as the primordial-$k_T$ smearing and nonperturbative uncertainties in the angular coefficients. The latter two are also retained in the unpolarized term, given that their impact on the cross section at low $p_T^V$ is significant within the finite-width bins of the helicity cross section variations. In contrast, we do not consider uncertainties in the unpolarized cross section from resummation, matching, and missing higher orders because they are largely redundant with respect to the explicit $\sigma^{U+L}$ variations. This approach results in a significant reduction in model-dependent assumptions with respect to the nominal analysis.

We validate the helicity fit approach by measuring a negligible $m_W$ bias in pseudo-data samples generated with different PDF sets and $p_T^W$ or $y^W$ spectra, and by measuring the Z boson mass in the W-like configuration. The expected $m_W$ uncertainty is evaluated for different prefit constraints on the helicity nuisance parameters. We observe only a mild dependence of the $m_W$ uncertainty on all helicity terms, except for $\sigma_3$, whose variations have a similar impact on $p_T^\mu$ as those resulting from $m_W$ variations. Therefore, in the $m_W$ extractions made to verify the stability of the measurement, we scale the prefit uncertainties of $\sigma_3$ and of all the other $\sigma_i$ terms by two independent factors.
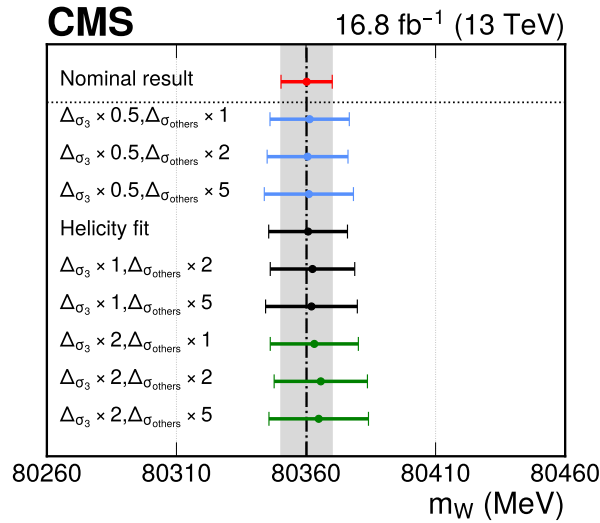


Figure A.13: The W boson mass measured with the helicity fit for different scaling scenarios of the prefit helicity cross section uncertainties, denoted by $\Delta_{\sigma_3}$ and $\Delta_{\sigma_{others}}$ for the $\sigma_3$ and the other components, respectively. The points are grouped and colored according to the scaling of $\sigma_3$. The black line indicates the nominal result, with its uncertainties shown in the gray band.

Figure A.13 shows the $m_W$ values measured with the helicity fit for different scenarios of the prefit helicity cross section uncertainties. We halved or doubled the default $\sigma_3$ prefit uncertainty, to study possible shifts of the central value under more aggressive or conservative theoretical assumptions. For each of those scenarios, we inflated the other helicity cross section uncertainties by factors of 2 or 5 (in addition to the nominal uncertainty). All eight extra cases give central $m_W$ values that are stable and consistent with both the baseline and helicity fit nominal results. Figure A.14 shows the W boson differential cross sections in $p_T^W$ and $|y^W|$, extracted

from the $(p_T^\mu, \eta^\mu, q^\mu)$ distributions through the decomposition of the helicity amplitudes in $p_T^W$ and $y^W$ bins.
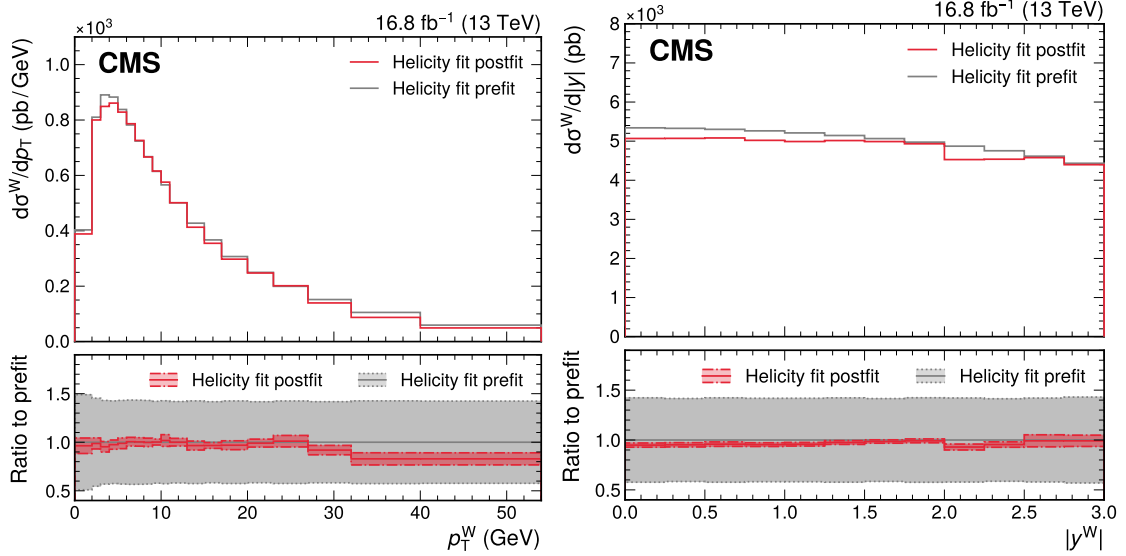


Figure A.14: Differential W boson production cross section, in the $W \to \mu\nu$ decay channel, in $p_T^W$ (left) and $|y^W|$ (right), measured from the $(p_T^\mu, \eta^\mu, q^\mu)$ distributions using the helicity fit approach (red). The SCETLIB+DYTURBO generator-level predictions, before incorporating in situ constraints, are also shown (in gray). The results are shown for the selection $|y^W| < 3.0$ and $p_T^W < 54 \, \text{GeV}$. The lower panel shows the ratio between the postfit and prefit spectra.

## A.11 Details regarding the W-like Z and W boson mass measurements

Figures A.15 and A.16 show the $(p_T^\mu, \eta^\mu)$ distributions, used in the binned maximum likelihood template fits to perform the W-like $m_Z$ and $m_W$ measurements, respectively. The $\eta^\mu$ binning allows sensitivity to discontinuities in the geometry of the detectors and maximally exploits in situ constraints of systematic uncertainties. The $p_T^\mu$ binning roughly corresponds to the $p_T^\mu$ resolution, useful to enhance the sensitivity to the measured mass, while avoiding fluctuations in the simulated templates that could potentially lead to undercoverage of the estimated uncertainties [48]. The predicted and observed $p_T^\mu$ distribution of the W-like analysis, with the prediction corrected by the best fit values of the nuisance parameters after the maximum likelihood fit to the $(p_T^\mu, \eta^\mu, q^\mu)$ distribution, is shown in Fig. A.17. The impact of a variation of $m_Z$ corresponding to the total uncertainty of the measurement is also shown, as well as the uncertainties in the prediction, illustrating the precision of the measurement.

The dominant uncertainties in $m_W$ are the $p_T^\mu$ scale and the PDFs. The individual systematic uncertainties in the W-like $m_Z$ and $m_W$ measurements are presented in Table A.4. The uncertainty breakdown labeled as "Nominal impact" is computed according to the procedure described in Ref. [25], where the data statistical uncertainty corresponds to a hypothetical analysis with no systematic uncertainties. The impact for all other sources of uncertainty corresponds to the amount by which the total uncertainty would decrease in quadrature if that source were removed from the analysis. The total uncertainty cannot be calculated as the sum in quadrature of the impacts because of correlations between the partial uncertainties.

This uncertainty breakdown is not directly comparable to that of ATLAS [10], which uses an alternative method to define the uncertainty contributions, referred to as "global" impacts [97]. In that approach, the data statistical uncertainty is, instead, computed with the nuisance pa-
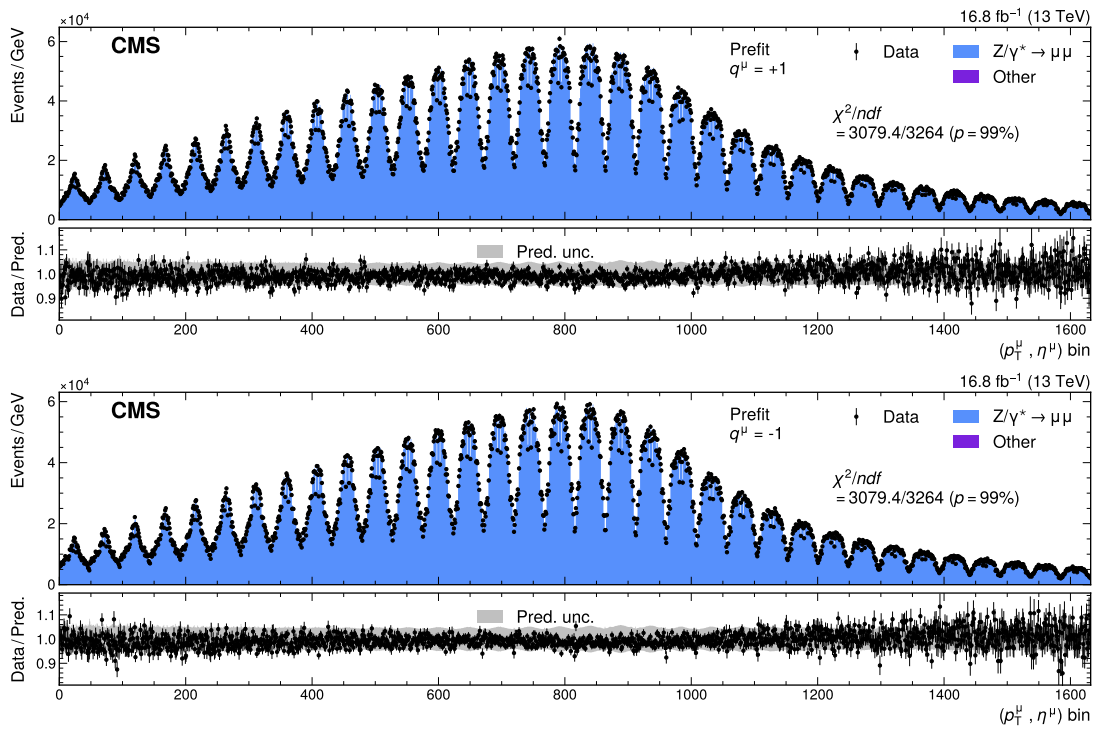
Figure A.15: Measured and predicted $(p_T^\mu, \eta^\mu)$ distributions used in the W-like $m_Z$ measurement, for positively (upper) and negatively (lower) charged muons. The two-dimensional distribution is "unrolled" such that each bin on the $x$-axis represents one $(p_T^\mu, \eta^\mu)$ cell. The gray band represents the uncertainty in the prediction, before the fit to the data. The bottom panel shows the ratio of the number of events observed in data to the nominal prediction. The vertical bars represent the statistical uncertainties in the data.
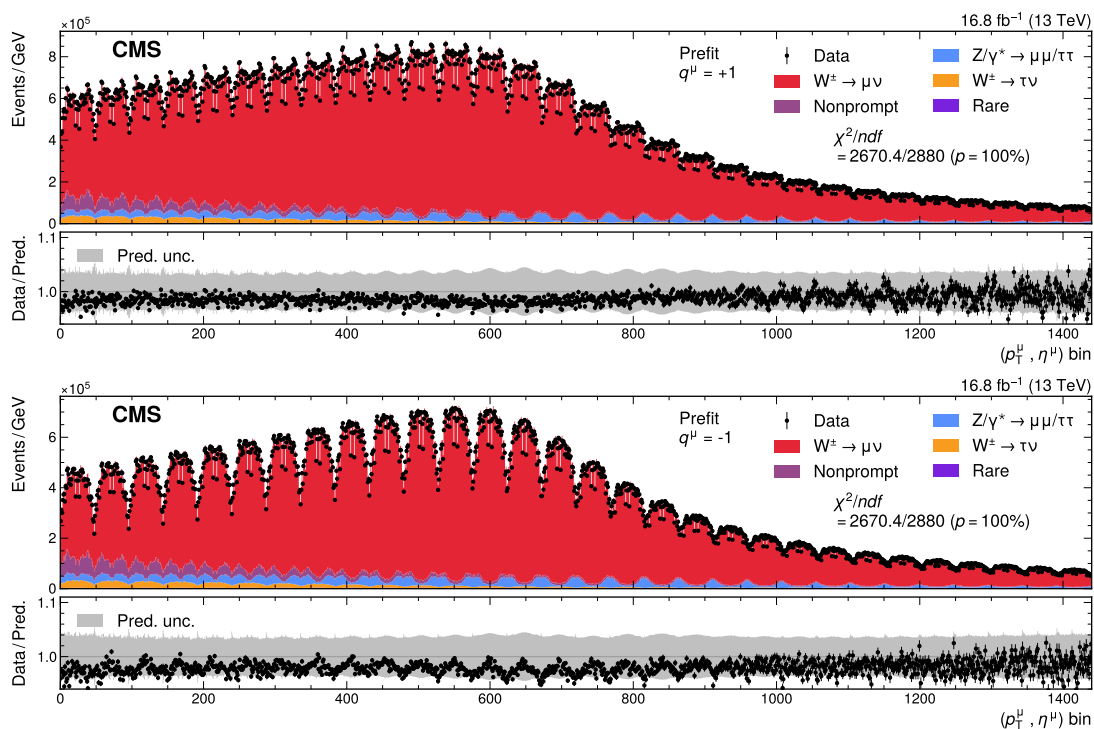
Figure A.16: Measured and predicted $(p_T^\mu, \eta^\mu)$ distributions used in the $m_W$ measurement, for positively (upper) and negatively (lower) charged muons. The two-dimensional distribution is "unrolled" such that each bin on the $x$-axis represents one $(p_T^\mu, \eta^\mu)$ cell. The gray band represents the uncertainty in the prediction, before the fit to the data. The bottom panel shows the ratio of the number of events observed in data to the nominal prediction. The vertical bars represent the statistical uncertainties in the data.
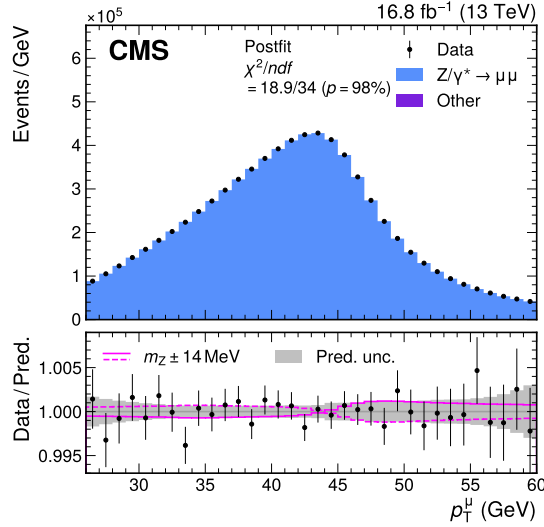
Figure A.17: Measured and simulated $p_T^\mu$ distributions, with the prediction adjusted according to the best fit values of nuisance parameters and of $m_Z$ obtained from the maximum likelihood fit of the W-like $m_Z$ analysis. The vertical bars represent the statistical uncertainties in the data. The bottom panel shows the ratio of the number of events observed in data to the nominal prediction. The solid and dashed purple lines represent, respectively, the relative impact of an increase and decrease of $m_Z$ by 14 MeV. The uncertainties in the predictions, after the systematic uncertainty profiling in the maximum likelihood fit, are shown by the shaded band.

Table A.4: Uncertainties in the W-like $m_Z$ and $m_W$ measurements, with contributions to the total uncertainty from individual sources separated according to the "nominal" [25] and "global" [97] definitions of the impacts.

| Source of uncertainty | Impact (MeV) | | | |
| | Nominal | | Global | |
| | in $m_Z$ | in $m_W$ | in $m_Z$ | in $m_W$ |
|---|---|---|---|---|
| Muon momentum scale | 5.6 | 4.8 | 5.3 | 4.4 |
| Muon reco. efficiency | 3.8 | 3.0 | 3.0 | 2.3 |
| W and Z angular coeffs. | 4.9 | 3.3 | 4.5 | 3.0 |
| Higher-order EW | 2.2 | 2.0 | 2.2 | 1.9 |
| $p_T^V$ modeling | 1.7 | 2.0 | 1.0 | 0.8 |
| PDF | 2.4 | 4.4 | 1.9 | 2.8 |
| Nonprompt-muon background | — | 3.2 | — | 1.7 |
| Integrated luminosity | 0.3 | 0.1 | 0.2 | 0.1 |
| MC sample size | 2.5 | 1.5 | 3.6 | 3.8 |
| Data sample size | 6.9 | 2.4 | 10.1 | 6.0 |
| Total uncertainty | 13.5 | 9.9 | 13.5 | 9.9 |

rameters present in the fit. If the data constrain the nuisance parameters in situ, beyond the externally imposed constraints, then fluctuations in the data and the simulated event samples become correlated with the fitted values of the nuisance parameters, which in turn increases the statistical components of the uncertainty. The impacts of systematic sources are computed considering fluctuations of the corresponding external measurements (i.e., of the so-called "global observables") within their uncertainties. In the presence of stronger in situ constraints, this method typically leads to smaller impacts than our approach. These two procedures only differ in the split between the statistical and systematic components of the uncertainty; they do

not impact the total uncertainty of the result. To facilitate the comparison with the uncertainty breakdown of the ATLAS measurement, Table A.4 also reports the leading uncertainties using global impacts.

Table A.5: Number of nuisance parameters for the main groups of systematic uncertainties, for the W-like $m_Z$ and $m_W$ fits. The number of parameters is displayed only once when it is the same for both fits, while "—" means that this source is not relevant. For completeness, subgroups of parameters are also reported as indented labels for a few groups.

| Systematic uncertainties | W-like $m_Z$ | $m_W$ |
|---|---|---|
| Muon efficiency | 3127 | 3658 |
|    Muon eff. veto | — | 531 |
|    Muon eff. syst. | 343 | |
|    Muon eff. stat. | 2784 | |
| Nonprompt-muon background | — | 387 |
| Prompt-muon background | 2 | 3 |
| Muon momentum scale | 314 | |
| L1 prefiring | 14 | |
| Integrated luminosity | 1 | |
| PDF (CT18Z) | 60 | |
| Angular coefficients | 177 | 353 |
|    W MiNNLO$_{PS}$ $\mu_F$, $\mu_R$ | — | 176 |
|    Z MiNNLO$_{PS}$ $\mu_F$, $\mu_R$ | 176 | |
|    Pythia shower $k_T$ | 1 | |
| $p_T^V$ modeling | 22 | 32 |
|    Nonperturbative | 4 | 10 |
|    Perturbative | 4 | 8 |
|    Theory nuisance parameters | 10 | |
|    c, b quark mass | 4 | |
| Higher-order EW | 6 | 7 |
| Z boson width | 1 | |
| Z boson mass | — | 1 |
| W boson width | — | 1 |
| $\sin^2 \theta_W$ | 1 | |
| Total | 3725 | 4833 |

Table A.5 shows a summary of the number of nuisance parameters included in the likelihood for the W-like $m_Z$ and $m_W$ fits. The parameters are categorized into groups, corresponding to the main sources of uncertainty reported in Table A.4, and gathering conceptually related systematic uncertainties. Uncertainties specific to W bosons, for instance the mass or width variations, are not implemented in the W-like $m_Z$ analysis because the W + jets background is negligible.

## A.12  Measurement of $m_{W+} - m_{W-}$

Our measurement assumes that the W$^+$ and W$^-$ bosons have identical masses, $m_{W+} = m_{W-}$, as required by CPT symmetry. This requirement reduces the impact of uncertainties that affect the two charges differently, including the PDFs, angular coefficients, and the alignment terms of the muon momentum calibration. By relaxing this requirement, we perform a measurement of the mass difference,

$$m_{W+} - m_{W-} = 57.0 \pm 30.3 \, \text{MeV}.$$

The significant increase in the uncertainty compared with the $m_W$ measurement is due to uncertainties that have a strong negative correlation between the two charges. In particular, the muon momentum calibration contributes an uncertainty of 22.0 MeV, the angular coefficients contribute 18.7 MeV, and the PDF uncertainty is 11.8 MeV. The statistical uncertainty of the data is 4.7 MeV. The $p$-value indicating the compatibility of this result and the expectation of $m_{W+} - m_{W-} = 0$ is 6.0%, or about 1.9 standard deviations. The correlation coefficient between $m_{W+}$ and $m_{W-}$ is $-0.40$, whereas the correlation between the mass difference and mass average is only 0.02. The small correlation between $m_W$ and $m_{W+} - m_{W-}$ is a consequence of a strong degree of anticorrelation for the alignment components of the $p_T^\mu$ calibration uncertainties, and the uncertainties in the $A_3$ angular coefficient.

As a validation of this result, we also perform the corresponding measurement in the case of the W-like $m_Z$ measurement using the positively and negatively charged muons. In this case, the two leptons are from the same object and, therefore, the comparison is purely a validation of the theoretical and experimental inputs. The result when selecting positively charged muons in odd event-number events is

$$m_{Z+} - m_{Z-} = 30.9 \pm 32.5 \, \text{MeV},$$

and for the reversed muon charge *vs.* event number selection we get

$$m_{Z+} - m_{Z-} = 6.4 \pm 32.3 \, \text{MeV}.$$

Apart from the PDFs, which are not relevant for this measurement, the breakdown of uncertainties is similar to the $m_{W+} - m_{W-}$ case. The muon momentum scale and the angular coefficients contribute uncertainties of 23.1 and 14.5 MeV, respectively. The statistical uncertainty of the data is 13.9 MeV.

Table A.6 shows the impacts on the difference between the measured mass with positive or negative muons in the W-like $m_Z$ and $m_W$ analyses, comparing with the nominal result from the simultaneous fit to both charges, and using nominal impacts. The breakdown of uncertainties from the global definition of the impacts is also reported, for completeness.

We have performed several additional checks that confirm that the small tension with the expectation of $m_{W+} = m_{W-}$ does not reflect a bias or an underestimation of our uncertainties that would impact our result. The alignment components of the muon momentum scale calibration and the $A_3$ angular coefficient uncertainties are the dominant sources affecting the $m_{W+} - m_{W-}$ measurement. Therefore, we repeat both measurements after varying the central value of these parameters by one standard deviation ($\sigma$) such that the charge difference is reduced, keeping their relative uncertainty fixed. Up variations of the $p_T^\mu$ scale alignment terms, and down variations of the $A_3$ coefficient uncertainties, each reduce $m_{W+} - m_{W-}$. The maximum shift in $m_{W+} - m_{W-}$ when varying these two terms, either independently or coherently, moves the result towards zero by $1.2\sigma$, compared with the $m_{W+} - m_{W-}$ measurement with the nominal uncertainty model. In the extreme configuration where the alignment term is varied by $3\sigma$, resulting in $m_{W+} - m_{W-} \approx 0$, the extracted $m_W$ differs from our nominal result by 0.6 MeV.

## A.13   Results with alternative parton distribution functions

We performed the $m_W$ measurement using alternative PDF sets, with and without scaling factors, following the procedure described in Section A.8. The results are shown in Table A.7 and Fig. A.18.

The scaling procedure, combined with the uncertainty profiling and in situ data constraints, improves the consistency between the $m_W$ results obtained with the different PDF sets. If no

Table A.6: Uncertainties in the W-like $m_Z$ and $m_W$ measurements, comparing the mass difference between charges and the nominal charge combination, using nominal (upper) and global (lower) impacts.

| Source of uncertainty | Nominal impact (MeV) | | | |
|---|---|---|---|---|
| | in $m_{Z^+} - m_{Z^-}$ | in $m_Z$ | in $m_{W^+} - m_{W^-}$ | in $m_W$ |
| Muon momentum scale | 23.1 | 5.6 | 21.6 | 4.8 |
| Muon reco. efficiency | 7.1 | 3.8 | 7.2 | 3.0 |
| W and Z angular coeffs. | 14.5 | 4.9 | 18.7 | 3.3 |
| Higher-order EW | 0.2 | 2.2 | 1.5 | 2.0 |
| $p_T^V$ modeling | 0.6 | 1.7 | 7.4 | 2.0 |
| PDF | 0.9 | 2.4 | 11.8 | 4.4 |
| Nonprompt-muon background | — | — | 7.5 | 3.2 |
| Integrated luminosity | <0.1 | 0.3 | 0.1 | 0.1 |
| MC sample size | 4.9 | 2.5 | 3.0 | 1.5 |
| Data sample size | 13.9 | 6.9 | 4.7 | 2.4 |
| Total uncertainty | 32.5 | 13.5 | 30.3 | 9.9 |

| Source of uncertainty | Global impact (MeV) | | | |
|---|---|---|---|---|
| | in $m_{Z^+} - m_{Z^-}$ | in $m_Z$ | in $m_{W^+} - m_{W^-}$ | in $m_W$ |
| Muon momentum scale | 21.2 | 5.3 | 20.0 | 4.4 |
| Muon reco. efficiency | 6.5 | 3.0 | 5.8 | 2.3 |
| W and Z angular coeffs. | 13.9 | 4.5 | 13.7 | 3.0 |
| Higher-order EW | 0.2 | 2.2 | 1.5 | 1.9 |
| $p_T^V$ modeling | 0.4 | 1.0 | 2.7 | 0.8 |
| PDF | 0.7 | 1.9 | 4.2 | 2.8 |
| Nonprompt-muon background | — | — | 4.8 | 1.7 |
| Integrated luminosity | <0.1 | 0.2 | 0.1 | 0.1 |
| MC sample size | 6.4 | 3.6 | 8.4 | 3.8 |
| Data sample size | 18.1 | 10.1 | 13.4 | 6.0 |
| Total uncertainty | 32.5 | 13.5 | 30.3 | 9.9 |

Table A.7: The $m_W$ values measured for different PDF sets, with uncertainties scaled following the procedure described in Section A.8 and with the default unscaled uncertainties.

| PDF set | Extracted $m_W$ (MeV) | |
|---|---|---|
| | Original $\sigma_{PDF}$ | Scaled $\sigma_{PDF}$ |
| CT18Z | 80 360.2 ± 9.9 | |
| CT18 | 80 361.8 ± 10.0 | |
| PDF4LHC21 | 80 363.2 ± 9.9 | |
| MSHT20 | 80 361.4 ± 10.0 | 80 361.7 ± 10.4 |
| MSHT20aN3LO | 80 359.9 ± 9.9 | 80 359.8 ± 10.3 |
| NNPDF3.1 | 80 359.3 ± 9.5 | 80 361.3 ± 10.4 |
| NNPDF4.0 | 80 355.1 ± 9.3 | 80 357.0 ± 10.8 |
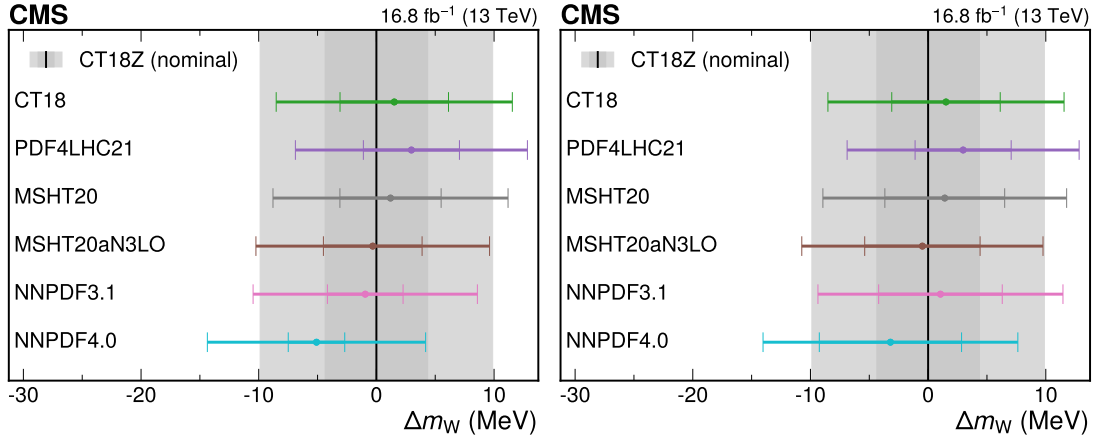
Figure A.18: Difference in $m_W$ values for six alternative recent PDF sets, when using the original uncertainty for the given set (left) and when the uncertainties are scaled to accommodate the central prediction of the other sets (right). Each point corresponds to the result obtained when using the indicated PDF set and its uncertainty for the simulated predictions. The inner bar shows the uncertainty from the PDF, and the outer bar shows the total uncertainty. The nominal result, using CT18Z, is shown by the black line, with the CT18Z PDF and total uncertainty shown in dark and light gray, respectively. The uncertainty scaling procedure described in Section A.8 improves the consistency of the $m_W$ values across the PDF sets and with the nominal result.

uncertainty scaling is used, the results vary by 8.1 MeV, from $80\,355.1 \pm 9.3$ MeV (NNPDF4.0) to $80\,363.2 \pm 9.9$ MeV (PDF4LHC21). If we use the uncertainty scaling, the spread of results is reduced to 6.2 MeV, ranging from $80\,357.0 \pm 10.8$ MeV (NNPDF4.0 with uncertainties scaled by 5.0) to $80\,363.2 \pm 9.9$ MeV (PDF4LHC21 with no scaling factor). The spread of these values is within the total PDF uncertainty of our nominal measurement (performed with CT18Z).

## A.14   Additional validation checks of experimental inputs

A number of additional tests were performed to ensure that the analysis is robust with respect to variations in the selections used.

The $m_Z$ extraction from $Z \to \mu\mu$ events is performed in subsets of events defined by the relative location of the two muons in the CMS detector. Figure A.19 shows that the nominal $m_Z$ result is compatible with the results obtained when both muons are central ($|\eta^\mu| < 0.9$), one is central and one is forward, or both are forward. The same exercise is performed depending on $\eta^\mu$, by requiring both muons on the $\eta^\mu < 0$ half of the detector, both on the positive half, and one in each half of the detector, with the same conclusions.

Concerning the W-like $m_Z$ and $m_W$ analyses, the $m_V$ extraction is performed in 24 bins of $\eta^\mu$. The results are shown in Fig. A.20, where the compatibility with the nominal result can also be appreciated.

Other tests that were performed and also showed no incompatibility with the corresponding nominal result include:

1. Performing the W-like $m_Z$ and $m_W$ analyses splitting events by the sign of $\eta^\mu$, for each half of the CMS detector separately.

2. Performing the $m_W$ analysis reducing the $p_T^\mu$ range considered by removing 4 GeV on the high end, on the low end, and on both ends.
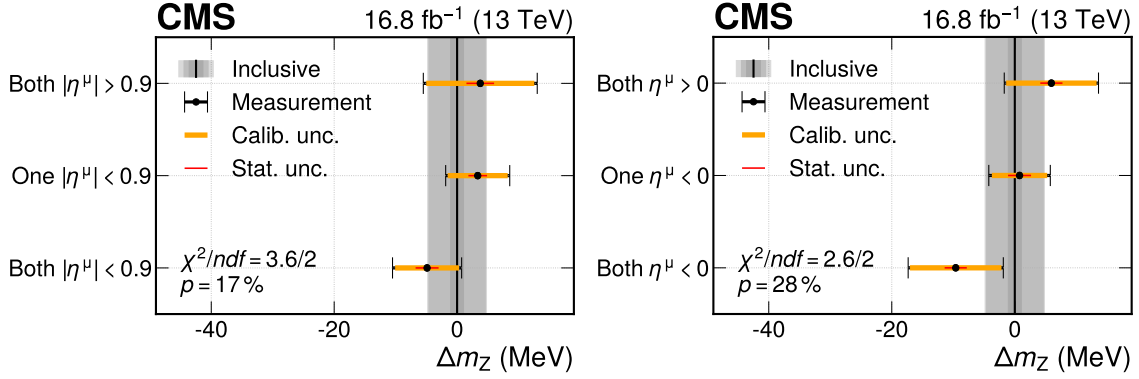
Figure A.19: The difference between the nominal $m_Z$ value measured from the $Z \to \mu\mu$ events and the result where $m_Z$ is allowed to vary, in three regions of the $\eta^\mu$ of the two muons. The results binned in $|\eta^\mu|$ (both central, one central and one forward, and both forward) are shown on the left and results binned in $\eta^\mu$ (both negative, one positive and one negative, and both positive) are shown on the right. The result of a fit with three $m_Z$ parameters is compared with the result with a single $m_Z$ parameter and the compatibility of the results is also shown, as assessed via the saturated goodness-of-fit test. The points show the $m_Z$ result for the indicated $\eta^\mu$ region and the horizontal bars represent the calibration (orange line), statistical (red line), and total (black line) uncertainties. The black vertical line represents the result with a single $m_Z$ parameter, with the three shaded gray bands representing the statistical (dark grey), calibration (intermediate grey), and total (light grey) uncertainties.
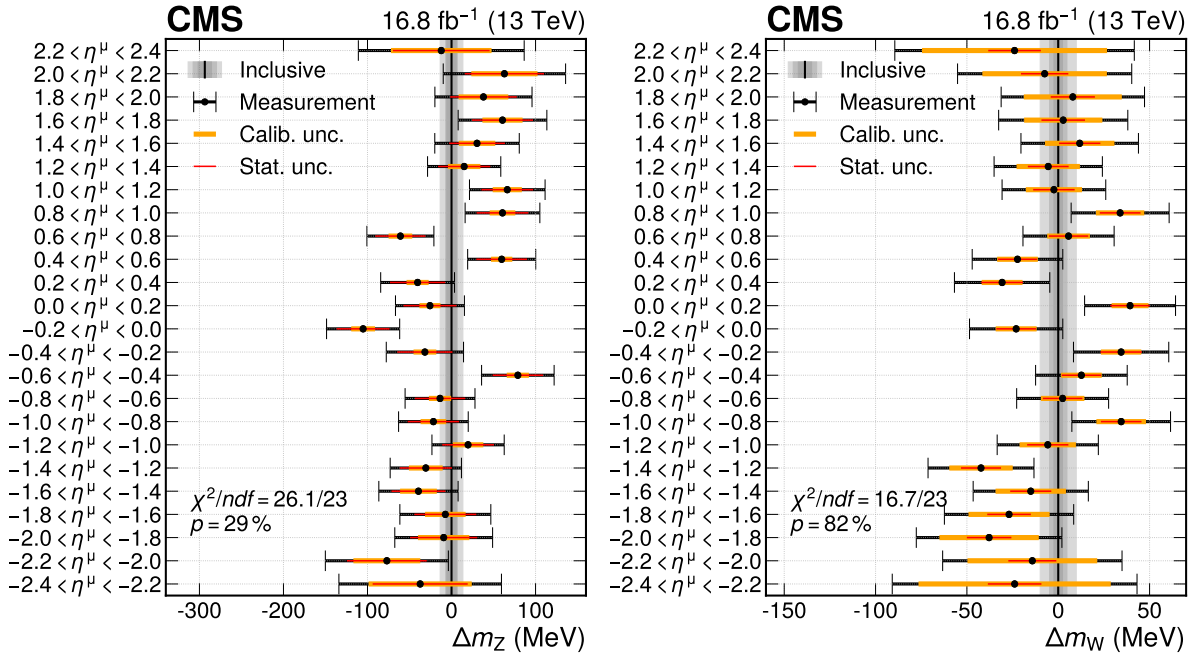


Figure A.20: For the W-like $m_Z$ analysis (left) and the $m_W$ measurement (right) the result of a fit with 24 $m_V$ parameters corresponding to different $\eta^\mu$ ranges is compared with the nominal $m_V$ fit result. The $\chi^2$-like compatibility of the two fits is also shown, assessed via the saturated goodness-of-fit test. The points show $m_V$ result for the indicated $\eta^\mu$ region, and the horizontal bars represent the calibration (orange line), statistical (red line), and total (black line) uncertainties. The black vertical line shows the result with a single $m_V$ parameter, with the shaded gray bands representing its statistical, calibration, and total uncertainties.

3. Performing the $m_W$ analysis treating the normalization of the W signal process unconstrained. A scaling factor of $0.979 \pm 0.026$ is obtained, in agreement with the SM expectation of unity.

Tabulated results are provided in the HEPData record for this work [98].

## Data availability

Release and preservation of data used by the CMS Collaboration as the basis for publications is guided by the CMS data preservation, re-use and open access policy.

## Code availability

The CMS core software is publicly available in our GitHub repository.

## References

[1] UA1 Collaboration, "Experimental observation of isolated large transverse energy electrons with associated missing energy at $\sqrt{s} = 540$ GeV", *Phys. Lett. B* **122** (1983) 103, `doi:10.1016/0370-2693(83)91177-2`.

[2] UA2 Collaboration, "Observation of single isolated electrons of high transverse momentum in events with missing transverse energy at the $\overline{p}p$ collider", *Phys. Lett. B* **122** (1983) 476, `doi:10.1016/0370-2693(83)91605-2`.

[3] S. Heinemeyer, W. Hollik, G. Weiglein, and L. Zeune, "Implications of LHC search results on the W boson mass prediction in the MSSM", *JHEP* **12** (2013) 084, `doi:10.1007/JHEP12(2013)084`, `arXiv:1311.1663`.

[4] D. López-Val and T. Robens, "$\Delta r$ and the W-boson mass in the singlet extension of the standard model", *Phys. Rev. D* **90** (2014) 114018, `doi:10.1103/PhysRevD.90.114018`, `arXiv:1406.1043`.

[5] Particle Data Group, S. Navas et al., "Review of particle physics", *Phys. Rev. D* **110** (2024) 030001, `doi:10.1103/PhysRevD.110.030001`.

[6] ALEPH, DELPHI, L3, OPAL, SLD, LEP Electroweak Working Group, SLD Electroweak Group, SLD Heavy Flavour Group Collaboration, "Precision electroweak measurements on the Z resonance", *Phys. Rept.* **427** (2006) 257, `doi:10.1016/j.physrep.2005.12.006`, `arXiv:hep-ex/0509008`.

[7] D0 Collaboration, "Measurement of the W boson mass with the D0 detector", *Phys. Rev. D* **89** (2014) 012005, `doi:10.1103/PhysRevD.89.012005`, `arXiv:1310.8628`.

[8] ATLAS Collaboration, "Measurement of the W-boson mass in pp collisions at $\sqrt{s} = 7$ TeV with the ATLAS detector", *Eur. Phys. J. C* **78** (2018) 110, `doi:10.1140/epjc/s10052-017-5475-4`, `arXiv:1701.07240`. [Erratum: `doi:10.1140/epjc/s10052-018-6354-3`].

[9] LHCb Collaboration, "Measurement of the W boson mass", *JHEP* **01** (2022) 036, `doi:10.1007/JHEP01(2022)036`, `arXiv:2109.01113`.

[10] ATLAS Collaboration, "Measurement of the W-boson mass and width with the ATLAS detector using proton-proton collisions at $\sqrt{s} = 7$ TeV", 2024. `arXiv:2403.15085`. Submitted to Eur. Phys. J. C.

[11] CDF Collaboration, "High-precision measurement of the W boson mass with the CDF II detector", *Science* **376** (2022) 170, `doi:10.1126/science.abk1781`.

[12] LHC-TeV MW Working Group, S. Amoroso et al., "Compatibility and combination of world W-boson mass measurements", *Eur. Phys. J. C* **84** (2024) 451, `doi:10.1140/epjc/s10052-024-12532-z`, `arXiv:2308.09417`.

[13] CMS Collaboration, "The CMS experiment at the CERN LHC", *JINST* **3** (2008) S08004, `doi:10.1088/1748-0221/3/08/S08004`.

[14] CMS Collaboration, "Performance of the CMS Level-1 trigger in proton-proton collisions at $\sqrt{s} = 13\,\text{TeV}$", *JINST* **15** (2020) P10017, `doi:10.1088/1748-0221/15/10/P10017`, `arXiv:2006.10165`.

[15] CMS Collaboration, "Performance of the CMS high-level trigger during LHC Run 2", *JINST* **19** (2024) P11021, `doi:10.1088/1748-0221/19/11/P11021`, `arXiv:2410.17038`.

[16] CMS Collaboration, "The CMS trigger system", *JINST* **12** (2017) P01020, `doi:10.1088/1748-0221/12/01/P01020`, `arXiv:1609.02366`.

[17] CMS Collaboration, "Electron and photon reconstruction and identification with the CMS experiment at the CERN LHC", *JINST* **16** (2021) P05014, `doi:10.1088/1748-0221/16/05/P05014`, `arXiv:2012.06888`.

[18] CMS Collaboration, "Performance of the CMS muon detector and muon reconstruction with proton-proton collisions at $\sqrt{s} = 13\,\text{TeV}$", *JINST* **13** (2018) P06015, `doi:10.1088/1748-0221/13/06/P06015`, `arXiv:1804.04528`.

[19] CMS Collaboration, "Description and performance of track and primary-vertex reconstruction with the CMS tracker", *JINST* **9** (2014) P10009, `doi:10.1088/1748-0221/9/10/P10009`, `arXiv:1405.6569`.

[20] CMS Collaboration, "Particle-flow reconstruction and global event description with the CMS detector", *JINST* **12** (2017) P10003, `doi:10.1088/1748-0221/12/10/P10003`, `arXiv:1706.04965`.

[21] E. Manca, O. Cerri, N. Foppiani, and G. Rolandi, "About the rapidity and helicity distributions of the W bosons produced at LHC", *JHEP* **12** (2017) 130, `doi:10.1007/JHEP12(2017)130`, `arXiv:1707.09344`.

[22] M. A. Ebert, J. K. L. Michel, I. W. Stewart, and F. J. Tackmann, "Drell–Yan $q_\text{T}$ resummation of fiducial power corrections at N³LL", *JHEP* **04** (2021) 102, `doi:10.1007/JHEP04(2021)102`, `arXiv:2006.11382`.

[23] G. Billis, J. K. L. Michel, and F. J. Tackmann, "Drell–Yan transverse-momentum spectra at N³LL′ and approximate N⁴LL with SCETlib", 2024. `arXiv:2411.16004`.

[24] F. J. Tackmann, "Beyond scale variations: perturbative theory uncertainties from nuisance parameters", 2024. `arXiv:2411.18606`.

[25] CMS Collaboration, "Measurements of the W boson rapidity, helicity, double-differential cross sections, and charge asymmetry in pp collisions at 13 TeV", *Phys. Rev. D* **102** (2020) 092012, `doi:10.1103/PhysRevD.102.092012`, `arXiv:2008.04174`.

[26] E. Mirkes, "Angular decay distribution of leptons from W bosons at NLO in hadronic collisions", *Nucl. Phys. B* **387** (1992) 3, `doi:10.1016/0550-3213(92)90046-E`.

[27] D. Y. Bardin, A. Leike, T. Riemann, and M. Sachwitz, "Energy dependent width effects in $e^+e^-$ annihilation near the Z boson pole", *Phys. Lett. B* **206** (1988) 539, `doi:10.1016/0370-2693(88)91627-9`.

[28] J. R. Klein and A. Roodman, "Blind analysis in nuclear and particle physics", *Ann. Rev. Nucl. Part. Sci.* **55** (2005) 141, `doi:10.1146/annurev.nucl.55.090704.151521`.

[29] CMS Collaboration, "Precision luminosity measurement in proton-proton collisions at $\sqrt{s} = 13$ TeV in 2015 and 2016 at CMS", *Eur. Phys. J. C* **81** (2021) 800, `doi:10.1140/epjc/s10052-021-09538-2`, `arXiv:2104.01927`.

[30] CMS Collaboration, "Strategies and performance of the CMS silicon tracker alignment during LHC Run 2", *Nucl. Instrum. Meth. A* **1037** (2022) 166795, `doi:10.1016/j.nima.2022.166795`, `arXiv:2111.08757`.

[31] Y. Feng, "A new deep-neural-network-based missing transverse momentum estimator, and its application to W recoil". PhD thesis, University of Maryland, College Park, 2020. `doi:10.13016/e6ze-zycc`.

[32] CMS Collaboration, "Performance of missing transverse momentum reconstruction in proton-proton collisions at $\sqrt{s} = 13$ TeV using the CMS detector", *JINST* **14** (2019) P07004, `doi:10.1088/1748-0221/14/07/P07004`, `arXiv:1903.06078`.

[33] P. F. Monni et al., "MiNNLO$_{PS}$: a new method to match NNLO QCD to parton showers", *JHEP* **05** (2020) 143, `doi:10.1007/JHEP05(2020)143`, `arXiv:1908.06987`. [Erratum: `doi:10.1007/JHEP02(2022)031`].

[34] P. F. Monni, E. Re, and M. Wiesemann, "MiNNLO$_{PS}$: optimizing $2 \rightarrow 1$ hadronic processes", *Eur. Phys. J. C* **80** (2020) 1075, `doi:10.1140/epjc/s10052-020-08658-5`, `arXiv:2006.04133`.

[35] T. Sjöstrand et al., "An introduction to PYTHIA 8.2", *Comput. Phys. Commun.* **191** (2015) 159, `doi:10.1016/j.cpc.2015.01.024`, `arXiv:1410.3012`.

[36] P. Golonka and Z. Wąs, "PHOTOS Monte Carlo: a precision tool for QED corrections in Z and W decays", *Eur. Phys. J. C* **45** (2006) 97, `doi:10.1140/epjc/s2005-02396-4`, `arXiv:hep-ph/0506026`.

[37] N. Davidson, T. Przedzinski, and Z. Wąs, "PHOTOS interface in C++: Technical and physics documentation", *Comput. Phys. Commun.* **199** (2016) 86, `doi:10.1016/j.cpc.2015.09.013`, `arXiv:1011.0937`.

[38] G. Billis, M. A. Ebert, J. K. L. Michel, and F. J. Tackmann, "A toolbox for $q_T$ and 0-jettiness subtractions at N$^3$LO", *Eur. Phys. J. Plus* **136** (2021) 214, `doi:10.1140/epjp/s13360-021-01155-y`, `arXiv:1909.00811`.

[39] T.-J. Hou et al., "New CTEQ global analysis of quantum chromodynamics with high-precision data from the LHC", *Phys. Rev. D* **103** (2021) 014013, `doi:10.1103/PhysRevD.103.014013`, `arXiv:1912.10053`.

[40] GEANT4 Collaboration, "GEANT4—a simulation toolkit", *Nucl. Instrum. Meth. A* **506** (2003) 250, `doi:10.1016/S0168-9002(03)01368-8`.

[41] S. Choi and H. Oh, "Improved extrapolation methods of data-driven background estimations in high energy physics", *Eur. Phys. J. C* **81** (2021) 643, `doi:10.1140/epjc/s10052-021-09404-1`, `arXiv:1906.10831`.

[42] W. Bizon et al., "The transverse momentum spectrum of weak gauge bosons at N$^3$LL+NNLO", *Eur. Phys. J. C* **79** (2019) 868, `doi:10.1140/epjc/s10052-019-7324-0`, `arXiv:1905.05171`.

[43] S. Camarda et al., "DYTurbo: Fast predictions for Drell–Yan processes", *Eur. Phys. J. C* **80** (2020) 251, `doi:10.1140/epjc/s10052-020-7757-5`, `arXiv:1910.07049`. [Erratum: `doi:10.1140/epjc/s10052-020-7972-0`].

[44] J. Campbell and T. Neumann, "Precision phenomenology with MCFM", *JHEP* **12** (2019) 034, `doi:10.1007/JHEP12(2019)034`, `arXiv:1909.09117`.

[45] J. Butterworth et al., "PDF4LHC recommendations for LHC Run II", *J. Phys. G* **43** (2016) 023001, `doi:10.1088/0954-3899/43/2/023001`, `arXiv:1510.03865`.

[46] J. S. Conway, "Incorporating nuisance parameters in likelihoods for multisource spectra", in *PHYSTAT 2011: Workshop on statistical issues related to discovery claims in search experiments and unfolding*, H. B. Prosper and L. Lyons, eds., CERN Yellow Reports: Conf. Proc., p. 115. CERN, Geneva, 2011. `arXiv:1103.0354`. `doi:10.5170/CERN-2011-006.115`.

[47] R. J. Barlow and C. Beeston, "Fitting using finite Monte Carlo samples", *Comput. Phys. Commun.* **77** (1993) 219, `doi:10.1016/0010-4655(93)90005-W`.

[48] C.-A. Alexe, J. L. Bendavid, L. Bianchini, and D. Bruschini, "Undercoverage in high-statistics counting experiments with finite MC samples", 2024. `arXiv:2401.10542`.

[49] B. Efron, "Bootstrap methods: another look at the jackknife", in *Breakthroughs in statistics: methodology and distribution*, S. Kotz and N. L. Johnson, eds., p. 569. Springer New York, New York, NY, 1992. `doi:10.1007/978-1-4612-4380-9_41`.

[50] Particle Data Group, P. A. Zyla et al., "Review of particle physics", *Prog. Theor. Exp. Phys.* **2020** (2020) 083C01, `doi:10.1093/ptep/ptaa104`.

[51] M. Abadi et al., "TensorFlow: Large-scale machine learning on heterogeneous distributed systems", 2016. `arXiv:1603.04467`. Software available from tensorflow.org.

[52] A. G. Baydin, B. A. Pearlmutter, A. A. Radul, and J. M. Siskind, "Automatic differentiation in machine learning: a survey", *Journal of Machine Learning Research* **18** (2018) 1, `arXiv:1502.05767`.

[53] J. K. Lindsey, "Parametric Statistical Inference". Oxford University Press, 1996. `doi:10.1093/oso/9780198523598.001.0001`, ISBN 9780198523598.

[54] ALEPH, DELPHI, L3, OPAL, LEP Electroweak Working Group, S. Schael et al., "Electroweak measurements in electron-positron collisions at W-boson-pair energies at LEP", *Phys. Rept.* **532** (2013) 119, `doi:10.1016/j.physrep.2013.07.004`, `arXiv:1302.3415`.

[55] D0 Collaboration, "Measurement of the W boson mass with the D0 detector", *Phys. Rev. Lett.* **108** (2012) 151804, `doi:10.1103/PhysRevLett.108.151804`, `arXiv:1203.0293`.

[56] CMS Collaboration, "Measurement of the top quark mass using a profile likelihood approach with the lepton+jets final states in proton-proton collisions at $\sqrt{s} = 13\,\text{TeV}$", *Eur. Phys. J. C* **83** (2023) 963, `doi:10.1140/epjc/s10052-023-12050-4`, `arXiv:2302.01967`.

[57] CMS Collaboration, "Measurement of the Drell–Yan forward-backward asymmetry and of the effective leptonic weak mixing angle in proton-proton collisions at $\sqrt{s} = 13\,\text{TeV}$", 2024. `arXiv:2408.07622`. Submitted to Physics Letters B.

[58] P. Nason, "A new method for combining NLO QCD with shower Monte Carlo algorithms", *JHEP* **11** (2004) 040, `doi:10.1088/1126-6708/2004/11/040`, `arXiv:hep-ph/0409146`.

[59] S. Frixione, P. Nason, and C. Oleari, "Matching NLO QCD computations with parton shower simulations: the POWHEG method", *JHEP* **11** (2007) 070, `doi:10.1088/1126-6708/2007/11/070`, `arXiv:0709.2092`.

[60] S. Alioli, P. Nason, C. Oleari, and E. Re, "A general framework for implementing NLO calculations in shower Monte Carlo programs: the POWHEG BOX", *JHEP* **06** (2010) 043, `doi:10.1007/JHEP06(2010)043`, `arXiv:1002.2581`.

[61] CMS Collaboration, "Extraction and validation of a new set of CMS PYTHIA 8 tunes from underlying-event measurements", *Eur. Phys. J. C* **80** (2020) 4, `doi:10.1140/epjc/s10052-019-7499-4`, `arXiv:1903.12179`.

[62] CMS Collaboration, "Measurements of differential Z boson production cross sections in proton-proton collisions at $\sqrt{s} = 13\,\text{TeV}$", *JHEP* **12** (2019) 061, `doi:10.1007/JHEP12(2019)061`, `arXiv:1909.04133`.

[63] NNPDF Collaboration, "Parton distributions from high-precision collider data", *Eur. Phys. J. C* **77** (2017) 663, `doi:10.1140/epjc/s10052-017-5199-5`, `arXiv:1706.00428`.

[64] NNPDF Collaboration, "The path to proton structure at 1% accuracy", *Eur. Phys. J. C* **82** (2022) 428, `doi:10.1140/epjc/s10052-022-10328-7`, `arXiv:2109.02653`.

[65] S. Bailey et al., "Parton distributions from LHC, HERA, Tevatron and fixed target data: MSHT20 PDFs", *Eur. Phys. J. C* **81** (2021) 341, `doi:10.1140/epjc/s10052-021-09057-0`, `arXiv:2012.04684`.

[66] PDF4LHC Working Group Collaboration, "The PDF4LHC21 combination of global PDF fits for the LHC Run III", *J. Phys. G* **49** (2022) 080501, `doi:10.1088/1361-6471/ac7216`, `arXiv:2203.05506`.

[67] T. Cridge, L. A. Harland-Lang, and R. S. Thorne, "Combining QED and approximate N$^3$LO QCD corrections in a global PDF fit: MSHT20qed_an3lo PDFs", *SciPost Phys.* **17** (2024) 026, `doi:10.21468/SciPostPhys.17.1.026`, `arXiv:2312.07665`.

[68] NNPDF Collaboration, "Illuminating the photon content of the proton within a global PDF analysis", *SciPost Phys.* **5** (2018) 008, `doi:10.21468/SciPostPhys.5.1.008`, `arXiv:1712.07053`.

[69] J. Alwall et al., "The automated computation of tree-level and next-to-leading order differential cross sections, and their matching to parton shower simulations", *JHEP* **07** (2014) 079, `doi:10.1007/JHEP07(2014)079`, `arXiv:1405.0301`.

[70] CMS Collaboration, "Technical proposal for the Phase-II upgrade of the Compact Muon Solenoid", CMS Technical Proposal CERN-LHCC-2015-010, CMS-TDR-15-02, 2015.

[71] CMS Collaboration, "Measurements of inclusive W and Z cross sections in pp collisions at $\sqrt{s} = 7$ TeV", *JHEP* **01** (2011) 080, `doi:10.1007/JHEP01(2011)080`, `arXiv:1012.2466`.

[72] CMS Collaboration, "Performance of the CMS muon trigger system in proton-proton collisions at $\sqrt{s} = 13$ TeV", *JINST* **16** (2021) P07001, `doi:10.1088/1748-0221/16/07/P07001`, `arXiv:2102.04790`.

[73] V. Blobel, C. Kleinwort, and F. Meier, "Fast alignment of a complex tracking detector using advanced track models", *Comput. Phys. Commun.* **182** (2011) 1760, `doi:10.1016/j.cpc.2011.03.017`, `arXiv:1103.3909`.

[74] V. Blobel, "A new fast track-fit algorithm based on broken lines", *Nucl. Instrum. Meth. A* **566** (2006) 14, `doi:10.1016/j.nima.2006.05.156`.

[75] CMS Collaboration, "Precision measurement of the structure of the CMS inner tracking system using nuclear interactions", *JINST* **13** (2018) P10034, `doi:10.1088/1748-0221/13/10/P10034`, `arXiv:1807.03289`.

[76] J. Allison et al., "GEANT4 developments and applications", *IEEE Trans. Nucl. Sci.* **53** (2006) 270, `doi:10.1109/TNS.2006.869826`.

[77] J. Allison et al., "Recent developments in GEANT4", *Nucl. Instrum. Meth. A* **835** (2016) 186, `doi:10.1016/j.nima.2016.06.125`.

[78] V. Klyukhin et al., "The CMS magnetic field measuring and monitoring systems", *Symmetry* **14** (2022) 169, `doi:10.3390/sym14010169`, `arXiv:2202.02562`.

[79] CMS Collaboration, "Alignment of the CMS tracker with LHC and cosmic ray data", *JINST* **9** (2014) P06009, `doi:10.1088/1748-0221/9/06/P06009`, `arXiv:1403.2286`.

[80] C. W. Bauer, S. Fleming, D. Pirjol, and I. W. Stewart, "An effective field theory for collinear and soft gluons: Heavy to light decays", *Phys. Rev. D* **63** (2001) 114020, `doi:10.1103/PhysRevD.63.114020`, `arXiv:hep-ph/0011336`.

[81] C. W. Bauer, D. Pirjol, and I. W. Stewart, "Soft collinear factorization in effective field theory", *Phys. Rev. D* **65** (2002) 054022, `doi:10.1103/PhysRevD.65.054022`, `arXiv:hep-ph/0109045`.

[82] J.-Y. Chiu, A. Jain, D. Neill, and I. Z. Rothstein, "A formalism for the systematic treatment of rapidity logarithms in quantum field theory", *JHEP* **05** (2012) 084, `doi:10.1007/JHEP05(2012)084`, `arXiv:1202.0814`.

[83] S. Camarda, L. Cieri, and G. Ferrera, "Drell–Yan lepton-pair production: $q_T$ resummation at N$^3$LL accuracy and fiducial cross sections at N$^3$LO", *Phys. Rev. D* **104** (2021) L111503, `doi:10.1103/PhysRevD.104.L111503`, `arXiv:2103.04974`.

[84] M. Grazzini, S. Kallweit, and M. Wiesemann, "Fully differential NNLO computations with MATRIX", *Eur. Phys. J. C* **78** (2018) 537, `doi:10.1140/epjc/s10052-018-5771-7`, `arXiv:1711.06631`.

[85] T. Becher and T. Neumann, "Fiducial $q_T$ resummation of color-singlet processes at N$^3$LL+NNLO", *JHEP* **03** (2021) 199, `doi:10.1007/JHEP03(2021)199`, `arXiv:2009.11437`.

[86] J. C. Collins and D. E. Soper, "Back-to-back jets in QCD", *Nucl. Phys. B* **193** (1981) 381, `doi:10.1016/0550-3213(81)90339-4`. [Erratum: `doi:10.1016/0550-3213(83)90235-3`].

[87] M. A. Ebert, J. K. L. Michel, I. W. Stewart, and Z. Sun, "Disentangling long and short distances in momentum-space TMDs", *JHEP* **07** (2022) 129, `doi:10.1007/JHEP07(2022)129`, `arXiv:2201.07237`.

[88] T. Cridge, L. A. Harland-Lang, A. D. Martin, and R. S. Thorne, "An investigation of the $\alpha_S$ and heavy quark mass dependence in the MSHT20 global PDF analysis", *Eur. Phys. J. C* **81** (2021) 744, `doi:10.1140/epjc/s10052-021-09533-7`, `arXiv:2106.10289`.

[89] J. C. Collins and D. E. Soper, "Angular distribution of dileptons in high-energy hadron collisions", *Phys. Rev. D* **16** (1977) 2219, `doi:10.1103/PhysRevD.16.2219`.

[90] C. M. Carloni Calame, G. Montagna, O. Nicrosini, and M. Treccani, "Higher order QED corrections to W boson mass determination at hadron colliders", *Phys. Rev. D* **69** (2004) 037301, `doi:10.1103/PhysRevD.69.037301`, `arXiv:hep-ph/0303102`.

[91] C. M. Carloni Calame, G. Montagna, O. Nicrosini, and M. Treccani, "Multiple photon corrections to the neutral-current Drell–Yan process", *JHEP* **05** (2005) 019, `doi:10.1088/1126-6708/2005/05/019`, `arXiv:hep-ph/0502218`.

[92] L. Barze et al., "Neutral current Drell–Yan with combined QCD and electroweak corrections in the POWHEG BOX", *Eur. Phys. J. C* **73** (2013) 2474, `doi:10.1140/epjc/s10052-013-2474-y`, `arXiv:1302.4606`.

[93] M. Chiesa, C. L. Del Pio, and F. Piccinini, "On electroweak corrections to neutral current Drell–Yan with the POWHEG BOX", *Eur. Phys. J. C* **84** (2024) 539, `doi:10.1140/epjc/s10052-024-12908-1`, `arXiv:2402.14659`.

[94] S. Bondarenko et al., "Hadron-hadron collision mode in ReneSANCe-v1.3.0", *Comput. Phys. Commun.* **285** (2023) 108646, `doi:10.1016/j.cpc.2022.108646`, `arXiv:2207.04332`.

[95] L. Barze et al., "Implementation of electroweak corrections in the POWHEG BOX: single W production", *JHEP* **04** (2012) 037, `doi:10.1007/JHEP04(2012)037`, `arXiv:1202.0465`.

[96] S. Alioli et al., "Precision studies of observables in pp $\rightarrow$ W $\rightarrow l\nu_l$ and pp $\rightarrow \gamma, Z \rightarrow l^+l^-$ processes at the LHC", *Eur. Phys. J. C* **77** (2017) 280, `doi:10.1140/epjc/s10052-017-4832-7`, `arXiv:1606.02330`.

[97] A. Pinto et al., "Uncertainty components in profile likelihood fits", *Eur. Phys. J. C* **84** (2024) 593, `doi:10.1140/epjc/s10052-024-12877-5`, `arXiv:2307.04007`.

[98] "HEPData record for this analysis", 2024. `doi:10.17182/hepdata.155627`.

## Acknowledgments

## Author contributions

All authors have contributed to the publication, being variously involved in the design and the construction of the detectors, in writing software, calibrating subsystems, operating the detectors and acquiring data, and finally analysing the processed data. The CMS Collaboration members discussed and approved the scientific results. The manuscript was prepared by a subgroup of authors appointed by the collaboration and subject to an internal collaboration-wide review process. All authors reviewed and approved the final version of the manuscript.

## Competing interests
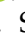
The authors declare no competing interests.

# B   The CMS Collaboration

**Yerevan Physics Institute, Yerevan, Armenia**
V. Chekhovsky, A. Hayrapetyan, V. Makarenko ⓘ, A. Tumasyan[1] ⓘ

**Institut für Hochenergiephysik, Vienna, Austria**
W. Adam ⓘ, J.W. Andrejkovic, L. Benato ⓘ, T. Bergauer ⓘ, S. Chatterjee ⓘ, K. Damanakis ⓘ, M. Dragicevic ⓘ, P.S. Hussain ⓘ, M. Jeitler[2] ⓘ, N. Krammer ⓘ, A. Li ⓘ, D. Liko ⓘ, I. Mikulec ⓘ, J. Schieck[2] ⓘ, R. Schöfbeck[2] ⓘ, D. Schwarz ⓘ, M. Sonawane ⓘ, W. Waltenberger ⓘ, C.-E. Wulz[2] ⓘ

**Universiteit Antwerpen, Antwerpen, Belgium**
T. Janssen ⓘ, H. Kwon ⓘ, T. Van Laer, P. Van Mechelen ⓘ
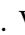
**Vrije Universiteit Brussel, Brussel, Belgium**
N. Breugelmans, J. D'Hondt ⓘ, S. Dansana ⓘ, A. De Moor ⓘ, M. Delcourt ⓘ, F. Heyen, Y. Hong ⓘ, S. Lowette ⓘ, I. Makarenko ⓘ, D. Müller ⓘ, S. Tavernier ⓘ, M. Tytgat[3] ⓘ, G.P. Van Onsem ⓘ, S. Van Putte ⓘ, D. Vannerom ⓘ
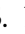
**Université Libre de Bruxelles, Bruxelles, Belgium**
B. Bilin ⓘ, B. Clerbaux ⓘ, A.K. Das, I. De Bruyn ⓘ, G. De Lentdecker ⓘ, H. Evard ⓘ, L. Favart ⓘ, P. Gianneios ⓘ, A. Khalilzadeh, F.A. Khan ⓘ, K. Lee ⓘ, A. Malara ⓘ, M.A. Shahzad, L. Thomas ⓘ, M. Vanden Bemden ⓘ, C. Vander Velde ⓘ, P. Vanlaer ⓘ
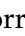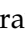
**Ghent University, Ghent, Belgium**
M. De Coen ⓘ, D. Dobur ⓘ, G. Gokbulut ⓘ, J. Knolle ⓘ, L. Lambrecht ⓘ, D. Marckx ⓘ, K. Skovpen ⓘ, N. Van Den Bossche ⓘ, J. van der Linden ⓘ, J. Vandenbroeck, L. Wezenbeek ⓘ
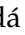
**Université Catholique de Louvain, Louvain-la-Neuve, Belgium**
S. Bein ⓘ, A. Benecke ⓘ, A. Bethani ⓘ, G. Bruno ⓘ, C. Caputo ⓘ, J. De Favereau De Jeneret ⓘ, C. Delaere ⓘ, I.S. Donertas ⓘ, A. Giammanco ⓘ, A.O. Guzel ⓘ, Sa. Jain ⓘ, V. Lemaitre, J. Lidrych ⓘ, P. Mastrapasqua ⓘ, T.T. Tran ⓘ, S. Turkcapar ⓘ

**Centro Brasileiro de Pesquisas Fisicas, Rio de Janeiro, Brazil**
G.A. Alves ⓘ, E. Coelho ⓘ, G. Correia Silva ⓘ, C. Hensel ⓘ, T. Menezes De Oliveira ⓘ, C. Mora Herrera[4] ⓘ, P. Rebello Teles ⓘ, M. Soeiro, E.J. Tonelli Manganote[5] ⓘ, A. Vilela Pereira[4] ⓘ

**Universidade do Estado do Rio de Janeiro, Rio de Janeiro, Brazil**
W.L. Aldá Júnior ⓘ, M. Barroso Ferreira Filho ⓘ, H. Brandao Malbouisson ⓘ, W. Carvalho ⓘ, J. Chinellato[6], E.M. Da Costa ⓘ, G.G. Da Silveira[7] ⓘ, D. De Jesus Damiao ⓘ, S. Fonseca De Souza ⓘ, R. Gomes De Souza, T. Laux Kuhn[7] ⓘ, M. Macedo ⓘ, J. Martins ⓘ, K. Mota Amarilo ⓘ, L. Mundim ⓘ, H. Nogima ⓘ, J.P. Pinheiro ⓘ, A. Santoro ⓘ, A. Sznajder ⓘ, M. Thiel ⓘ

**Universidade Estadual Paulista, Universidade Federal do ABC, São Paulo, Brazil**
C.A. Bernardes[7] ⓘ, L. Calligaris ⓘ, T.R. Fernandez Perez Tomei ⓘ, E.M. Gregores ⓘ, I. Maietto Silverio ⓘ, P.G. Mercadante ⓘ, S.F. Novaes ⓘ, B. Orzari ⓘ, Sandra S. Padula ⓘ, V. Scheurer

**Institute for Nuclear Research and Nuclear Energy, Bulgarian Academy of Sciences, Sofia, Bulgaria**
A. Aleksandrov ⓘ, G. Antchev ⓘ, R. Hadjiiska ⓘ, P. Iaydjiev ⓘ, M. Misheva ⓘ, M. Shopova ⓘ, G. Sultanov ⓘ

**University of Sofia, Sofia, Bulgaria**
A. Dimitrov (iD), L. Litov (iD), B. Pavlov (iD), P. Petkov (iD), A. Petrov (iD), E. Shumka (iD)

**Instituto De Alta Investigación, Universidad de Tarapacá, Casilla 7 D, Arica, Chile**
S. Keshri (iD), D. Laroze (iD), S. Thakur (iD)
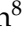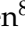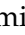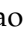
**Beihang University, Beijing, China**
T. Cheng (iD), T. Javaid (iD), L. Yuan (iD)
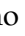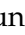
**Department of Physics, Tsinghua University, Beijing, China**
Z. Hu (iD), Z. Liang, J. Liu

**Institute of High Energy Physics, Beijing, China**
G.M. Chen[8] (iD), H.S. Chen[8] (iD), M. Chen[8] (iD), F. Iemmi (iD), C.H. Jiang, A. Kapoor[9] (iD), H. Liao (iD), Z.-A. Liu[10] (iD), R. Sharma[11] (iD), J.N. Song[10], J. Tao (iD), C. Wang[8], J. Wang (iD), Z. Wang[8], H. Zhang (iD), J. Zhao (iD)

**State Key Laboratory of Nuclear Physics and Technology, Peking University, Beijing, China**
A. Agapitos (iD), Y. Ban (iD), A. Carvalho Antunes De Oliveira (iD), S. Deng (iD), B. Guo, C. Jiang (iD), A. Levin (iD), C. Li (iD), Q. Li (iD), Y. Mao, S. Qian, S.J. Qian (iD), X. Qin, X. Sun (iD), D. Wang (iD), H. Yang, Y. Zhao, C. Zhou (iD)

**Guangdong Provincial Key Laboratory of Nuclear Science and Guangdong-Hong Kong Joint Laboratory of Quantum Matter, South China Normal University, Guangzhou, China**
S. Yang (iD)

**Sun Yat-Sen University, Guangzhou, China**
Z. You (iD)

**University of Science and Technology of China, Hefei, China**
K. Jaffel (iD), N. Lu (iD)

**Nanjing Normal University, Nanjing, China**
G. Bauer[12], B. Li[13], H. Wang (iD), K. Yi[14] (iD), J. Zhang (iD)

**Institute of Modern Physics and Key Laboratory of Nuclear Physics and Ion-beam Application (MOE) - Fudan University, Shanghai, China**
Y. Li

**Zhejiang University, Hangzhou, Zhejiang, China**
Z. Lin (iD), C. Lu (iD), M. Xiao (iD)

**Universidad de Los Andes, Bogota, Colombia**
C. Avila (iD), D.A. Barbosa Trujillo, A. Cabrera (iD), C. Florez (iD), J. Fraga (iD), J.A. Reyes Vega

**Universidad de Antioquia, Medellin, Colombia**
J. Jaramillo (iD), C. Rendón (iD), M. Rodriguez (iD), A.A. Ruales Barbosa (iD), J.D. Ruiz Alvarez (iD)

**University of Split, Faculty of Electrical Engineering, Mechanical Engineering and Naval Architecture, Split, Croatia**
D. Giljanovic (iD), N. Godinovic (iD), D. Lelas (iD), A. Sculac (iD)

**University of Split, Faculty of Science, Split, Croatia**
M. Kovac (iD), A. Petkovic (iD), T. Sculac (iD)

**Institute Rudjer Boskovic, Zagreb, Croatia**
P. Bargassa (iD), V. Brigljevic (iD), B.K. Chitroda (iD), D. Ferencek (iD), K. Jakovcic, A. Starodumov[15] (iD),

T. Susa

**University of Cyprus, Nicosia, Cyprus**
A. Attikis, K. Christoforou, A. Hadjiagapiou, C. Leonidou, J. Mousa, C. Nicolaou, L. Paizanos, F. Ptochos, P.A. Razis, H. Rykaczewski, H. Saka, A. Stepennov

**Charles University, Prague, Czech Republic**
M. Finger, M. Finger Jr., A. Kveton

**Escuela Politecnica Nacional, Quito, Ecuador**
E. Ayala

**Universidad San Francisco de Quito, Quito, Ecuador**
E. Carrera Jarrin

**Academy of Scientific Research and Technology of the Arab Republic of Egypt, Egyptian Network of High Energy Physics, Cairo, Egypt**
B. El-mahdy, S. Khalil[16], E. Salama[17,18]

**Center for High Energy Physics (CHEP-FU), Fayoum University, El-Fayoum, Egypt**
M. Abdullah Al-Mashad, M.A. Mahmoud

**National Institute of Chemical Physics and Biophysics, Tallinn, Estonia**
K. Ehataht, M. Kadastik, T. Lange, C. Nielsen, J. Pata, M. Raidal, L. Tani, C. Veelken

**Department of Physics, University of Helsinki, Helsinki, Finland**
K. Osterberg, M. Voutilainen
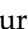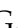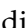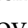
**Helsinki Institute of Physics, Helsinki, Finland**
N. Bin Norjoharuddeen, E. Brücken, F. Garcia, P. Inkaew, K.T.S. Kallonen, T. Lampén, K. Lassila-Perini, S. Lehti, T. Lindén, M. Myllymäki, M.m. Rantanen, J. Tuominiemi
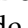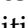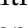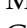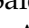
**Lappeenranta-Lahti University of Technology, Lappeenranta, Finland**
H. Kirschenmann, P. Luukka, H. Petrow

**IRFU, CEA, Université Paris-Saclay, Gif-sur-Yvette, France**
M. Besancon, F. Couderc, M. Dejardin, D. Denegri, J.L. Faure, F. Ferri, S. Ganjour, P. Gras, G. Hamel de Monchenault, M. Kumar, V. Lohezic, J. Malcles, F. Orlandi, L. Portales, A. Rosowsky, M.Ö. Sahin, A. Savoy-Navarro[19], P. Simkina, M. Titov, M. Tornago

**Laboratoire Leprince-Ringuet, CNRS/IN2P3, Ecole Polytechnique, Institut Polytechnique de Paris, Palaiseau, France**
F. Beaudette, G. Boldrini, P. Busson, A. Cappati, C. Charlot, M. Chiusi, T.D. Cuisset, F. Damas, O. Davignon, A. De Wit, I.T. Ehle, B.A. Fontana Santos Alves, S. Ghosh, A. Gilbert, R. Granier de Cassagnac, B. Harikrishnan, L. Kalipoliti, G. Liu, M. Nguyen, S. Obraztsov, C. Ochando, R. Salerno, J.B. Sauvan, Y. Sirois, G. Sokmen, L. Urda Gómez, E. Vernazza, A. Zabi, A. Zghiche
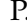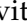
**Université de Strasbourg, CNRS, IPHC UMR 7178, Strasbourg, France**
J.-L. Agram[20], J. Andrea, D. Bloch, J.-M. Brom, E.C. Chabert, C. Collard, S. Falke, U. Goerlach, R. Haeberle, A.-C. Le Bihan, M. Meena, O. Poncet, G. Saha, M.A. Sessini, P. Van Hove, P. Vaucelle

**Centre de Calcul de l'Institut National de Physique Nucleaire et de Physique des Particules, CNRS/IN2P3, Villeurbanne, France**
A. Di Florio

**Institut de Physique des 2 Infinis de Lyon (IP2I ), Villeurbanne, France**
D. Amram, S. Beauceron, B. Blancon, G. Boudoul, N. Chanon, D. Contardo, P. Depasse, C. Dozen[21], H. El Mamouni, J. Fay, S. Gascon, M. Gouzevitch, C. Greenberg, G. Grenier, B. Ille, E. Jourd'huy, I.B. Laktineh, M. Lethuillier, L. Mirabito, S. Perries, A. Purohit, M. Vander Donckt, P. Verdier, J. Xiao

**Georgian Technical University, Tbilisi, Georgia**
G. Adamov, I. Lomidze, Z. Tsamalaidze[22]
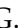
**RWTH Aachen University, I. Physikalisches Institut, Aachen, Germany**
V. Botta, S. Consuegra Rodríguez, L. Feld, K. Klein, M. Lipinski, D. Meuser, A. Pauls, D. Pérez Adán, N. Röwert, M. Teroerde

**RWTH Aachen University, III. Physikalisches Institut A, Aachen, Germany**
S. Diekmann, A. Dodonova, N. Eich, D. Eliseev, F. Engelke, J. Erdmann, M. Erdmann, B. Fischer, T. Hebbeker, K. Hoepfner, F. Ivone, A. Jung, M.y. Lee, F. Mausolf, M. Merschmeyer, A. Meyer, S. Mukherjee, F. Nowotny, A. Pozdnyakov, Y. Rath, W. Redjeb, F. Rehm, H. Reithler, V. Sarkisovi, A. Schmidt, C. Seth, A. Sharma, J.L. Spah, F. Torres Da Silva De Araujo[23], S. Wiedenbeck, S. Zaleski
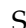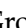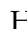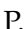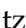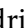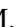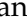
**RWTH Aachen University, III. Physikalisches Institut B, Aachen, Germany**
C. Dziwok, G. Flügge, T. Kress, A. Nowack, O. Pooth, A. Stahl, T. Ziemons, A. Zotz
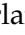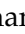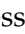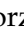
**Deutsches Elektronen-Synchrotron, Hamburg, Germany**
H. Aarup Petersen, M. Aldaya Martin, J. Alimena, S. Amoroso, Y. An, J. Bach, S. Baxter, M. Bayatmakou, H. Becerril Gonzalez, O. Behnke, A. Belvedere, F. Blekman[24], K. Borras[25], A. Campbell, A. Cardini, F. Colombina, M. De Silva, G. Eckerlin, D. Eckstein, L.I. Estevez Banos, E. Gallo[24], A. Geiser, V. Guglielmi, M. Guthoff, A. Hinzmann, L. Jeppe, B. Kaech, M. Kasemann, C. Kleinwort, R. Kogler, M. Komm, D. Krücker, W. Lange, D. Leyva Pernia, K. Lipka[26], W. Lohmann[27], F. Lorkowski, R. Mankel, I.-A. Melzer-Pellmann, M. Mendizabal Morentin, A.B. Meyer, G. Milella, K. Moral Figueroa, A. Mussgiller, L.P. Nair, J. Niedziela, A. Nürnberg, J. Park, E. Ranken, A. Raspereza, D. Rastorguev, J. Rübenach, L. Rygaard, M. Scham[28,25], S. Schnake[25], P. Schütze, C. Schwanenberger[24], D. Selivanova, K. Sharko, M. Shchedrolosiev, D. Stafford, F. Vazzoler, A. Ventura Barroso, R. Walsh, D. Wang, Q. Wang, K. Wichmann, L. Wiens[25], C. Wissing, Y. Yang, S. Zakharov, A. Zimermmane Castro Santos

**University of Hamburg, Hamburg, Germany**
A. Albrecht, S. Albrecht, M. Antonello, S. Bollweg, M. Bonanomi, P. Connor, K. El Morabit, Y. Fischer, E. Garutti, A. Grohsjean, J. Haller, D. Hundhausen, H.R. Jabusch, G. Kasieczka, P. Keicher, R. Klanner, W. Korcari, T. Kramer, C.c. Kuo, V. Kutzner, F. Labe, J. Lange, A. Lobanov, C. Matthies, L. Moureaux, M. Mrowietz, A. Nigamova, Y. Nissan, A. Paasch, K.J. Pena Rodriguez, T. Quadfasel, B. Raciti, M. Rieger, D. Savoiu, J. Schindler, P. Schleper, M. Schröder, J. Schwandt, M. Sommerhalder, H. Stadie, G. Steinbrück, A. Tews, B. Wiederspan, M. Wolf
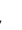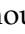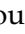
**Karlsruher Institut fuer Technologie, Karlsruhe, Germany**

S. Brommer, E. Butz, T. Chwalek, A. Dierlamm, G.G. Dincer, U. Elicabuk, N. Faltermann, M. Giffels, A. Gottmann, F. Hartmann[29], R. Hofsaess, M. Horzela, U. Husemann, J. Kieseler, M. Klute, O. Lavoryk, J.M. Lawhorn, M. Link, A. Lintuluoto, S. Maier, M. Mormile, Th. Müller, M. Neukum, M. Oh, E. Pfeffer, M. Presilla, G. Quast, K. Rabbertz, B. Regnery, R. Schmieder, N. Shadskiy, I. Shvetsov, H.J. Simonis, L. Sowa, L. Stockmeier, K. Tauqeer, M. Toms, B. Topko, N. Trevisani, T. Voigtländer, R.F. Von Cube, J. Von Den Driesch, M. Wassmer, S. Wieland, F. Wittig, R. Wolf, X. Zuo

**Institute of Nuclear and Particle Physics (INPP), NCSR Demokritos, Aghia Paraskevi, Greece**

G. Anagnostou, G. Daskalakis, A. Kyriakis, A. Papadopoulos[29], A. Stakia

**National and Kapodistrian University of Athens, Athens, Greece**

G. Melachroinos, Z. Painesis, I. Paraskevas, N. Saoulidou, K. Theofilatos, E. Tziaferi, K. Vellidis, I. Zisopoulos

**National Technical University of Athens, Athens, Greece**

G. Bakas, T. Chatzistavrou, G. Karapostoli, K. Kousouris, I. Papakrivopoulos, E. Siamarkou, G. Tsipolitis

**University of Ioánnina, Ioánnina, Greece**

I. Bestintzanos, I. Evangelou, C. Foudas, C. Kamtsikis, P. Katsoulis, P. Kokkas, P.G. Kosmoglou Kioseoglou, N. Manthos, I. Papadopoulos, J. Strologas

**HUN-REN Wigner Research Centre for Physics, Budapest, Hungary**

C. Hajdu, D. Horvath[30,31], K. Márton, A.J. Rádl[32], F. Sikler, V. Veszpremi

**MTA-ELTE Lendület CMS Particle and Nuclear Physics Group, Eötvös Loránd University, Budapest, Hungary**

M. Csanád, K. Farkas, A. Fehérkuti[33], M.M.A. Gadallah[34], Á. Kadlecsik, P. Major, G. Pásztor, G.I. Veres
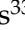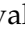
**Faculty of Informatics, University of Debrecen, Debrecen, Hungary**

B. Ujvari, G. Zilizi
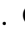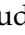
**HUN-REN ATOMKI - Institute of Nuclear Research, Debrecen, Hungary**

G. Bencze, S. Czellar, J. Molnar, Z. Szillasi

**Karoly Robert Campus, MATE Institute of Technology, Gyongyos, Hungary**

T. Csorgo[33], F. Nemes[33], T. Novak

**Panjab University, Chandigarh, India**

S. Bansal, S.B. Beri, V. Bhatnagar, G. Chaudhary, S. Chauhan, N. Dhingra[35], A. Kaur, A. Kaur, H. Kaur, M. Kaur, S. Kumar, T. Sheokand, J.B. Singh, A. Singla

**University of Delhi, Delhi, India**

A. Bhardwaj, A. Chhetri, B.C. Choudhary, A. Kumar, A. Kumar, M. Naimuddin, K. Ranjan, M.K. Saini, S. Saumya

**Saha Institute of Nuclear Physics, HBNI, Kolkata, India**

S. Baradia, S. Barman[36], S. Bhattacharya, S. Das Gupta, S. Dutta, S. Dutta, S. Sarkar

**Indian Institute of Technology Madras, Madras, India**

M.M. Ameen, P.K. Behera, S.C. Behera, S. Chatterjee, G. Dash, P. Jana, P. Kalbhor, S. Kamble, J.R. Komaragiri[37], D. Kumar[37], T. Mishra, B. Parida[38], P.R. Pujahari, N.R. Saha, A.K. Sikdar, R.K. Singh, P. Verma, S. Verma, A. Vijay

**Tata Institute of Fundamental Research-A, Mumbai, India**
S. Dugad, G.B. Mohanty, M. Shelake, P. Suryadevara
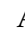
**Tata Institute of Fundamental Research-B, Mumbai, India**
A. Bala, S. Banerjee, S. Bhowmik, R.M. Chatterjee, M. Guchait, Sh. Jain, A. Jaiswal, B.M. Joshi, S. Kumar, G. Majumder, K. Mazumdar, S. Parolia, A. Thachayath
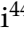
**National Institute of Science Education and Research, An OCC of Homi Bhabha National Institute, Bhubaneswar, Odisha, India**
S. Bahinipati[39], C. Kar, D. Maity[40], P. Mal, K. Naskar[40], A. Nayak[40], S. Nayak, K. Pal, P. Sadangi, S.K. Swain, S. Varghese[40], D. Vats[40]
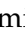
**Indian Institute of Science Education and Research (IISER), Pune, India**
S. Acharya[41], A. Alpana, S. Dube, B. Gomber[41], P. Hazarika, B. Kansal, A. Laha, B. Sahu[41], S. Sharma, K.Y. Vaish

**Isfahan University of Technology, Isfahan, Iran**
H. Bakhshiansohi[42], A. Jafari[43], M. Zeinali[44]
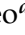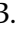
**Institute for Research in Fundamental Sciences (IPM), Tehran, Iran**
S. Bashiri, S. Chenarani[45], S.M. Etesami, Y. Hosseini, M. Khakzad, E. Khazaie, M. Mohammadi Najafabadi, S. Tizchang[46]

**University College Dublin, Dublin, Ireland**
M. Felcini, M. Grunewald

**INFN Sezione di Bari[a], Università di Bari[b], Politecnico di Bari[c], Bari, Italy**
M. Abbrescia[a,b], A. Colaleo[a,b], D. Creanza[a,c], B. D'Anzi[a,b], N. De Filippis[a,c], M. De Palma[a,b], W. Elmetenawee[a,b,47], N. Ferrara[a,b], L. Fiore[a], G. Iaselli[a,c], L. Longo[a], M. Louka[a,b], G. Maggi[a,c], M. Maggi[a], I. Margjeka[a], V. Mastrapasqua[a,b], S. My[a,b], S. Nuzzo[a,b], A. Pellecchia[a,b], A. Pompili[a,b], G. Pugliese[a,c], R. Radogna[a,b], D. Ramos[a], A. Ranieri[a], L. Silvestris[a], F.M. Simone[a,c], Ü. Sözbilir[a], A. Stamerra[a,b], D. Troiano[a,b], R. Venditti[a,b], P. Verwilligen[a], A. Zaza[a,b]
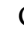
**INFN Sezione di Bologna[a], Università di Bologna[b], Bologna, Italy**
G. Abbiendi[a], C. Battilana[a,b], D. Bonacorsi[a,b], P. Capiluppi[a,b], A. Castro[†a,b], F.R. Cavallo[a], M. Cuffiani[a,b], G.M. Dallavalle[a], T. Diotalevi[a,b], F. Fabbri[a], A. Fanfani[a,b], D. Fasanella[a], P. Giacomelli[a], L. Giommi[a,b], C. Grandi[a], L. Guiducci[a,b], S. Lo Meo[a,48], M. Lorusso[a,b], L. Lunerti[a], S. Marcellini[a], G. Masetti[a], F.L. Navarria[a,b], G. Paggi[a,b], A. Perrotta[a], F. Primavera[a,b], A.M. Rossi[a,b], S. Rossi Tisbeni[a,b], T. Rovelli[a,b], G.P. Siroli[a,b]
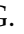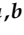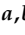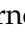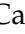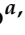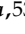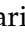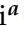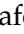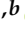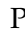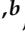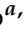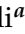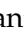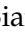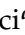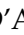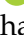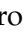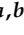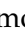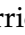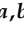
**INFN Sezione di Catania[a], Università di Catania[b], Catania, Italy**
S. Costa[a,b,49], A. Di Mattia[a], A. Lapertosa[a], R. Potenza[a,b], A. Tricomi[a,b,49]
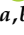
**INFN Sezione di Firenze[a], Università di Firenze[b], Firenze, Italy**
P. Assiouras[a], G. Barbagli[a], G. Bardelli[a,b], B. Camaiani[a,b], A. Cassese[a], R. Ceccarelli[a], V. Ciulli[a,b], C. Civinini[a], R. D'Alessandro[a,b], E. Focardi[a,b], T. Kello[a], G. Latino[a,b], P. Lenzi[a,b], M. Lizzo[a], M. Meschini[a], S. Paoletti[a], A. Papanastassiou[a,b], G. Sguazzoni[a], L. Viliani[a]

**INFN Laboratori Nazionali di Frascati, Frascati, Italy**

L. Benussi [iD], S. Bianco [iD], S. Meola[50] [iD], D. Piccolo [iD]

**INFN Sezione di Genova[a], Università di Genova[b], Genova, Italy**

M. Alves Gallo Pereira[a] [iD], F. Ferro[a] [iD], E. Robutti[a] [iD], S. Tosi[a,b] [iD]

**INFN Sezione di Milano-Bicocca[a], Università di Milano-Bicocca[b], Milano, Italy**

A. Benaglia[a] [iD], F. Brivio[a] [iD], F. Cetorelli[a,b] [iD], F. De Guio[a,b] [iD], M.E. Dinardo[a,b] [iD], P. Dini[a] [iD], S. Gennai[a] [iD], R. Gerosa[a,b] [iD], A. Ghezzi[a,b] [iD], P. Govoni[a,b] [iD], L. Guzzi[a] [iD], G. Lavizzari[a,b], M.T. Lucchini[a,b] [iD], M. Malberti[a] [iD], S. Malvezzi[a] [iD], A. Massironi[a] [iD], D. Menasce[a] [iD], L. Moroni[a] [iD], M. Paganoni[a,b] [iD], S. Palluotto[a,b] [iD], D. Pedrini[a] [iD], A. Perego[a,b] [iD], B.S. Pinolini[a], G. Pizzati[a,b] [iD], S. Ragazzi[a,b] [iD], T. Tabarelli de Fatis[a,b] [iD]

**INFN Sezione di Napoli[a], Università di Napoli 'Federico II'[b], Napoli, Italy; Università della Basilicata[c], Potenza, Italy; Scuola Superiore Meridionale (SSM)[d], Napoli, Italy**

S. Buontempo[a] [iD], A. Cagnotta[a,b] [iD], F. Carnevali[a,b], N. Cavallo[a,c] [iD], F. Fabozzi[a,c] [iD], A.O.M. Iorio[a,b] [iD], L. Lista[a,b,51] [iD], P. Paolucci[a,29] [iD], B. Rossi[a] [iD]

**INFN Sezione di Padova[a], Università di Padova[b], Padova, Italy; Università di Trento[c], Trento, Italy**

R. Ardino[a] [iD], P. Azzi[a] [iD], N. Bacchetta[a,52] [iD], D. Bisello[a,b] [iD], P. Bortignon[a] [iD], G. Bortolato[a,b], A.C.M. Bulla[a] [iD], R. Carlin[a,b] [iD], T. Dorigo[a,53] [iD], F. Gasparini[a,b] [iD], U. Gasparini[a,b] [iD], S. Giorgetti[a], E. Lusiani[a] [iD], M. Margoni[a,b] [iD], A.T. Meneguzzo[a,b] [iD], M. Migliorini[a,b] [iD], M. Passaseo[a] [iD], J. Pazzini[a,b] [iD], P. Ronchese[a,b] [iD], R. Rossin[a,b] [iD], M. Sgaravatto[a] [iD], F. Simonetto[a,b] [iD], M. Tosi[a,b] [iD], A. Triossi[a,b] [iD], S. Ventura[a] [iD], M. Zanetti[a,b] [iD], P. Zotto[a,b] [iD], A. Zucchetta[a,b] [iD]

**INFN Sezione di Pavia[a], Università di Pavia[b], Pavia, Italy**

A. Braghieri[a] [iD], S. Calzaferri[a] [iD], D. Fiorina[a] [iD], P. Montagna[a,b] [iD], V. Re[a] [iD], C. Riccardi[a,b] [iD], P. Salvini[a] [iD], I. Vai[a,b] [iD], P. Vitulo[a,b] [iD]

**INFN Sezione di Perugia[a], Università di Perugia[b], Perugia, Italy**

S. Ajmal[a,b] [iD], M.E. Ascioti[a,b], G.M. Bilei[a] [iD], C. Carrivale[a,b], D. Ciangottini[a,b] [iD], L. Fanò[a,b] [iD], V. Mariani[a,b] [iD], M. Menichelli[a] [iD], F. Moscatelli[a,54] [iD], A. Rossi[a,b] [iD], A. Santocchia[a,b] [iD], D. Spiga[a] [iD], T. Tedeschi[a,b] [iD]

**INFN Sezione di Pisa[a], Università di Pisa[b], Scuola Normale Superiore di Pisa[c], Pisa, Italy; Università di Siena[d], Siena, Italy**

C. Aimè[a,b] [iD], C.A. Alexe[a,c] [iD], P. Asenov[a,b] [iD], P. Azzurri[a] [iD], G. Bagliesi[a] [iD], V. Bertacchi[a,c] [iD], R. Bhattacharya[a] [iD], L. Bianchini[a,b] [iD], T. Boccali[a] [iD], E. Bossini[a] [iD], D. Bruschini[a,c] [iD], R. Castaldi[a] [iD], M.A. Ciocci[a,b] [iD], M. Cipriani[a,b] [iD], V. D'Amante[a,d] [iD], R. Dell'Orso[a] [iD], S. Donato[a] [iD], R. Forti[a,b] [iD], A. Giassi[a] [iD], F. Ligabue[a,c] [iD], A.C. Marini[a] [iD], D. Matos Figueiredo[a] [iD], A. Messineo[a,b] [iD], S. Mishra[a] [iD], V.K. Muraleedharan Nair Bindhu[a,b,40] [iD], M. Musich[a,b] [iD], S. Nandan[a] [iD], F. Palla[a] [iD], A. Rizzi[a,b] [iD], G. Rolandi[a,c] [iD], S. Roy Chowdhury[a] [iD], T. Sarkar[a] [iD], A. Scribano[a] [iD], P. Spagnolo[a] [iD], F. Tenchini[a,b] [iD], R. Tenchini[a] [iD], G. Tonelli[a,b] [iD], N. Turini[a,d] [iD], F. Vaselli[a,c] [iD], A. Venturi[a] [iD], P.G. Verdini[a] [iD]

**INFN Sezione di Roma[a], Sapienza Università di Roma[b], Roma, Italy**

P. Barria[a] [iD], C. Basile[a,b] [iD], F. Cavallari[a] [iD], L. Cunqueiro Mendez[a,b] [iD], D. Del Re[a,b] [iD], E. Di Marco[a,b] [iD], M. Diemoz[a] [iD], F. Errico[a,b] [iD], R. Gargiulo[a,b], E. Longo[a,b] [iD], L. Martikainen[a,b] [iD], J. Mijuskovic[a,b] [iD], G. Organtini[a,b] [iD], F. Pandolfi[a] [iD], R. Paramatti[a,b] [iD], C. Quaranta[a,b] [iD], S. Rahatlou[a,b] [iD], C. Rovelli[a] [iD], F. Santanastasio[a,b] [iD], L. Soffi[a] [iD],

V. Vladimirov[a,b]

**INFN Sezione di Torino[a], Università di Torino[b], Torino, Italy; Università del Piemonte Orientale[c], Novara, Italy**
N. Amapane[a,b] (iD), R. Arcidiacono[a,c] (iD), S. Argiro[a,b] (iD), M. Arneodo[a,c] (iD), N. Bartosik[a] (iD), R. Bellan[a,b] (iD), C. Biino[a] (iD), C. Borca[a,b] (iD), N. Cartiglia[a] (iD), M. Costa[a,b] (iD), R. Covarelli[a,b] (iD), N. Demaria[a] (iD), L. Finco[a] (iD), M. Grippo[a,b] (iD), B. Kiani[a,b] (iD), F. Legger[a] (iD), F. Luongo[a,b] (iD), C. Mariotti[a] (iD), L. Markovic[a,b] (iD), S. Maselli[a] (iD), A. Mecca[a,b] (iD), L. Menzio[a,b], P. Meridiani[a] (iD), E. Migliore[a,b] (iD), M. Monteno[a] (iD), R. Mulargia[a] (iD), M.M. Obertino[a,b] (iD), G. Ortona[a] (iD), L. Pacher[a,b] (iD), N. Pastrone[a] (iD), M. Pelliccioni[a] (iD), M. Ruspa[a,c] (iD), F. Siviero[a,b] (iD), V. Sola[a,b] (iD), A. Solano[a,b] (iD), A. Staiano[a] (iD), C. Tarricone[a,b] (iD), D. Trocino[a] (iD), G. Umoret[a,b] (iD), R. White[a,b] (iD)

**INFN Sezione di Trieste[a], Università di Trieste[b], Trieste, Italy**
J. Babbar[a,b] (iD), S. Belforte[a] (iD), V. Candelise[a,b] (iD), M. Casarsa[a] (iD), F. Cossutti[a] (iD), K. De Leo[a] (iD), G. Della Ricca[a,b] (iD)

**Kyungpook National University, Daegu, Korea**
S. Dogra (iD), J. Hong (iD), J. Kim, D. Lee, H. Lee, S.W. Lee (iD), C.S. Moon (iD), Y.D. Oh (iD), M.S. Ryu (iD), S. Sekmen (iD), B. Tae, Y.C. Yang (iD)

**Department of Mathematics and Physics - GWNU, Gangneung, Korea**
M.S. Kim (iD)

**Chonnam National University, Institute for Universe and Elementary Particles, Kwangju, Korea**
G. Bak (iD), P. Gwak (iD), H. Kim (iD), D.H. Moon (iD)

**Hanyang University, Seoul, Korea**
E. Asilar (iD), J. Choi (iD), D. Kim (iD), T.J. Kim (iD), J.A. Merlin, Y. Ryou

**Korea University, Seoul, Korea**
S. Choi (iD), S. Han, B. Hong (iD), K. Lee, K.S. Lee (iD), S. Lee (iD), J. Yoo (iD)

**Kyung Hee University, Department of Physics, Seoul, Korea**
J. Goh (iD), S. Yang (iD)

**Sejong University, Seoul, Korea**
Y. Kang (iD), H. S. Kim (iD), Y. Kim, S. Lee

**Seoul National University, Seoul, Korea**
J. Almond, J.H. Bhyun, J. Choi (iD), J. Choi, W. Jun (iD), J. Kim (iD), Y.W. Kim (iD), S. Ko (iD), H. Lee (iD), J. Lee (iD), J. Lee (iD), B.H. Oh (iD), S.B. Oh (iD), H. Seo (iD), U.K. Yang, I. Yoon (iD)

**University of Seoul, Seoul, Korea**
W. Jang (iD), D.Y. Kang, S. Kim (iD), B. Ko, J.S.H. Lee (iD), Y. Lee (iD), I.C. Park (iD), Y. Roh, I.J. Watson (iD)

**Yonsei University, Department of Physics, Seoul, Korea**
S. Ha (iD), K. Hwang (iD), B. Kim (iD), H.D. Yoo (iD)

**Sungkyunkwan University, Suwon, Korea**
M. Choi (iD), M.R. Kim (iD), H. Lee, Y. Lee (iD), I. Yu (iD)

**College of Engineering and Technology, American University of the Middle East (AUM), Dasman, Kuwait**
T. Beyrouthy (iD), Y. Gharbia (iD)

**Kuwait University - College of Science - Department of Physics, Safat, Kuwait**

F. Alazemi (iD)

**Riga Technical University, Riga, Latvia**
K. Dreimanis (iD), A. Gaile (iD), C. Munoz Diaz (iD), D. Osite (iD), G. Pikurs, A. Potrebko (iD), M. Seidel (iD), D. Sidiropoulos Kontos (iD)

**University of Latvia (LU), Riga, Latvia**
N.R. Strautnieks (iD)

**Vilnius University, Vilnius, Lithuania**
M. Ambrozas (iD), A. Juodagalvis (iD), A. Rinkevicius (iD), G. Tamulaitis (iD)

**National Centre for Particle Physics, Universiti Malaya, Kuala Lumpur, Malaysia**
I. Yusuff[55] (iD), Z. Zolkapli

**Universidad de Sonora (UNISON), Hermosillo, Mexico**
J.F. Benitez (iD), A. Castaneda Hernandez (iD), H.A. Encinas Acosta, L.G. Gallegos Maríñez, M. León Coello (iD), J.A. Murillo Quijada (iD), A. Sehrawat (iD), L. Valencia Palomo (iD)

**Centro de Investigacion y de Estudios Avanzados del IPN, Mexico City, Mexico**
G. Ayala (iD), H. Castilla-Valdez (iD), H. Crotte Ledesma, E. De La Cruz-Burelo (iD), I. Heredia-De La Cruz[56] (iD), R. Lopez-Fernandez (iD), J. Mejia Guisao (iD), A. Sánchez Hernández (iD)

**Universidad Iberoamericana, Mexico City, Mexico**
C. Oropeza Barrera (iD), D.L. Ramirez Guadarrama, M. Ramírez García (iD)

**Benemerita Universidad Autonoma de Puebla, Puebla, Mexico**
I. Bautista (iD), F.E. Neri Huerta (iD), I. Pedraza (iD), H.A. Salazar Ibarguen (iD), C. Uribe Estrada (iD)

**University of Montenegro, Podgorica, Montenegro**
I. Bubanja (iD), N. Raicevic (iD)

**University of Canterbury, Christchurch, New Zealand**
P.H. Butler (iD)

**National Centre for Physics, Quaid-I-Azam University, Islamabad, Pakistan**
A. Ahmad (iD), M.I. Asghar, A. Awais (iD), M.I.M. Awan, H.R. Hoorani (iD), W.A. Khan (iD)
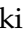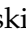
**AGH University of Krakow, Krakow, Poland**
V. Avati, A. Bellora (iD), L. Forthomme (iD), L. Grzanka (iD), M. Malawski (iD), K. Piotrzkowski

**National Centre for Nuclear Research, Swierk, Poland**
H. Bialkowska (iD), M. Bluj (iD), M. Górski (iD), M. Kazana (iD), M. Szleper (iD), P. Zalewski (iD)
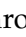
**Institute of Experimental Physics, Faculty of Physics, University of Warsaw, Warsaw, Poland**
K. Bunkowski (iD), K. Doroba (iD), A. Kalinowski (iD), M. Konecki (iD), J. Krolikowski (iD), A. Muhammad (iD)

**Warsaw University of Technology, Warsaw, Poland**
P. Fokow (iD), K. Pozniak (iD), W. Zabolotny (iD)
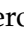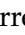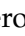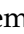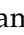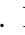
**Laboratório de Instrumentação e Física Experimental de Partículas, Lisboa, Portugal**
M. Araujo (iD), D. Bastos (iD), C. Beirão Da Cruz E Silva (iD), A. Boletti (iD), M. Bozzo (iD), T. Camporesi (iD), G. Da Molin (iD), P. Faccioli (iD), M. Gallinaro (iD), J. Hollar (iD), N. Leonardo (iD), G.B. Marozzo (iD), A. Petrilli (iD), M. Pisano (iD), J. Seixas (iD), J. Varela (iD), J.W. Wulff
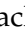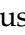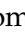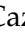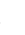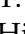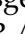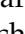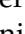
**Faculty of Physics, University of Belgrade, Belgrade, Serbia**
P. Adzic (iD), P. Milenovic (iD)
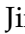
**VINCA Institute of Nuclear Sciences, University of Belgrade, Belgrade, Serbia**
D. Devetak, M. Dordevic (iD), J. Milosevic (iD), L. Nadderd (iD), V. Rekovic, M. Stojanovic (iD)

**Centro de Investigaciones Energéticas Medioambientales y Tecnológicas (CIEMAT), Madrid, Spain**
J. Alcaraz Maestre (iD), Cristina F. Bedoya (iD), J.A. Brochero Cifuentes (iD), Oliver M. Carretero (iD), M. Cepeda (iD), M. Cerrada (iD), N. Colino (iD), B. De La Cruz (iD), A. Delgado Peris (iD), A. Escalante Del Valle (iD), D. Fernández Del Val (iD), J.P. Fernández Ramos (iD), J. Flix (iD), M.C. Fouz (iD), O. Gonzalez Lopez (iD), S. Goy Lopez (iD), J.M. Hernandez (iD), M.I. Josa (iD), J. Llorente Merino (iD), C. Martin Perez (iD), E. Martin Viscasillas (iD), D. Moran (iD), C. M. Morcillo Perez (iD), Á. Navarro Tobar (iD), C. Perez Dengra (iD), A. Pérez-Calero Yzquierdo (iD), J. Puerta Pelayo (iD), I. Redondo (iD), J. Sastre (iD), J. Vazquez Escobar (iD)

**Universidad Autónoma de Madrid, Madrid, Spain**
J.F. de Trocóniz (iD)

**Universidad de Oviedo, Instituto Universitario de Ciencias y Tecnologías Espaciales de Asturias (ICTEA), Oviedo, Spain**
B. Alvarez Gonzalez (iD), J. Cuevas (iD), J. Fernandez Menendez (iD), S. Folgueras (iD), I. Gonzalez Caballero (iD), P. Leguina (iD), E. Palencia Cortezon (iD), J. Prado Pico, V. Rodríguez Bouza (iD), A. Soto Rodríguez (iD), A. Trapote (iD), C. Vico Villalba (iD), P. Vischia (iD)

**Instituto de Física de Cantabria (IFCA), CSIC-Universidad de Cantabria, Santander, Spain**
S. Blanco Fernández (iD), I.J. Cabrillo (iD), A. Calderon (iD), J. Duarte Campderros (iD), M. Fernandez (iD), G. Gomez (iD), C. Lasaosa García (iD), R. Lopez Ruiz (iD), C. Martinez Rivero (iD), P. Martinez Ruiz del Arbol (iD), F. Matorras (iD), P. Matorras Cuevas (iD), E. Navarrete Ramos (iD), J. Piedra Gomez (iD), L. Scodellaro (iD), I. Vila (iD), J.M. Vizan Garcia (iD)

**University of Colombo, Colombo, Sri Lanka**
B. Kailasapathy[57] (iD), D.D.C. Wickramarathna (iD)

**University of Ruhuna, Department of Physics, Matara, Sri Lanka**
W.G.D. Dharmaratna[58] (iD), K. Liyanage (iD), N. Perera (iD)

**CERN, European Organization for Nuclear Research, Geneva, Switzerland**
D. Abbaneo (iD), C. Amendola (iD), E. Auffray (iD), J. Baechler, D. Barney (iD), A. Bermúdez Martínez (iD), M. Bianco (iD), A.A. Bin Anuar (iD), A. Bocci (iD), L. Borgonovi (iD), C. Botta (iD), A. Bragagnolo (iD), E. Brondolin (iD), C.E. Brown (iD), C. Caillol (iD), G. Cerminara (iD), N. Chernyavskaya (iD), D. d'Enterria (iD), A. Dabrowski (iD), A. David (iD), A. De Roeck (iD), M.M. Defranchis (iD), M. Deile (iD), M. Dobson (iD), M. Dünser (iD), G. Franzoni (iD), W. Funk (iD), S. Giani, D. Gigi, K. Gill (iD), F. Glege (iD), M. Glowacki, J. Hegeman (iD), J.K. Heikkilä (iD), B. Huber (iD), V. Innocente (iD), T. James (iD), P. Janot (iD), O. Kaluzinska (iD), O. Karacheban[27] (iD), G. Karathanasis (iD), S. Laurila (iD), P. Lecoq, E. Leutgeb (iD), C. Lourenço (iD), M. Magherini (iD), L. Malgeri (iD), M. Mannelli (iD), M. Matthewman, A. Mehta (iD), F. Meijers (iD), S. Mersi (iD), E. Meschi (iD), V. Milosevic (iD), F. Monti (iD), F. Moortgat (iD), M. Mulders (iD), I. Neutelings (iD), S. Orfanelli, F. Pantaleo (iD), G. Petrucciani (iD), A. Pfeiffer (iD), M. Pierini (iD), M. Pitt (iD), H. Qu (iD), D. Rabady (iD), B. Ribeiro Lopes (iD), F. Riti (iD), M. Rovere (iD), H. Sakulin (iD), R. Salvatico (iD), S. Sanchez Cruz (iD), S. Scarfi (iD), C. Schwick, M. Selvaggi (iD), A. Sharma (iD), K. Shchelina (iD), P. Silva (iD), P. Sphicas[59] (iD), A.G. Stahl Leiton (iD), A. Steen (iD), S. Summers (iD), D. Treille (iD), P. Tropea (iD), D. Walter (iD), J. Wanczyk[60] (iD), J. Wang, S. Wuchterl (iD), P. Zehetner (iD), P. Zejdl (iD), W.D. Zeuner

**PSI Center for Neutron and Muon Sciences, Villigen, Switzerland**

T. Bevilacqua[61] (iD), L. Caminada[61] (iD), A. Ebrahimi (iD), W. Erdmann (iD), R. Horisberger (iD), Q. Ingram (iD), H.C. Kaestli (iD), D. Kotlinski (iD), C. Lange (iD), M. Missiroli[61] (iD), L. Noehte[61] (iD), T. Rohe (iD), A. Samalan

**ETH Zurich - Institute for Particle Physics and Astrophysics (IPA), Zurich, Switzerland**
T.K. Aarrestad (iD), M. Backhaus (iD), G. Bonomelli (iD), A. Calandri (iD), C. Cazzaniga (iD), K. Datta (iD), P. De Bryas Dexmiers D'archiac[60] (iD), A. De Cosa (iD), G. Dissertori (iD), M. Dittmar, M. Donegà (iD), F. Eble (iD), M. Galli (iD), K. Gedia (iD), F. Glessgen (iD), C. Grab (iD), N. Härringer (iD), T.G. Harte, D. Hits (iD), W. Lustermann (iD), A.-M. Lyon (iD), R.A. Manzoni (iD), M. Marchegiani (iD), L. Marchese (iD), A. Mascellani[60] (iD), F. Nessi-Tedaldi (iD), F. Pauss (iD), V. Perovic (iD), S. Pigazzini (iD), B. Ristic (iD), R. Seidita (iD), J. Steggemann[60] (iD), A. Tarabini (iD), D. Valsecchi (iD), R. Wallny (iD)
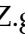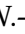
**Universität Zürich, Zurich, Switzerland**
C. Amsler[62] (iD), P. Bärtschi (iD), M.F. Canelli (iD), K. Cormier (iD), M. Huwiler (iD), W. Jin (iD), A. Jofrehei (iD), B. Kilminster (iD), S. Leontsinis (iD), S.P. Liechti (iD), A. Macchiolo (iD), P. Meiring (iD), F. Meng (iD), J. Motta (iD), A. Reimers (iD), P. Robmann, M. Senger (iD), E. Shokr, F. Stäger (iD), R. Tramontano (iD)
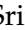
**National Central University, Chung-Li, Taiwan**
C. Adloff[63], D. Bhowmik, C.M. Kuo, W. Lin, P.K. Rout (iD), P.C. Tiwari[37] (iD)

**National Taiwan University (NTU), Taipei, Taiwan**
L. Ceard, K.F. Chen (iD), Z.g. Chen, A. De Iorio (iD), W.-S. Hou (iD), T.h. Hsu, Y.w. Kao, S. Karmakar (iD), G. Kole (iD), Y.y. Li (iD), R.-S. Lu (iD), E. Paganis (iD), X.f. Su (iD), J. Thomas-Wilsker (iD), L.s. Tsai, D. Tsionou, H.y. Wu, E. Yazgan (iD)
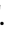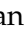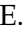
**High Energy Physics Research Unit, Department of Physics, Faculty of Science, Chulalongkorn University, Bangkok, Thailand**
C. Asawatangtrakuldee (iD), N. Srimanobhas (iD), V. Wachirapusitanand (iD)

**Tunis El Manar University, Tunis, Tunisia**
Y. Maghrbi (iD)

**Çukurova University, Physics Department, Science and Art Faculty, Adana, Turkey**
D. Agyel (iD), F. Boran (iD), F. Dolek (iD), I. Dumanoglu[64] (iD), E. Eskut (iD), Y. Guler[65] (iD), E. Gurpinar Guler[65] (iD), C. Isik (iD), O. Kara, A. Kayis Topaksu (iD), Y. Komurcu (iD), G. Onengut (iD), K. Ozdemir[66] (iD), A. Polatoz (iD), B. Tali[67] (iD), U.G. Tok (iD), E. Uslan (iD), I.S. Zorbakir (iD)

**Middle East Technical University, Physics Department, Ankara, Turkey**
M. Yalvac[68] (iD)

**Bogazici University, Istanbul, Turkey**
B. Akgun (iD), I.O. Atakisi (iD), E. Gülmez (iD), M. Kaya[69] (iD), O. Kaya[70] (iD), S. Tekten[71] (iD)
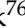
**Istanbul Technical University, Istanbul, Turkey**
A. Cakir (iD), K. Cankocak[64,72] (iD), S. Sen[73] (iD)

**Istanbul University, Istanbul, Turkey**
O. Aydilek[74] (iD), B. Hacisahinoglu (iD), I. Hos[75] (iD), B. Kaynak (iD), S. Ozkorucuklu (iD), O. Potok (iD), H. Sert (iD), C. Simsek (iD), C. Zorbilmez (iD)

**Yildiz Technical University, Istanbul, Turkey**
S. Cerci (iD), B. Isildak[76] (iD), D. Sunar Cerci (iD), T. Yetkin (iD)
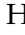
**Institute for Scintillation Materials of National Academy of Science of Ukraine, Kharkiv, Ukraine**
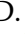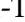
A. Boyaryntsev, B. Grynyov

**National Science Centre, Kharkiv Institute of Physics and Technology, Kharkiv, Ukraine**
L. Levchuk
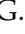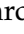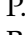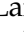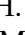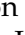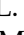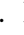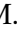
**University of Bristol, Bristol, United Kingdom**
D. Anthony, J.J. Brooke, A. Bundock, F. Bury, E. Clement, D. Cussans, H. Flacher, J. Goldstein, H.F. Heath, M.-L. Holmberg, L. Kreczko, S. Paramesvaran, L. Robertshaw, V.J. Smith, K. Walkingshaw Pass

**Rutherford Appleton Laboratory, Didcot, United Kingdom**
A.H. Ball, K.W. Bell, A. Belyaev[77], C. Brew, R.M. Brown, D.J.A. Cockerill, C. Cooke, A. Elliot, K.V. Ellis, K. Harder, S. Harper, J. Linacre, K. Manolopoulos, D.M. Newbold, E. Olaiya, D. Petyt, T. Reis, A.R. Sahasransu, G. Salvi, T. Schuh, C.H. Shepherd-Themistocleous, I.R. Tomalin, K.C. Whalen, T. Williams

**Imperial College, London, United Kingdom**
I. Andreou, R. Bainbridge, P. Bloch, O. Buchmuller, C.A. Carrillo Montoya, G.S. Chahal[78], D. Colling, J.S. Dancu, I. Das, P. Dauncey, G. Davies, M. Della Negra, S. Fayer, G. Fedi, G. Hall, A. Howard, G. Iles, C.R. Knight, P. Krueper, J. Langford, K.H. Law, J. León Holgado, L. Lyons, A.-M. Magnan, B. Maier, S. Mallios, M. Mieskolainen, J. Nash[79], M. Pesaresi, P.B. Pradeep, B.C. Radburn-Smith, A. Richards, A. Rose, K. Savva, C. Seez, R. Shukla, A. Tapper, K. Uchida, G.P. Uttley, T. Virdee[29], M. Vojinovic, N. Wardle, D. Winterbottom

**Brunel University, Uxbridge, United Kingdom**
J.E. Cole, A. Khan, P. Kyberd, I.D. Reid

**Baylor University, Waco, Texas, USA**
S. Abdullin, A. Brinkerhoff, E. Collins, M.R. Darwish, J. Dittmann, K. Hatakeyama, V. Hegde, J. Hiltbrand, B. McMaster, J. Samudio, S. Sawant, C. Sutantawibul, J. Wilson
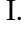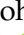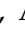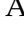
**Catholic University of America, Washington, DC, USA**
R. Bartek, A. Dominguez, A.E. Simsek, S.S. Yu
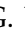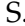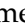
**The University of Alabama, Tuscaloosa, Alabama, USA**
B. Bam, A. Buchot Perraguin, R. Chudasama, S.I. Cooper, C. Crovella, S.V. Gleyzer, E. Pearson, C.U. Perez, P. Rumerio[80], E. Usai, R. Yi
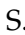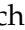
**Boston University, Boston, Massachusetts, USA**
A. Akpinar, C. Cosby, G. De Castro, Z. Demiragli, C. Erice, C. Fangmeier, C. Fernandez Madrazo, E. Fontanesi, D. Gastler, F. Golf, S. Jeon, J. O'cain, I. Reed, J. Rohlf, K. Salyer, D. Sperka, D. Spitzbart, I. Suarez, A. Tsatsos, A.G. Zecchinelli

**Brown University, Providence, Rhode Island, USA**
G. Barone, G. Benelli, D. Cutts, L. Gouskos, M. Hadley, U. Heintz, K.W. Ho, J.M. Hogan[81], T. Kwon, G. Landsberg, K.T. Lau, J. Luo, S. Mondal, T. Russell, S. Sagir[82], X. Shen, M. Stamenkovic, N. Venkatasubramanian
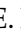
**University of California, Davis, Davis, California, USA**
S. Abbott, B. Barton, C. Brainerd, R. Breedon, H. Cai, M. Calderon De La Barca Sanchez, M. Chertok, M. Citron, J. Conway, P.T. Cox,

R. Erbacher, F. Jensen, O. Kukral, G. Mocellin, M. Mulhearn, S. Ostrom, W. Wei, S. Yoo, F. Zhang
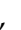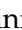
**University of California, Los Angeles, California, USA**

K. Adamidis, M. Bachtis, D. Campos, R. Cousins, A. Datta, G. Flores Avila, J. Hauser, M. Ignatenko, M.A. Iqbal, T. Lam, Y.f. Lo, E. Manca, A. Nunez Del Prado, D. Saltzberg, V. Valuev

**University of California, Riverside, Riverside, California, USA**

R. Clare, J.W. Gary, G. Hanson

**University of California, San Diego, La Jolla, California, USA**

A. Aportela, A. Arora, J.G. Branson, S. Cittolin, S. Cooperstein, D. Diaz, J. Duarte, L. Giannini, Y. Gu, J. Guiang, R. Kansal, V. Krutelyov, R. Lee, J. Letts, M. Masciovecchio, F. Mokhtar, S. Mukherjee, M. Pieri, D. Primosch, M. Quinnan, V. Sharma, M. Tadel, E. Vourliotis, F. Würthwein, Y. Xiang, A. Yagil
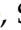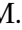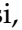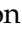
**University of California, Santa Barbara - Department of Physics, Santa Barbara, California, USA**

A. Barzdukas, L. Brennan, C. Campagnari, K. Downham, C. Grieco, M.M. Hussain, J. Incandela, J. Kim, A.J. Li, P. Masterson, H. Mei, J. Richman, S.N. Santpur, U. Sarica, R. Schmitz, F. Setti, J. Sheplock, D. Stuart, T.Á. Vámi, X. Yan, D. Zhang

**California Institute of Technology, Pasadena, California, USA**

S. Bhattacharya, A. Bornheim, O. Cerri, J. Mao, H.B. Newman, G. Reales Gutiérrez, M. Spiropulu, J.R. Vlimant, C. Wang, S. Xie, R.Y. Zhu
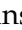
**Carnegie Mellon University, Pittsburgh, Pennsylvania, USA**

J. Alison, S. An, P. Bryant, M. Cremonesi, V. Dutta, T. Ferguson, T.A. Gómez Espinosa, A. Harilal, A. Kallil Tharayil, M. Kanemura, C. Liu, T. Mudholkar, S. Murthy, P. Palit, K. Park, M. Paulini, A. Roberts, A. Sanchez, W. Terrill

**University of Colorado Boulder, Boulder, Colorado, USA**
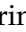
J.P. Cumalat, W.T. Ford, A. Hart, A. Hassani, N. Manganelli, J. Pearkes, C. Savard, N. Schonbeck, K. Stenson, K.A. Ulmer, S.R. Wagner, N. Zipper, D. Zuolo

**Cornell University, Ithaca, New York, USA**
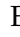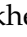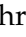
J. Alexander, X. Chen, D.J. Cranshaw, J. Dickinson, J. Fan, X. Fan, S. Hogan, P. Kotamnives, J. Monroy, M. Oshiro, J.R. Patterson, M. Reid, A. Ryd, J. Thom, P. Wittich, R. Zou

**Fermi National Accelerator Laboratory, Batavia, Illinois, USA**

M. Albrow, M. Alyari, O. Amram, G. Apollinari, A. Apresyan, L.A.T. Bauerdick, D. Berry, J. Berryhill, P.C. Bhat, K. Burkett, J.N. Butler, A. Canepa, G.B. Cerati, H.W.K. Cheung, F. Chlebana, G. Cummings, I. Dutta, V.D. Elvira, J. Freeman, A. Gandrakota, Z. Gecse, L. Gray, D. Green, A. Grummer, S. Grünendahl, D. Guerrero, O. Gutsche, R.M. Harris, T.C. Herwig, J. Hirschauer, B. Jayatilaka, S. Jindariani, M. Johnson, U. Joshi, T. Klijnsma, B. Klima, K.H.M. Kwok, S. Lammel, C. Lee, D. Lincoln, R. Lipton, T. Liu, K. Maeshima, D. Mason, P. McBride, P. Merkel, S. Mrenna, S. Nahn, J. Ngadiuba, D. Noonan, S. Norberg, V. Papadimitriou, N. Pastika, K. Pedro, C. Pena[83], F. Ravera,

66

A. Reinsvold Hall[84], L. Ristori, M. Safdari, E. Sexton-Kennedy, N. Smith, A. Soha, L. Spiegel, S. Stoynev, J. Strait, L. Taylor, S. Tkaczyk, N.V. Tran, L. Uplegger, E.W. Vaandering, I. Zoi
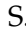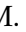
**University of Florida, Gainesville, Florida, USA**
C. Aruta, P. Avery, D. Bourilkov, P. Chang, V. Cherepanov, R.D. Field, C. Huh, E. Koenig, M. Kolosova, J. Konigsberg, A. Korytov, K. Matchev, N. Menendez, G. Mitselmakher, K. Mohrman, A. Muthirakalayil Madhu, N. Rawal, S. Rosenzweig, Y. Takahashi, J. Wang
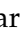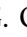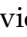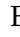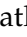
**Florida State University, Tallahassee, Florida, USA**
T. Adams, A. Al Kadhim, A. Askew, S. Bower, R. Hashmi, R.S. Kim, S. Kim, T. Kolberg, G. Martinez, H. Prosper, P.R. Prova, M. Wulansatiti, R. Yohay, J. Zhang
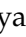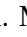
**Florida Institute of Technology, Melbourne, Florida, USA**
B. Alsufyani, S. Butalla, S. Das, T. Elkafrawy[18], M. Hohlmann, E. Yanes
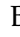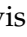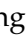
**University of Illinois Chicago, Chicago, Illinois, USA**
M.R. Adams, A. Baty, C. Bennett, R. Cavanaugh, R. Escobar Franco, O. Evdokimov, C.E. Gerber, M. Hawksworth, A. Hingrajiya, D.J. Hofman, J.h. Lee, D. S. Lemos, C. Mills, S. Nanda, G. Oh, B. Ozek, D. Pilipovic, R. Pradhan, E. Prifti, P. Roy, T. Roy, S. Rudrabhatla, N. Singh, M.B. Tonjes, N. Varelas, M.A. Wadud, Z. Ye, J. Yoo
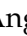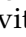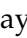
**The University of Iowa, Iowa City, Iowa, USA**
M. Alhusseini, D. Blend, K. Dilsiz[85], L. Emediato, G. Karaman, O.K. Köseyan, J.-P. Merlo, A. Mestvirishvili[86], O. Neogi, H. Ogul[87], Y. Onel, A. Penzo, C. Snyder, E. Tiras[88]
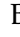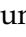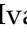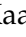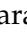
**Johns Hopkins University, Baltimore, Maryland, USA**
B. Blumenfeld, L. Corcodilos, J. Davis, A.V. Gritsan, L. Kang, S. Kyriacou, P. Maksimovic, M. Roguljic, J. Roskes, S. Sekhar, M. Swartz
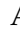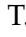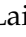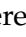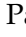
**The University of Kansas, Lawrence, Kansas, USA**
A. Abreu, L.F. Alcerro Alcerro, J. Anguiano, S. Arteaga Escatel, P. Baringer, A. Bean, Z. Flowers, D. Grove, J. King, G. Krintiras, M. Lazarovits, C. Le Mahieu, J. Marquez, M. Murray, M. Nickel, S. Popescu[89], C. Rogan, C. Royon, S. Sanders, C. Smith, G. Wilson
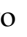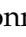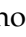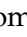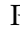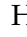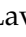
**Kansas State University, Manhattan, Kansas, USA**
B. Allmond, R. Gujju Gurunadha, A. Ivanov, K. Kaadze, Y. Maravin, J. Natoli, D. Roy, G. Sorrentino

**University of Maryland, College Park, Maryland, USA**
A. Baden, A. Belloni, J. Bistany-riebman, Y.M. Chen, S.C. Eno, N.J. Hadley, S. Jabeen, R.G. Kellogg, T. Koeth, B. Kronheim, Y. Lai, S. Lascio, A.C. Mignerey, S. Nabili, C. Palmer, C. Papageorgakis, M.M. Paranjpe, E. Popova[90], A. Shevelev, L. Wang, L. Zhang

**Massachusetts Institute of Technology, Cambridge, Massachusetts, USA**
C. Baldenegro Barrera, J. Bendavid, S. Bright-Thonney, I.A. Cali, P.c. Chou, M. D'Alfonso, J. Eysermans, C. Freer, G. Gomez-Ceballos, M. Goncharov, G. Grosso, P. Harris, D. Hoang, D. Kovalskyi, J. Krupa, L. Lavezzo, Y.-J. Lee, K. Long, C. Mcginn, A. Novak, M.I. Park, C. Paus, C. Reissel, C. Roland, G. Roland,

S. Rothman (iD), G.S.F. Stephans (iD), Z. Wang (iD), B. Wyslouch (iD), T. J. Yang (iD)
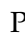
**University of Minnesota, Minneapolis, Minnesota, USA**
B. Crossman (iD), C. Kapsiak (iD), M. Krohn (iD), D. Mahon (iD), J. Mans (iD), B. Marzocchi (iD), M. Revering (iD), R. Rusack (iD), R. Saradhy (iD), N. Strobbe (iD)
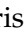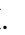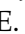
**University of Nebraska-Lincoln, Lincoln, Nebraska, USA**
K. Bloom (iD), D.R. Claes (iD), G. Haza (iD), J. Hossain (iD), C. Joo (iD), I. Kravchenko (iD), A. Rohilla (iD), J.E. Siado (iD), W. Tabb (iD), A. Vagnerini (iD), A. Wightman (iD), F. Yan (iD), D. Yu (iD)

**State University of New York at Buffalo, Buffalo, New York, USA**
H. Bandyopadhyay (iD), L. Hay (iD), H.w. Hsia, I. Iashvili (iD), A. Kalogeropoulos (iD), A. Kharchilava (iD), M. Morris (iD), D. Nguyen (iD), S. Rappoccio (iD), H. Rejeb Sfar, A. Williams (iD), P. Young (iD)

**Northeastern University, Boston, Massachusetts, USA**
G. Alverson (iD), E. Barberis (iD), J. Bonilla (iD), B. Bylsma, M. Campana (iD), J. Dervan (iD), Y. Haddad (iD), Y. Han (iD), I. Israr (iD), A. Krishna (iD), P. Levchenko (iD), J. Li (iD), M. Lu (iD), R. Mccarthy (iD), D.M. Morse (iD), T. Orimoto (iD), A. Parker (iD), L. Skinnari (iD), E. Tsai, D. Wood (iD)
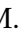
**Northwestern University, Evanston, Illinois, USA**
S. Dittmer (iD), K.A. Hahn (iD), D. Li (iD), Y. Liu (iD), M. Mcginnis (iD), Y. Miao (iD), D.G. Monk (iD), M.H. Schmitt (iD), A. Taliercio (iD), M. Velasco
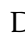
**University of Notre Dame, Notre Dame, Indiana, USA**
G. Agarwal (iD), R. Band (iD), R. Bucci, S. Castells (iD), A. Das (iD), R. Goldouzian (iD), M. Hildreth (iD), K. Hurtado Anampa (iD), T. Ivanov (iD), C. Jessop (iD), K. Lannon (iD), J. Lawrence (iD), N. Loukas (iD), L. Lutton (iD), J. Mariano, N. Marinelli, I. Mcalister, T. McCauley (iD), C. Mcgrady (iD), C. Moore (iD), Y. Musienko[22] (iD), H. Nelson (iD), M. Osherson (iD), A. Piccinelli (iD), R. Ruchti, A. Townsend (iD), Y. Wan, M. Wayne (iD), H. Yockey, M. Zarucki (iD), L. Zygala (iD)

**The Ohio State University, Columbus, Ohio, USA**
A. Basnet (iD), M. Carrigan (iD), L.S. Durkin (iD), C. Hill (iD), M. Joyce (iD), M. Nunez Ornelas (iD), K. Wei, D.A. Wenzl, B.L. Winer (iD), B. R. Yates (iD)
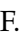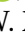
**Princeton University, Princeton, New Jersey, USA**
H. Bouchamaoui (iD), K. Coldham, P. Das (iD), G. Dezoort (iD), P. Elmer (iD), P. Fackeldey (iD), A. Frankenthal (iD), B. Greenberg (iD), N. Haubrich (iD), K. Kennedy, G. Kopp (iD), S. Kwan (iD), D. Lange (iD), A. Loeliger (iD), D. Marlow (iD), I. Ojalvo (iD), J. Olsen (iD), F. Simpson (iD), D. Stickland (iD), C. Tully (iD), L.H. Vage

**University of Puerto Rico, Mayaguez, Puerto Rico, USA**
S. Malik (iD), R. Sharma

**Purdue University, West Lafayette, Indiana, USA**
A.S. Bakshi (iD), S. Chandra (iD), R. Chawla (iD), A. Gu (iD), L. Gutay, M. Jones (iD), A.W. Jung (iD), A.M. Koshy, M. Liu (iD), G. Negro (iD), N. Neumeister (iD), G. Paspalaki (iD), S. Piperov (iD), J.F. Schulte (iD), A. K. Virdi (iD), F. Wang (iD), A. Wildridge (iD), W. Xie (iD), Y. Yao (iD)

**Purdue University Northwest, Hammond, Indiana, USA**
J. Dolen (iD), N. Parashar (iD), A. Pathak (iD)

**Rice University, Houston, Texas, USA**
D. Acosta (iD), A. Agrawal (iD), T. Carnahan (iD), K.M. Ecklund (iD), P.J. Fernández Manteca (iD), S. Freed, P. Gardner, F.J.M. Geurts (iD), I. Krommydas (iD), W. Li (iD), J. Lin (iD), O. Miguel Colin (iD),
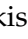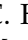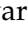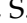
B.P. Padley, R. Redjimi, J. Rotter, E. Yigitbasi, Y. Zhang

**University of Rochester, Rochester, New York, USA**
A. Bodek, P. de Barbaro, R. Demina, J.L. Dulemba, A. Garcia-Bellido, O. Hindrichs, A. Khukhunaishvili, N. Parmar, P. Parygin[90], R. Taus

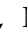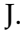**Rutgers, The State University of New Jersey, Piscataway, New Jersey, USA**
B. Chiarito, J.P. Chou, S.V. Clark, D. Gadkari, Y. Gershtein, E. Halkiadakis, M. Heindl, C. Houghton, D. Jaroslawski, S. Konstantinou, I. Laflotte, A. Lath, R. Montalvo, K. Nash, J. Reichert, P. Saha, S. Salur, S. Schnetzer, S. Somalwar, R. Stone, S.A. Thayil, S. Thomas, J. Vora

**University of Tennessee, Knoxville, Tennessee, USA**
D. Ally, A.G. Delannoy, S. Fiorendi, S. Higginbotham, T. Holmes, A.R. Kanuganti, N. Karunarathna, L. Lee, E. Nibigira, S. Spanier

**Texas A&M University, College Station, Texas, USA**
D. Aebi, M. Ahmad, T. Akhter, K. Androsov[60], O. Bouhali[91], R. Eusebi, J. Gilmore, T. Huang, T. Kamon[92], H. Kim, S. Luo, R. Mueller, D. Overton, A. Safonov

**Texas Tech University, Lubbock, Texas, USA**
N. Akchurin, J. Damgov, Y. Feng, N. Gogate, Y. Kazhykarim, K. Lamichhane, S.W. Lee, C. Madrid, A. Mankel, T. Peltola, I. Volobouev

**Vanderbilt University, Nashville, Tennessee, USA**
E. Appelt, Y. Chen, S. Greene, A. Gurrola, W. Johns, R. Kunnawalkam Elayavalli, A. Melo, D. Rathjens, F. Romeo, P. Sheldon, S. Tuo, J. Velkovska, J. Viinikainen
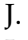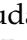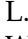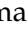
**University of Virginia, Charlottesville, Virginia, USA**
B. Cardwell, H. Chung, B. Cox, J. Hakala, R. Hirosky, A. Ledovskoy, C. Mantilla, C. Neu, C. Ramón Álvarez

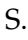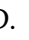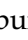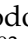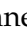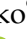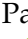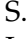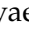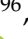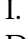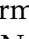**Wayne State University, Detroit, Michigan, USA**
S. Bhattacharya, P.E. Karchin

**University of Wisconsin - Madison, Madison, Wisconsin, USA**
A. Aravind, S. Banerjee, K. Black, T. Bose, E. Chavez, S. Dasu, P. Everaerts, C. Galloni, H. He, M. Herndon, A. Herve, C.K. Koraka, A. Lanaro, R. Loveless, J. Madhusudanan Sreekala, A. Mallampalli, A. Mohammadi, S. Mondal, G. Parida, L. Pétré, D. Pinna, A. Savin, V. Shang, V. Sharma, W.H. Smith, D. Teague, H.F. Tsoi, W. Vetens, A. Warden

**Authors affiliated with an international laboratory covered by a cooperation agreement with CERN**
S. Afanasiev, V. Alexakhin, D. Budkouski, I. Golutvin[†], I. Gorbunov, V. Karjavine, O. Kodolova[93,90], V. Korenkov, A. Lanev, A. Malakhov, V. Matveev[94], A. Nikitenko[95,93], V. Palichik, V. Perelygin, M. Savina, V. Shalaev, S. Shmatov, S. Shulha, V. Smirnov, O. Teryaev, N. Voytishin, B.S. Yuldashev[†96], A. Zarubin, I. Zhizhin, Yu. Andreev, A. Dermenev, S. Gninenko, N. Golubev, A. Karneyeu, D. Kirpichnikov, M. Kirsanov, N. Krasnikov, I. Tlisova, A. Toropin

**Authors affiliated with an institute formerly covered by a cooperation agreement with CERN**
G. Gavrilov, V. Golovtcov, Y. Ivanov, V. Kim[97], V. Murzin, V. Oreshkin, D. Sosnov, V. Sulimov, L. Uvarov, A. Vorobyev[†], T. Aushev, K. Ivanov,

V. Gavrilov, N. Lychkovskaya, V. Popov, A. Zhokin, R. Chistov[97], M. Danilov[97], S. Polikarpov[97], V. Andreev, M. Azarkin, M. Kirakosyan, A. Terkulov, E. Boos, V. Bunichev, M. Dubinin[83], L. Dudko, V. Klyukhin, O. Lukina, M. Perfilov, V. Savrin, P. Volkov, G. Vorotnikov, V. Blinov[97], T. Dimova[97], A. Kozyrev[97], O. Radchenko[97], Y. Skovpen[97], V. Kachanov, S. Slabospitskii, A. Uzunian, A. Babaev, V. Borshch, D. Druzhkin

†: Deceased
[1]Also at Yerevan State University, Yerevan, Armenia
[2]Also at TU Wien, Vienna, Austria
[3]Also at Ghent University, Ghent, Belgium
[4]Also at Universidade do Estado do Rio de Janeiro, Rio de Janeiro, Brazil
[5]Also at FACAMP - Faculdades de Campinas, Sao Paulo, Brazil
[6]Also at Universidade Estadual de Campinas, Campinas, Brazil
[7]Also at Federal University of Rio Grande do Sul, Porto Alegre, Brazil
[8]Also at University of Chinese Academy of Sciences, Beijing, China
[9]Also at China Center of Advanced Science and Technology, Beijing, China
[10]Also at University of Chinese Academy of Sciences, Beijing, China
[11]Also at China Spallation Neutron Source, Guangdong, China
[12]Now at Henan Normal University, Xinxiang, China
[13]Also at University of Shanghai for Science and Technology, Shanghai, China
[14]Now at The University of Iowa, Iowa City, Iowa, USA
[15]Also at an institute formerly covered by a cooperation agreement with CERN
[16]Also at Zewail City of Science and Technology, Zewail, Egypt
[17]Also at British University in Egypt, Cairo, Egypt
[18]Now at Ain Shams University, Cairo, Egypt
[19]Also at Purdue University, West Lafayette, Indiana, USA
[20]Also at Université de Haute Alsace, Mulhouse, France
[21]Also at Istinye University, Istanbul, Turkey
[22]Also at an international laboratory covered by a cooperation agreement with CERN
[23]Also at The University of the State of Amazonas, Manaus, Brazil
[24]Also at University of Hamburg, Hamburg, Germany
[25]Also at RWTH Aachen University, III. Physikalisches Institut A, Aachen, Germany
[26]Also at Bergische University Wuppertal (BUW), Wuppertal, Germany
[27]Also at Brandenburg University of Technology, Cottbus, Germany
[28]Also at Forschungszentrum Jülich, Juelich, Germany
[29]Also at CERN, European Organization for Nuclear Research, Geneva, Switzerland
[30]Also at HUN-REN ATOMKI - Institute of Nuclear Research, Debrecen, Hungary
[31]Now at Universitatea Babes-Bolyai - Facultatea de Fizica, Cluj-Napoca, Romania
[32]Also at MTA-ELTE Lendület CMS Particle and Nuclear Physics Group, Eötvös Loránd University, Budapest, Hungary
[33]Also at HUN-REN Wigner Research Centre for Physics, Budapest, Hungary
[34]Also at Physics Department, Faculty of Science, Assiut University, Assiut, Egypt
[35]Also at Punjab Agricultural University, Ludhiana, India
[36]Also at University of Visva-Bharati, Santiniketan, India
[37]Also at Indian Institute of Science (IISc), Bangalore, India
[38]Also at Amity University Uttar Pradesh, Noida, India
[39]Also at IIT Bhubaneswar, Bhubaneswar, India
[40]Also at Institute of Physics, Bhubaneswar, India
[41]Also at University of Hyderabad, Hyderabad, India

[42]Also at Deutsches Elektronen-Synchrotron, Hamburg, Germany

[43]Also at Isfahan University of Technology, Isfahan, Iran

[44]Also at Sharif University of Technology, Tehran, Iran

[45]Also at Department of Physics, University of Science and Technology of Mazandaran, Behshahr, Iran

[46]Also at Department of Physics, Faculty of Science, Arak University, ARAK, Iran

[47]Also at Helwan University, Cairo, Egypt

[48]Also at Italian National Agency for New Technologies, Energy and Sustainable Economic Development, Bologna, Italy

[49]Also at Centro Siciliano di Fisica Nucleare e di Struttura Della Materia, Catania, Italy

[50]Also at Università degli Studi Guglielmo Marconi, Roma, Italy

[51]Also at Scuola Superiore Meridionale, Università di Napoli 'Federico II', Napoli, Italy

[52]Also at Fermi National Accelerator Laboratory, Batavia, Illinois, USA

[53]Also at Lulea University of Technology, Lulea, Sweden

[54]Also at Consiglio Nazionale delle Ricerche - Istituto Officina dei Materiali, Perugia, Italy

[55]Also at Department of Applied Physics, Faculty of Science and Technology, Universiti Kebangsaan Malaysia, Bangi, Malaysia

[56]Also at Consejo Nacional de Ciencia y Tecnología, Mexico City, Mexico

[57]Also at Trincomalee Campus, Eastern University, Sri Lanka, Nilaveli, Sri Lanka

[58]Also at Saegis Campus, Nugegoda, Sri Lanka

[59]Also at National and Kapodistrian University of Athens, Athens, Greece

[60]Also at Ecole Polytechnique Fédérale Lausanne, Lausanne, Switzerland

[61]Also at Universität Zürich, Zurich, Switzerland

[62]Also at Stefan Meyer Institute for Subatomic Physics, Vienna, Austria

[63]Also at Laboratoire d'Annecy-le-Vieux de Physique des Particules, IN2P3-CNRS, Annecy-le-Vieux, France

[64]Also at Near East University, Research Center of Experimental Health Science, Mersin, Turkey

[65]Also at Konya Technical University, Konya, Turkey

[66]Also at Izmir Bakircay University, Izmir, Turkey

[67]Also at Adiyaman University, Adiyaman, Turkey

[68]Also at Bozok Universitetesi Rektörlügü, Yozgat, Turkey

[69]Also at Marmara University, Istanbul, Turkey

[70]Also at Milli Savunma University, Istanbul, Turkey

[71]Also at Kafkas University, Kars, Turkey

[72]Now at Istanbul Okan University, Istanbul, Turkey

[73]Also at Hacettepe University, Ankara, Turkey

[74]Also at Erzincan Binali Yildirim University, Erzincan, Turkey

[75]Also at Istanbul University - Cerrahpasa, Faculty of Engineering, Istanbul, Turkey

[76]Also at Yildiz Technical University, Istanbul, Turkey

[77]Also at School of Physics and Astronomy, University of Southampton, Southampton, United Kingdom

[78]Also at IPPP Durham University, Durham, United Kingdom

[79]Also at Monash University, Faculty of Science, Clayton, Australia

[80]Also at Università di Torino, Torino, Italy

[81]Also at Bethel University, St. Paul, Minnesota, USA

[82]Also at Karamanoğlu Mehmetbey University, Karaman, Turkey

[83]Also at California Institute of Technology, Pasadena, California, USA

[84]Also at United States Naval Academy, Annapolis, Maryland, USA